Single-Molecule Dynamics at the Solid-Liquid Interface

by

Joshua Nolan Mabry

B.S., Cornell University, 2010

A thesis submitted to the Faculty of the Graduate School of the University of Colorado in partial fulfillment of the requirement for the degree of Doctor of Philosophy

Department of Chemical and Biological Engineering

2015

This thesis entitled:

"Single-Molecule Dynamics at the Solid-Liquid Interface"
written by Joshua Nolan Mabry

has been approved for the Department of Chemical and Biological Engineering

_____	_____
Daniel K. Schwartz	Date
_____	_____
Joel Kaar	Date

The final copy of this thesis has been examined by the signatories, and we find that both the content and the form meet acceptable presentation standards of scholarly work in the above mentioned disciple.

Abstract

Mabry, Joshua Nolan (Ph.D., Department of Chemical and Biological Engineering)

Single-Molecule Dynamics at the Solid-Liquid Interface

Thesis directed by Professor Daniel K. Schwartz

The overall objective of this work was to develop new analytical methods for characterizing molecular dynamics at the solid-liquid interface. We used single-molecule imaging, based on total internal reflection fluorescence microscopy, to observe surface-active molecules at silica-aqueous interfaces and leveraged high-throughput computational tools to create massive datasets capturing broad distributions of molecular kinetics and detailed information on surface lateral heterogeneity. We developed novel statistical approaches to learn about the molecular-level physical processes in unprecedented detail. With respect to specific applications, we first demonstrated how single-molecule imaging yields a deeper understanding of chromatographic media. We used a combination of single-molecule observations and macroscopic reversed phase liquid chromatography to characterize the surface activity of a hydrophobic analyte across a range of solution conditions, focusing on how anomalous surface sites affected the adsorption kinetics and retention in the column. The other two projects described in this thesis focused on understanding molecular mobility and structure—important variables to consider in the self-assembly of nanodevices and surface coatings. Building off of our understanding of hydrophobic systems, we carefully studied surface diffusion at the interface of a hydrophobic surface and aqueous solution and found that diffusion

could be rationally manipulated by changing the polarity of the solution, although the average diffusive behavior was strongly affected by the prevalence of anomalous surface sites. Finally, we developed a new surface mapping method to correlate the conformation and adsorption behavior of molecular building blocks on surfaces. We characterized alpha-helical peptides on deliberately patterned and nominally uniform surfaces of varying hydrophobicity and found that the peptide conformation and adsorption kinetics were sensitive to microscopic, lateral surface heterogeneity. In all of this work, spatial variations in surface chemistry were observed to profoundly affect surface dynamics with significant impact on self-assembly and chemical separation processes. More generally, we found that surface heterogeneity is seemingly ubiquitous and changes considerably the correct interpretation of ensemble-averaged experiments and molecular simulations.

Acknowledgements

I appreciate having had the opportunity to interact with many intelligent scientists, engineers, and support staff over the past five years at the University of Colorado Boulder. My development as a scientist was driven most by my advisor Dan Schwartz. Dan challenged me to think critically about science, first in the classroom and later in the laboratory. Dan always brought his powerful intellect to bear on any research questions that I brought to him and gave selflessly of his time. He also taught me to value the greater scientific enterprise and to strive to be a well-rounded physical scientist. I truly appreciated that he incorporated my ideas into funding proposals and new student research projects so that I could influence the direction of the group beyond my own projects.

Importantly, Dan provided a stable funding environment and recruited some very talented students and postdocs, with whom I had the pleasure of working. My co-authors Blake Langdon and Michael Skaug provided endless encouragement and critical analysis of my work. Significant technical assistance was provided by Mark Kastantin, Nathan Nelson, and Rob Walder. Indira Sriram, Stephanie Malone, and Carolyn Schoenbaum were an invaluable source of advice and critical insight. Dapeng Wang generously allowed me to join him in an interesting follow-up project to my work on surface diffusion. I enjoyed working alongside Saonti Chakroborty, Jon Monserud, Heidi Chin, Katherine Macri, and Aaron McUmber, as well. I also have appreciated the company of the following new

students in our lab: James Weltz, Yu Cai, Lucas Ellis, and Jeremiah Traeger. Undergraduates Brennan Coffey and Roya Mirhossaini provided much needed outside perspectives over their years in the lab. Many of the faculty have also provided support and encouragement over the years, especially Joel Kaar, Will Medlin, Al Weimer, Charles Musgrave, Diego Krapf, Matt Glaser, and Tom Perkins. In my first year of graduate school, fellow graduate student Katherine Rice graciously offered her materials for use in experiments. Walter Paxton of Sandia National Laboratory in Albuquerque also provided instruction in surface chemistry and patterning techniques.

I was able to engage in this challenging work because I had strong backing from my family, especially my wife Kelly Mabry. Kelly, more than anyone else, cheered on my research, even when confronting research challenges herself. My parents Phillip and Elizabeth and my sister Carole also provided unfailing encouragement and support. I also acknowledge all of the wonderful teachers and professors who prepared me for this endeavor. While in graduate school, I was lucky to have assistance from the department staff, including Andrew Schmidt, Jen Gifford, Dragan Mejic, and Dominque De Vangel.

I have thankfully been fully supported by government funding sources throughout graduate school. I acknowledge primary support from the U.S. Department of Energy Basic Energy Sciences, Chemical Sciences, Geosciences, and Biosciences Division (DE-SC0001854) for all aspects of the research reported here, including instrumentation, salary and stipend support, materials/supplies, etc. I was partially supported by a U.S.

Department of Education Graduate Assistance in Areas of National Need Fellowship (P200A120125). This work utilized the Janus supercomputer, which is supported by the National Science Foundation (award number CNS-0821794) and the University of Colorado Boulder. The Janus supercomputer is a joint effort of the University of Colorado Boulder, the University of Colorado Denver and the National Center for Atmospheric Research. Data storage resources were provided by NSF-MRI Grant ACI-1126839, MRI: Acquisition of a Scalable Petascale Storage Infrastructure for Data-Collections and Data-Intensive Discovery. Circular dichroism spectroscopy instrumentation was provided by NIH 1S10RR028036-01. I also thank Adrianne M. Rosales and Kristi S. Anseth for kindly providing access to and assistance with their high performance liquid chromatography instrument.

Table of Contents

CHAPTER 1: INTRODUCTION 1

1.1 CHEMICAL ENVIRONMENT OF THE SOLID-LIQUID INTERFACE 2

1.1.1 Silica-Based Surfaces.....2

1.1.2 Surface Characterization.....4

1.1.3 Solution Effects.....7

1.2 ADSORBATE DYNAMICS.....9

1.2.1 Adsorption.....9

2.2 Surface Diffusion.....12

1.2.3 Conformational Change.....16

1.3 FLUORESCENCE PHENOMENA AND MEASUREMENT TECHNIQUES 18

1.3.1 Fluorescence RECOVERY AFTER PHOTOBLEACHING 20

1.3.2 Fluorescence Correlation Spectroscopy.....21

1.3.3 Total Internal Reflection Fluorescence Microscopy.....22

1.3.4 Förster Resonance Energy Transfer.....24

1.4 OBJECTIVES 26

1.5 REFERENCES 27

CHAPTER 2: SINGLE-MOLECULE INSIGHTS INTO RETENTION AT A REVERSED-PHASE CHROMATOGRAPHIC INTERFACE.....34

2.1 ABSTRACT.....34

2.2 INTRODUCTION.....35

2.3 EXPERIMENTAL SECTION 38

2.3.1 Single-Molecule Experiments.....38

2.3.2 Single-Molecule Data Analysis 39

2.3.2.1 Correlation Analysis of Adsorption Event Positions 39

2.3.2.2 Super-Resolution Imaging and Adsorption Site Analysis 41

2.3.2.3 Adsorption/Desorption Kinetics and Adsorption Equilibrium Calculations 42

2.3.3.1 Experiments.....*43*
2.3.3.2 Stochastic Model of Chromatography.....*44*
2.4 RESULTS AND DISCUSSION.....47
2.4.1 Mapping Adsorption Sites.....47
2.4.2 Heterogeneous Adsorption Site Residence Time Distributions..51
2.4.3 Correlation of Adsorption and Desorption Kinetics.....53
2.4.4 Retention in Single-Molecule and Macroscopic RPLC Experiments.....55
2.4.4 Chromatographic Peak Tailing.....58
2.5 CONCLUSIONS.....59
2.7 REFERENCES.....61
CHAPTER 3: TUNING THE FLIGHT LENGTH OF MOLECULES DIFFUSING ON A HYDROPHOBIC SURFACE.....65
3.1 ABSTRACT.....65
3.2 INTRODUCTION.....66
3.3 RESULTS AND DISCUSSION.....69
3.3 EXPERIMENTAL METHODS.....76
3.4 REFERENCES.....79
CHAPTER 4: CAPTURING CONFORMATION-DEPENDENT MOLECULE-SURFACE INTERACTIONS WHEN SURFACE CHEMISTRY IS HETEROGENEOUS.....82
4.1 ABSTRACT.....82
4.2 INTRODUCTION.....83
4.3 RESULTS AND DISCUSSION.....86
4.3.1 Peptide Conformation in Solution and on the Surface.....86
4.3.2 Identifying Distinct Regions of a Heterogeneous Surface.....92
4.3.3 Contributions of Adsorption/Desorption and Folding/Unfolding Processes to Average Conformation.....97
4.3.4 Heterogeneous Peptide Behavior on Nominally Uniform Surfaces.....100
4.4 CONCLUSION.....103

4.5 METHODS 104
4.5.1 Solutions of End-Labeled Peptide 104
4.5.2 Surface Preparation and Characterization 105
4.5.3 Single-Molecule Total Internal Reflection Fluorescence Microscopy (TIRFM) 106
4.5.4 Quantification of Förster Resonance Energy Transfer (FRET) 107
4.5.5 Calculation of Likelihood of Conformational States 108
4.5.6 Characterization of Desorption and Folding/Unfolding Kinetics 109
4.6 REFERENCES 110
BIBLIOGRAPHY 116
APPENDIX A: SUPPORTING INFORMATION FOR CH. 2 131
A.1 SINGLE-MOLECULE IMAGING EXPERIMENTAL DETAILS 131
A.1.1 Surface Preparation 131
A.1.2 Single-Molecule TIRFM 131
A.2 RANGE OF RETENTION MEASUREMENTS 133
A.3 FITTING ADSORPTION EVENT COUNT DATA 134
A.4 FITTING SINGLE-MOLECULE RESIDENCE TIME DISTRIBUTIONS 136
A.4.1 Number of Populations 136
A.4.2 Dependence of Population Fractions on Solution Conditions 141
A.5 CORRELATION BETWEEN SITE RESIDENCE TIMES AND ADSORPTION RATES 143
A.6 CALCULATION OF SINGLE-MOLECULE STEP SIZE DISTRIBUTIONS 144
A.7 POWER STUDIES DEMONSTRATING NO PHOTOPHYSICAL EFFECTS 145
A.8 CHROMATOGRAMS SHOWING NO DEPENDENCE ON ANALYTE CONCENTRATION 146
A.9 STOCHASTIC MODEL OF CHROMATOGRAPHY 148
A.9.1 Theoretical Model 148
A.9.2 Estimation of True Residence Time Distribution 150
A.9.3 Fitting Experimental Peak Asymmetry Results 154
A.9.4 Sensitivity to Characteristic Residence Time Constants 155
A.10 EXPERIMENTAL AND MODEL CHROMATOGRAMS 156

A.10.1 Analysis of Uracil Chromatographic Peaks 158
A.11 References 158
APPENDIX B: SUPPORTING INFORMATION FOR CH. 3 160
B.1 End-to-End Distances of Molecular Trajectories 160
B.2 Apparent Diffusion of Confined Molecules 161
B.3 Statistical Description of Molecular Mobility 166
B.4 Evidence of Surface Heterogeneity 168
B.5 Theoretical Flight Length Distribution 172
B.6 References 172
APPENDIX C: SUPPORTING INFORMATION FOR CH. 4 174
C.1 Circular Dichroism Measurements 174
C.2 Peptide End-to-End Distance Calculations 176
C.3 Surface Patterning 177
C.3.1 Procedure 177
C.3.2 Photomask Imaging 178
C.3.4 Dye-Labeled Amine Monolayer Preparation 178
C.3.5 Pattern Characterization 179
C.4 MAPT Images of Control Surfaces 181
C.5 Measurement of Folding and Unfolding Rates 182
C.6 Distributions of Surface Residence and Initial Conformational State Times 184
C.7 Effect of Incident Laser Power on Surface Residence Times 186
C.8 References 187

List of Tables

Table 2.1: Eq 2.4 fit parameters for site residence time distributions 51

Table 2.2: Chromatographic figures of merit 57

Table A1: Adsorption event count histogram fit parameters. 135

Table A2: Parameters for residence time distribution fits 142

Table A3: Adsorption site residence time distribution fit parameters 143

Table A4: Chromatographic figures of merit at different BFA concentrations...147

Table A5: Model parameters and results for best fit to peak asymmetry data 156

Table A6: Chromatographic figures of merit for uracil.....158

Table B1: Parameters for the fits of Equation 3.2 shown in Figure B4. 165

Table B2: Fit parameters for the Equation 3.3 fits shown in Figure B5. 167

Table B3: Adsorption event count histogram fit parameters. 171

Table C1: Parameters for surface residence time distribution fits. 185

Table C2: Parameters for initial conformational state time distribution fits. 185

List of Figures

Figure 1.1: Simulation snapshots at different C_{18} ligand densities on silica in 50/50 mol % water/methanol. 4

Figure 1.2: AFM techniques (bold) and the various biochemical, physical, and chemical properties that can be measured. 5

Figure 1.3: Tip-enhanced, optical spectroscopic imaging with sub-diffraction limited spatial resolution. 6

Figure 1.4: Influence of organic modifier concentration on retention factor in reversed-phase liquid chromatography. 8

Figure 1.5: Kinetics of BSA adsorption on gold surfaces as measured by surface plasmon resonance spectroscopy. 10

Figure 1.6: Hypothetical energy diagram for adsorption of C16 fatty acid at the water-silica interface. 12

Figure 1.7: Displacement distributions at the annotated Δt for (a) PEG, (b) BSA, (c) Atto6G, and (d) BODIPY. 14

Figure 1.8: Chain length scaling of polymer surface dynamics and kinetics. 15

Figure 1.9: Surface residence time distributions for different organophosphorus hydrolase protein conformations.....17

Figure 1.10: Typical fluorescent dyes: brightness vs. wavelength of maximum absorption. Inset: Typical absorbance and fluorescence emission spectra. 19

Figure 1.11: FRAP of lipid bilayer. 21

Figure 1.12: Detecting nanodomains in membranes using FCS. 22

Figure 1.13: Prism-based TIRFM. 23

Figure 1.14: DNA hairpin conformation by FRET measurements. 25
Figure 2.1: Pair autocorrelation function of molecule adsorption positions.....46
Figure 2.2: Super-resolution map of BFA adsorption events in 62% methanol....48
Figure 2.3: Probability histogram of site adsorption events. 49
Figure 2.4: Adsorption site residence time distributions. 50
Figure 2.5: Dependence of average solute behavior on methanol concentration ..54
Figure 2.6: Experimental chromatogram for BFA with 56% methanol mobile phase. 57
Figure 3.1: Schematic depiction of surface diffusion. 69
Figure 3.2: Selected trajectories and detailed statistics of surface diffusion in different solutions. 72
Figure 3.3 Flying mode diffusion coefficients.....75
Figure 4.1: Schematic of mapping technique. 87
Figure 4.2: Peptide end-to-end distance distributions.....89
Figure 4.3: MAPT Images. 93
Figure 4.4: Spatial dependence of adsorption and conformational states.....96
Figure 4.5: Conformational state dynamics. 98
Figure 4.6: Likelihood of helical peptide conformation for observations in adsorption map pixels with N_{pixel} adsorption events. 101
Figure A1: Adsorption event count histogram fit with increasing numbers of components. 136
Figure A2: Residence time distribution fits for increasing numbers of populations.137
Figure A3: Fitted distributions of residence times.....139
Figure A4: Residence time distribution fit by maximum entropy method 140
Figure A5: Residence time distribution fits with fixed population fractions.....142

Figure A6: Adsorption site residence time distributions. 143
Figure A7: Single-molecule step-size distributions. 144
Figure A8: Residence time distributions at different laser power levels. 146
Figure A9: Experimental chromatograms for BFA at different sample concentrations. 147
Figure A10: Experimental and theoretical chromatographic figures of merit 154
Figure A11: Experimental and theoretical chromatographic figures of merit for $\alpha = 100$ 156
Figure A12: Experimental and theoretical model chromatograms 157
Figure B1: End-to-End Distance Distributions. 161
Figure B2: Step-size distributions for trajectories with end-to-end distance < 50 nm at different lag times. 162
Figure B3: Complementary cumulative squared step-size distributions for trajectories with end-to-end distance < 50 nm in 0% methanol. 163
Figure B4: Complementary cumulative squared step-size distributions for trajectories with end-to-end distance < 50 nm. 164
Figure B5: Complementary cumulative squared step-size distributions for trajectories with end-to-end distance > 200 nm. 166
Figure B6: Mean squared displacement as a function of lag time 168
Figure B7: Super-resolution maps of adsorption sites 169
Figure B8: Probability histograms of site adsorption events 171
Figure C1: Circular dichroism spectra of peptide in solution. 175
Figure C2: Patterning test images. 180
Figure C3: Control adsorption map. 181
Figure C4: Control conformation map. 182

Figure C5: Complementary cumulative distributions of state times. 184
Figure C6: Residence time distributions at different laser power levels. 186

CHAPTER 1: INTRODUCTION

Our interest in the Schwartz Group in molecular dynamics at the solid-liquid interface primarily stems from the desire to understand and ultimately to control the self-organization of molecular building blocks.[1] Confinement of molecules to two dimensions can lead to more efficient assembly processes, since diffusion can be enhanced[2] and molecular orientation and structure stabilized.[3] Interfacial self-assembly may ultimately enable the bottom-up fabrication of nanodevices with desirable optical and electronic properties.[4] The dynamics of assembly involve non-covalent interactions: van der Waals, electrostatic, hydrophobic, hydrogen-bonding, and coordination bonds.[5] Molecular interactions in solution have been studied extensively, to the point that *ab initio* calculations can evaluate binding energies of small molecules well within experimental accurary.[6] Larger biomolecules such as DNA and proteins can provide a scaffold for assembling hierarchical structures,[7] but the interactions of macromolecules with the chemical environment cannot be predicted with the requisite accuracy from first-principles to enable rational design of complex structures.[8] After several decades of development, coarse-grained molecular dynamics simulations can sample the free energy landscape and predict which conformations and structures in solution are likely to be observed.[9] Dynamic properties are less well-understood and more difficult to predict, especially at long timescales, with advanced sampling methods rarely accessing millisecond dynamics.[10] The application of theoretical tools to molecular dynamics at the

solid-liquid interface is significantly complicated by the inherent heterogeneity of solid surfaces.[11] Therefore, there remains a significant need for *experimental* methods of characterizing the dynamics of molecules at solid-liquid interfaces. Ultimately, the lengthscales, timescales, and energies accessible to computational and experimental methods will fully converge, and self-assembly strategies will be guided by mechanistic understanding.

1.1 Chemical Environment of the Solid-Liquid Interface

1.1.1 Silica-Based Surfaces

Silica, in the form of quartz or sand, is abundant in nature, and contact between biomolecules and silica surfaces in aqueous solutions is ubiquitous.[12] Accordingly, pure silica is chemically inert towards most biomolecules in aqueous solution.[13] The chemical inertness and high specific surface area of silica gel ($\sim 10^3$ m^2 g^{-1})[14] make it incredibly useful as a support for catalysts,[15] as a desiccant,[16] and as a liquid chromatography stationary phase material.[17] Of course, silicon wafers support the vast majority of microelectronic devices,[18] and silicon oxide is often used as a dielectric layer.[19] Accordingly, silica is an extremely relevant surface for bottom-up assembly because it can be patterned using established top-down methods, as well, to control surface features over multiple lengthscales.[20-21]

The macroscopic property of silica investigated most heavily in this work is wettability, specifically hydrophobicity in aqueous systems. The surface of silica is hydrophilic, when a significant number of hydrogen-bonding silanol (SiOH) groups are present.[22] The density of silanols is commonly increased by treating the surface with ozone, which reacts with SiH to form SiOH, up to a maximum density of ~5 silanols nm^{-2}.[23-24] By reacting silanol groups with alkylsilanes, the surface can be rendered hydrophobic, with a water contact angle of >90°.[25-26] Exposure to hexamethyldisilazane (HMDS) vapor, in particular, forms a trimethylsilyl (TMS) surface by the following reaction.

$$2\ \text{Si–OH} + (CH_3)_3SiNHSi(CH_3)_3 \rightarrow 2\ \text{Si–O–}\ Si(CH_3)_3 + NH_3 \qquad (1.1)$$

One underappreciated aspect of the silica surface is its inherent chemical heterogeneity due to the presence of different types of silanol (e.g. isolated, vicinal, and geminal silanols) and siloxane groups that naturally arise upon exposure to water.[27] Chemical functionalization reduces this heterogeneity to a limited extent. In the case of alkylsilane modification, only about half of the silanols undergo reaction due to steric interactions of the alkyl groups.[24,28] Furthermore, when an alkylsilane-modified surface is exposed to aqueous solution, hydrolytic cleavage of the siloxane bonds occurs, reducing alkyl ligand density over time and increasing the silanol density.[29] This is known to decrease the performance of silica-based chromatography stationary phase materials because the polar silanol groups can interact in anomalous fashion with the analytes being separated.[30-33] The increasing spatial heterogeneity of the surface at lower alkyl ligand densities

(specifically the uneven lateral distribution of ligands) can be seen in snapshots from molecular simulations (Figure 1.1).[28,34] Surface heterogeneity can also bias the nucleation of self-assembled structures, hindering the ability to achieve long-range order.[35] Throughout this work, we focus on the effects of surface spatial heterogeneity, not only because of its impact on technology, but also because it greatly affects the physical picture of molecules interacting with surfaces.

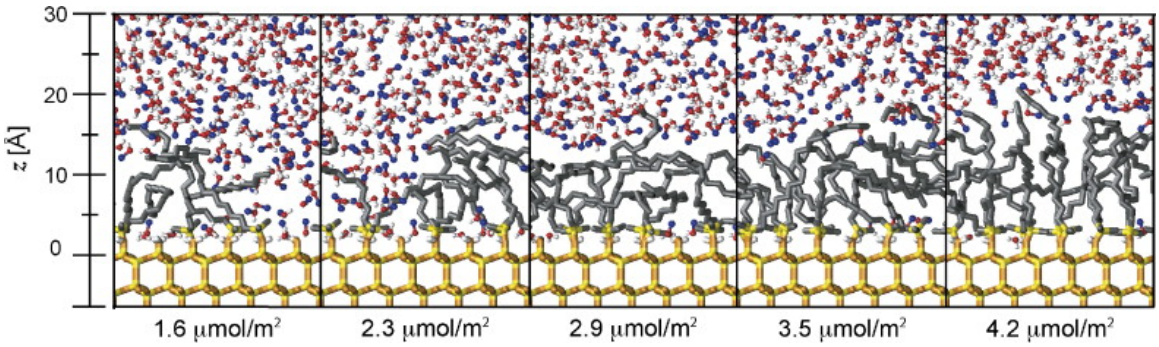

Figure 1.1: Simulation snapshots at different C_{18} ligand densities on silica in 50/50 mol % water/methanol. Adapted from Rafferty, *et. al.*[28] Reprinted by permission from Elsevier B.V: *J. Chromatogr. A.*, Copyright 2008.

1.1.2 Surface Characterization

Averaged information about surface chemistry is available from a host of techniques, including infrared spectroscopy, ellipsometry, x-ray photoelectron spectroscopy, secondary ion mass spectrometry, and contact angle goniometry, while molecular-level simulations can provide insight into the effect of surface chemistry on dynamic processes.[25,36] However, real surfaces are both chemically and topographically

heterogeneous across a wide range of length scales, making it difficult to connect averaged surface properties to molecular processes.[37] Surface heterogeneity can be characterized by scanning probe microscopy and chemical imaging techniques to provide semi-quantitative information on surface chemistry and topography.[38]

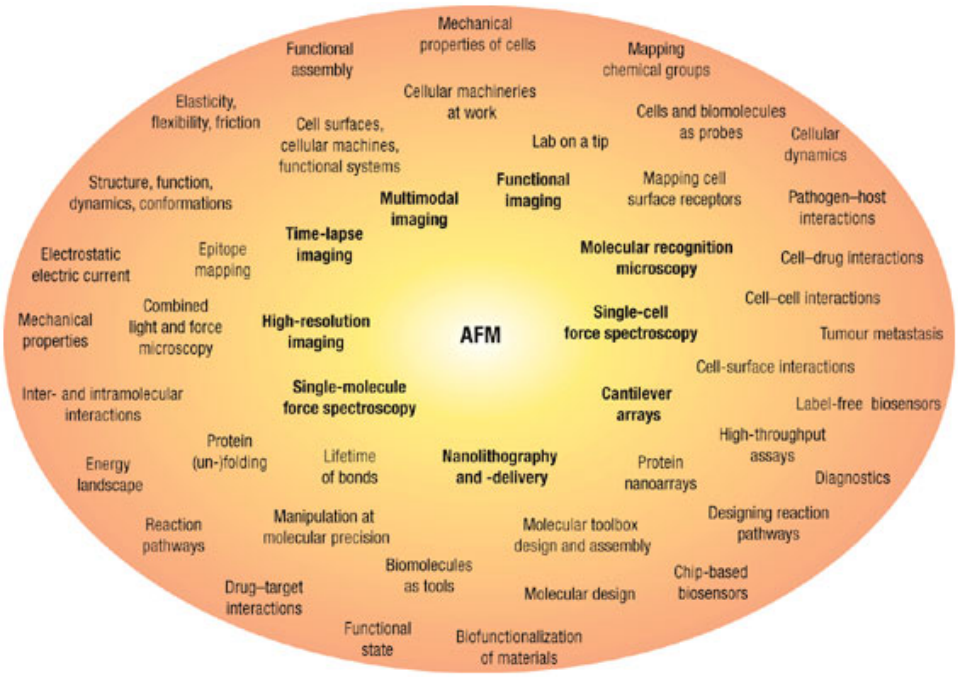

Figure 1.2: AFM techniques (bold) and the various biochemical, physical, and chemical properties that can be measured. Adapted from Müller and Dufrêne.[39] Reprinted by permission from Macmillan Publishers Ltd: *Nat. Nano.*, Copyright 2008.

The atomic force microscopy (AFM) tip has been called the "molecular toolbox" and a "lab-on-a-tip" because it can be physically, chemically, or biologically functionalized[39-40] and applied to study a broad range of phenomena (Figure 1.2). While tips are commonly functionalized to have specific interactions with a surface, the observed data is a

convolution of surface features, tip geometry, and chemistry.[41] The time resolution of AFM techniques is also limited by the raster speed of the probe, typically requiring image acquisition times $>10^{-2}$ s.[42] In contrast to purely optical techniques, the spatial resolution of AFM-based techniques is, however, very high, approaching atomic resolution in carefully controlled systems.[43]

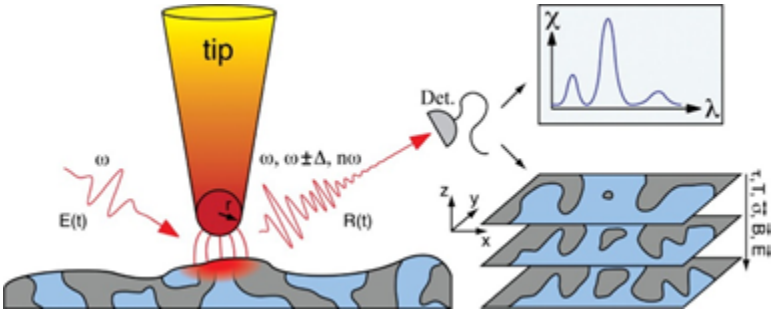

Figure 1.3: Tip-enhanced, optical spectroscopic imaging with sub-diffraction limited spatial resolution. Adapted from Atkin, *et. al*. Reprinted by permission from Taylor and Francis: *Adv. Phys.*, Copyright 2012.

The exquisite spatial control of AFM cantilevers has been leveraged in nano-optical imaging systems, where the AFM tip is used as an antenna for optical spectroscopy, to achieve sub-diffraction limited resolution of chemical domains, in materials systems like block copolymers (Figure 1.3).[44] However, quantitative reproducibility and even temporal stability are fundamental and perhaps intrinsic challenges for scanning probe microscopy methods because of tip-to-tip variability and changes to tip geometry during scanning conditions (due to contamination and/or wear). Of course, even if reliable information on surface chemistry and topography can be obtained, connecting heterogeneous surface structure to function remains a difficult task, since the mechanistic details of surface processes in heterogeneous environments remain largely unknown.

1.1.3 Solution Effects

Surface-sensitive measurements of molecular phenomena can be made under ultra-high vacuum conditions, on carefully prepared crystalline substrates, with incredible precision and accuracy using electron-based microscopy and spectroscopy.[45] A detailed picture has developed for molecular dynamics at the solid-gas interface, and simulations can accurately describe many phenomena such as adsorption.[46-47] The molecular structure of the solid-liquid interface is richer and more dynamic than the solid-gas interface and has profound importance for many applications including sensing and catalysis. However, the introduction of a liquid solution to the solid surface precludes the use of electron-based tools because electrons cannot penetrate the bulk phase. A more limited set of primarily optical techniques are available to probe the solid-liquid interface, and one of the most-established techniques is non-linear optical spectroscopy.[48] It has revealed that large organic and small solvent molecules in contact with the surface have orientational order that depends on the surface chemistry.[49] The anisotropy and ordering of the solution near the surface present a significantly different chemical environment than the bulk solution. This complicates attempts to tether functional biomolecules like enzymes to the surface or to rationally manipulate molecular building blocks like DNA origami that are designed to function in isotropic bulk solution.

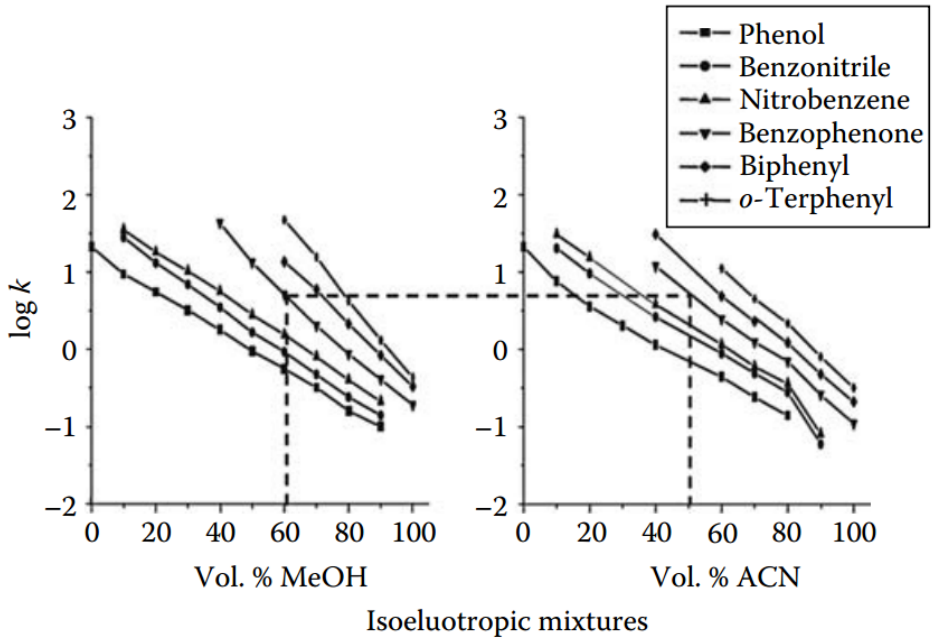

Figure 1.4: Influence of organic modifier concentration on retention factor in reversed-phase liquid chromatography. Adapted from Corradini, et. al.[17] Reprinted by permission from Taylor and Francis: Adv. in Phys., Copyright 2012.

Despite the complexity of the fine structure of solvent molecules at the interface, many interfacial phenomena can be rationally manipulated by subtly changing the composition of the bulk solvent. For example, changing solution conditions can shift the adsorption equilibrium coefficient and enable fast and convenient separations by liquid chromatography.[17] In reversed phase liquid chromatography, adsorption is driven by hydrophobic effects, and decreasing the solution polarity (e.g. adding methanol or acetonitrile to an aqueous solution) makes adsorption less favorable.[50] This is apparent in the experimental retention factors ($k \propto$ adsorption equilibrium coefficient) for hydrophobic solutes in different solutions presented in Figure 1.4. In ion exchange chromatography, the ionic strength of the solution is varied to control retention of

charged molecules, typically proteins, onto the stationary phase.[51] We emphasize phenomenological effects of solution conditions in chromatography because they have been studied intensively for over 100 years[52] and provide a valuable source of insight into the dynamics of molecules at solid-liquid interfaces.

1.2 Adsorbate Dynamics

Molecular dynamics at the solid-liquid interface dominate technologically important processes ranging from heterogeneous catalysis[53-54] to chromatographic separations[55-56] to biosensors[57-58] to the formation of organic monolayers.[59-60] To be able to rationally improve these technologies, one must understand how molecules behave at the interface. An isolated molecule can undergo processes including adsorption, surface diffusion, conformational change, and desorption. Multiple adsorbed molecules can interact and undergo chemical reaction, oligomerization, or specific binding. This thesis focuses only on the interactions of isolated, amphiphilic molecules with surfaces, while keeping in mind the implications for higher order phenomena.

1.2.1 Adsorption

Adsorption of amphiphilic molecules, i.e. surfactants, on solid surfaces is a fundamental process governed by a number of forces such as electrostatic attraction, hydrogen

bonding and non-polar interactions and involves desolvation of the interface.[61] Thermodynamically, adsorption typically occurs when the favorable enthalpy of adsorption is greater than the loss of entropy of the adsorbed solute.[62] Macroscopically, adsorption is often characterized by measuring the increase in surface coverage over time, when a bare surface is exposed to a solution containing the adsorbate at a known concentration. Adsorption kinetics are extracted from the change in surface coverage over time, while thermodynamic isotherms are populated from steady-state coverage.[63] Figure 1.5 shows an example sensorgram for protein adsorption onto different surfaces, noting the upper bound to the measurable kinetics imposed by mass transfer limitations.

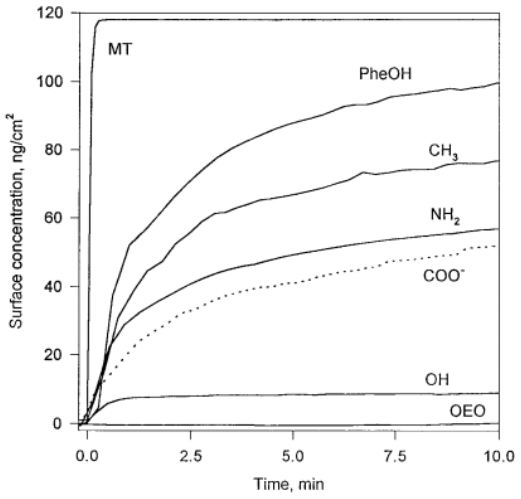

Figure 1.5: Kinetics of BSA adsorption on gold surfaces as measured by surface plasmon resonance spectroscopy. Surface were modified with indicated monolayers, described in the reference source in detail. MT represents adsorption process with mass transport limitation. Adapted from Silin, *et. al*.[64] Reprinted by permission from Elsevier BV: *J. Colloid Interface Sci.* Copyright 1997.

Kinetic models are often fit to ensemble-averaged adsorption data, but since the increase in surface coverage arises from a convolution of mass transfer and adsorption and desorption kinetics, it is difficult to accurately extract the kinetic parameters.[65] The most

common theoretical treatment of adsorption considers the steps to include transport from the bulk solution to the near-surface layer and then a first-order kinetic process of attachment to the surface.[58] In Monte Carlo simulations, the near-surface layer has a thickness equal to the lattice spacing and the timescale for adsorption is scaled by the bulk diffusion coefficient, but the layer thickness does not have a clear physical definition upon which to base the rates of exchange.[66-67] In single-molecule observations, the attachment rate is directly measured without needing to assume a model for adsorption. .[62,68] Previous single-molecule studies extracted rates of attachment of amphiphilic molecules to silica surfaces and found that the attachment process had a positive activation energy, similar in magnitude to a hydrogen bond.[68] This was consistent with the picture presented in Figure 1.6, of adsorption of an amphiphilic fatty acid molecule to silica requiring the removal of a solvent molecule. Thus, adsorption can be viewed as a competition between adsorbate and solvent molecules for surface adsorption sites.

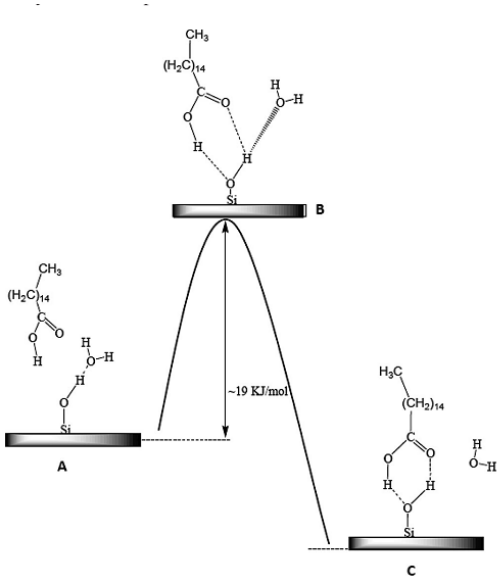

Figure 1.6: Hypothetical energy diagram for adsorption of C16 fatty acid at the water-silica interface. Adapted from Honciuc, *et. al*.[62] Reprinted with permission from American Chemical Society: *J. Phys. Chem. C.* Copyright 2009.

2.2 Surface Diffusion

Molecules adsorbed to a solid surface were traditionally thought to explore the surface by 2D Brownian motion described by Gaussian statistics, and this type of surface diffusion model is often incorporated into models of more complex processes like chromatography[55] or crystal growth.[69] The detailed mechanism of surface diffusion has a profound impact on the efficiency of search processes, especially in heterogeneous catalysis where a reactive molecule must find catalytic surface sites or in biosensors where an analyte must reach the recognition element.[70] For many geometrical configurations of surface elements, the optimal search strategy is an intermittent strategy combining periods of slow local searching separated by ballistic displacements.[71] This is

often the case at the solid-liquid interface, when molecules diffuse by an intermittent hopping mechanism.

Hopping molecules translate across the surface by desorbing, diffusing through the bulk solution, and readsorbing.[72-76] Isolated molecules on a hydrophobic surface desorb very frequently on the timescale of single-molecule imaging,[75] and for a desorbed molecule in the near vicinity of a surface, the probability of readsorbing and executing a "hop" is actually quite high. In a previous study in our group, experimental data for small molecules (BODIPY and Atto6G) and macromolecules (bovine serum albumin (BSA) and 40 kDa polyethylene glycol (PEG)) adsorbed to hydrophobic TMS surfaces was described by a continuous time random walk (CTRW) model, where adsorbed molecules remained immobile for a random waiting time prior to desorbing into bulk solution and readsorbing to execute steps across the surface (Figure 1.7). At short lag times, most of the step size distributions had pronounced power law tails, but at longer lag times, the central limit theorem applied and the distributions became Gaussian. Broad step-size distributions (approximately power-law) had been theoretically predicted for hopping through bulk solution and were used in the simulations.[66] The effect of the hopping was that an adsorbed molecule made large displacements across the surface much more often than would have been expected for a molecule undergoing 2D diffusion with Gaussian-distributed step sizes.

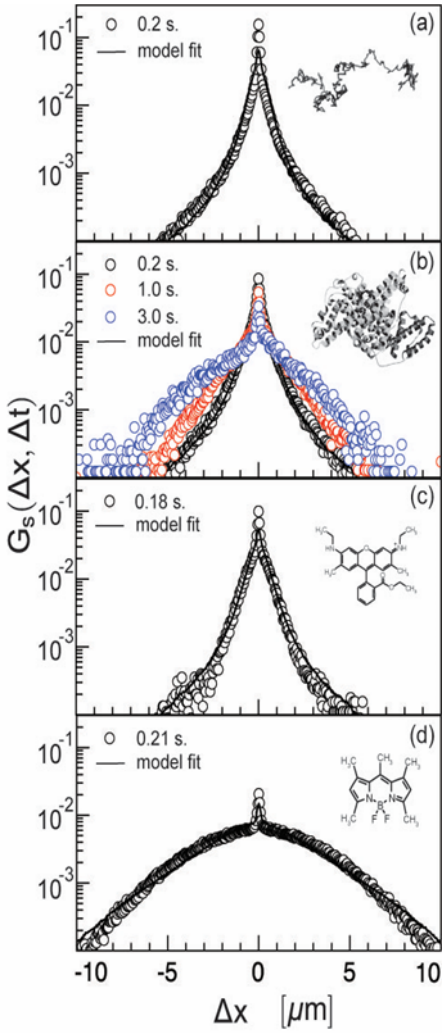

Figure 1.7: Displacement distributions at the annotated Δt for (a) PEG, (b) BSA, (c) Atto6G, and (d) BODIPY. Symbols are experimental data measured using single-molecule tracking and the solid lines are simulated data using the model described in the text. Adapted from Skaug, Mabry, and Schwartz.[74] Reprinted with permission from American Physical Society: *Phys. Rev. Lett.* Copyright 2013.

As shown in Figure 1.7, PEG diffused at the surface by a hopping mechanism, and so we applied the same analytical approach to look at the molecular weight dependence of PEG surface diffusion. Since diffusion through the bulk water was fast compared to the timescale of imaging, the primary contribution to the scaling of the diffusion coefficient, was the desorption rate. Consequently, the diffusion coefficient scaled in proportion to the desorption rate constant (Figure 1.8).[74-75]

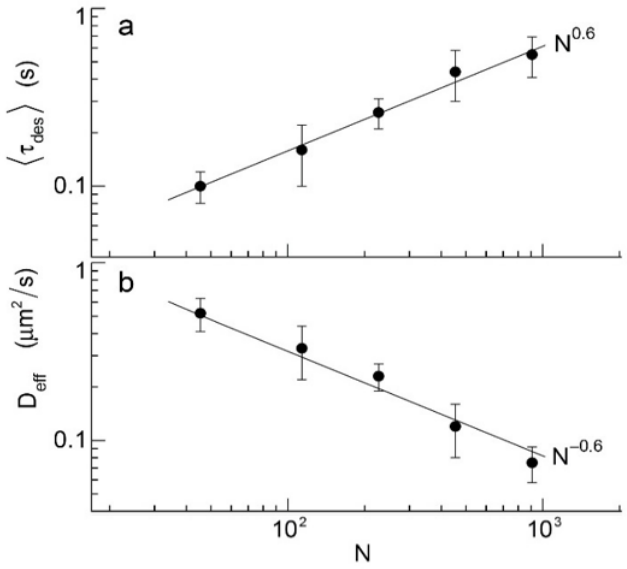

Figure 1.8: Chain length scaling of polymer surface dynamics and kinetics. (a) The mean waiting time $\langle \tau_{des} \rangle$ and (b) the effective surface diffusion coefficient D_{eff} versus the chain length N. Symbols are experimental data and the solid lines depict the power-law scaling with best-fit exponents of 0.6 ± 0.1 and -0.6 ± 0.2 for data in (a) and (b) respectively. Adapted from Skaug, Mabry, and Schwartz.[75] Reprinted with permission from American Chemical Society: *JACS*. Copyright 2014.

Importantly, the desorption of the entire polymer (with chain length N) from the surface could be thought of as a series of independent desorption events (the desorption of each train). In this scenario, the characteristic desorption time was proportional to the fraction of adsorbed monomers.[77] We found the characteristic desorption time scaled roughly as $N^{0.6}$ for PEG desorbing from a solid hydrophobic surface.[75] This suggested that $N^{0.6}$ PEG monomers attached to the hydrophobic surface with the polymer adsorbed in a three-dimensional loop-train-tail conformation, in direct contrast to the two-dimensional

"pancake" conformation inferred from previous measurements of surface diffusion using a model-dependent analysis of fluorescence correlation spectroscopy data.[78] If the adsorbed chains had adopted strictly 2-dimensional pancake conformations, the number of adsorbed monomers would have increased in proportion to *N* and the waiting times would have fallen off exponentially with chain length rather than as a power-law as we observed. These detailed results on the conformation of an adsorbed polymer highlight the types of theoretical insights that can be gained from single-molecule observations, and we have attempted to build on this statistically rigorous approach in the work presented in this thesis.

1.2.3 Conformational Change

When a macromolecule, such as a peptide, protein, or DNA, adsorbs to a surface, it may retain its solution conformation after adsorption (i.e. become pinned to the surface) or it may be induced to (un)fold into a different conformation. Irreversible binding of proteins to surface is observed macroscopically and believed to result from surface-induced unfolding (i.e. the loss of secondary structure).[64-65] In spectroscopic studies, utilizing circular dichroism and fluorescence and other techniques, the average structure of an adsorbed protein population has appeared to become more disordered over time.[79-81] The mechanistic details of this process are subject to speculation but have not been extensively characterized. One recent study in our group demonstrated, that while unfolded proteins remain on the surface longer, they are not necessarily irreversibly

adsorbed (Figure 1.9).[82] This implies that the surface could also affect the balance of the populations of folded and unfolded proteins in solution.

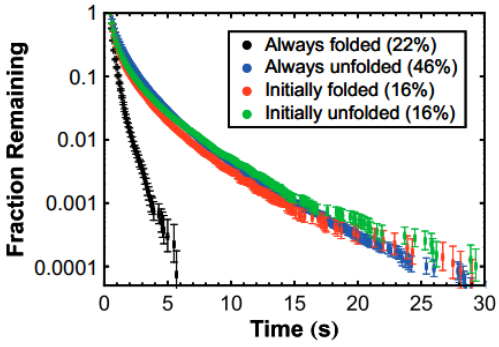

Figure 1.9: Surface residence time distributions for different organophosphorus hydrolase protein conformations. Adapted from McLoughlin, *et. al.*[82] Reprinted with permission from National Academy of Sciences USA: *PNAS.* Copyright 2013.

For many applications, such as the separation of proteins by chromatography or the immobilization of enzymes to impart reusability, surface-induced denaturation is highly undesirable. Since protein folding is largely driven by hydrophobic interactions, unsurprisingly, surface hydrophobicity has been correlated with the loss of structure of adsorbed proteins and peptides.[83-84] The variety of protein immobilization methods is incredibly large, with non-covalent adsorption, physical entrapment, covalent linkage, and affinity immobilization methods and many derivatives all in use.[85] The rational design of support materials is severely limited, however, by the lack of techniques to study the full ensemble of adsorbed proteins and the heterogeneity of the surface.

1.3 Fluorescence Phenomena and Measurement Techniques

Fluorescence spectroscopy and microscopy are primary research tools in the biological sciences because fluorescence can be detected from low concentrations of probe molecules and localized with high spatial precision without disrupting the function of cells.[86] With biological applications driving their intensive development, fluorescence techniques have become well-suited for the study of macromolecules in aqueous systems at moderate temperatures, which contrasts with other highly sensitive materials-characterization techniques requiring cryogenic temperatures and ultra-high vacuum conditions.[87] Practically, to detect fluorescence above background photon emission, the fluorescent molecules must be bright, with high absorbance and quantum yield, and the Stokes shift must be large (> 20 nm). Easily detectable fluorophores are almost always highly conjugated, aromatic molecules, and common examples are given in Figure 1.10. The inset of Figure 1.10 shows the prototypical excitation and emission spectra for fluorophores. Molecules such as fluorescein and Cy5 shown in the top two rows of Figure 1.10 have been used successfully in our laboratory for single-molecule imaging at the solid-liquid interface and previously with less sophisticated techniques. In the past two decades, many different fluorescence spectroscopy and microscopy techniques have been applied to studying interfacial processes, and we describe several of the most important techniques in the following sections.

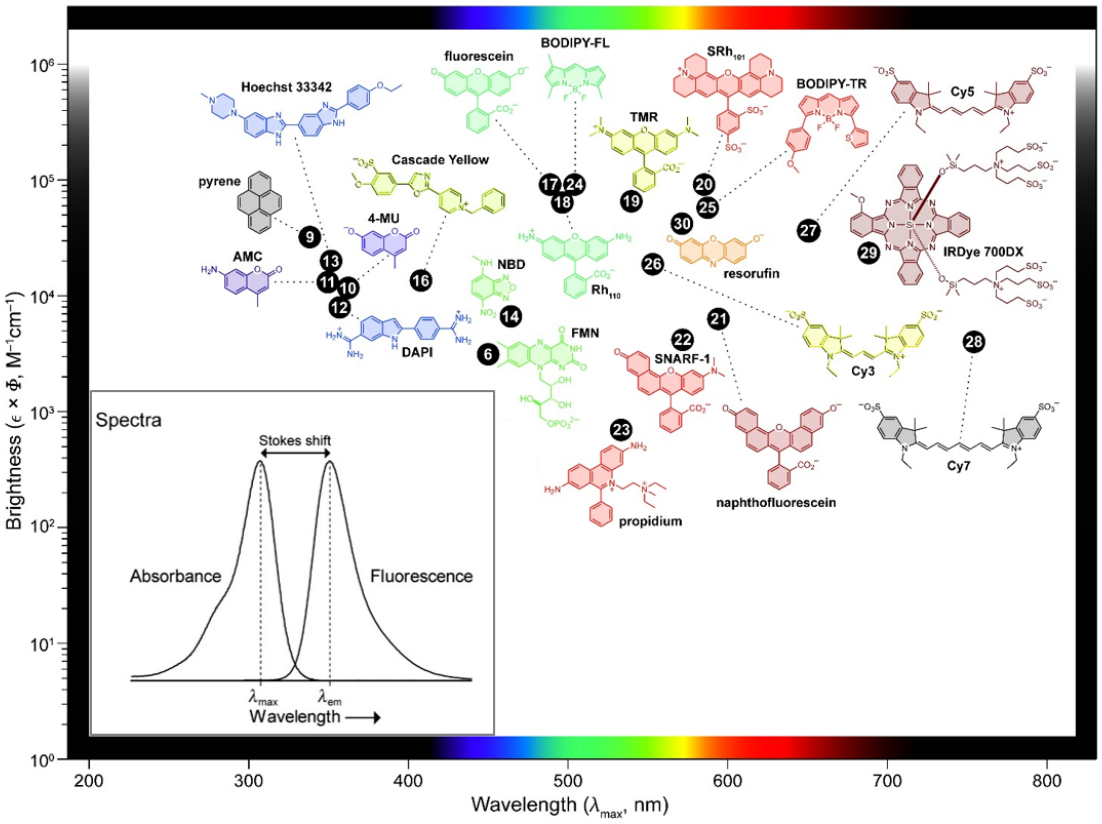

Figure 1.10: Typical fluorescent dyes: brightness vs. wavelength of maximum absorption. Inset: Typical absorbance and fluorescence emission spectra. Adapted from Lavis, *et. al.*[88] Reprinted with permission from American Chemical Society: *ACS Chem. Biol.* Copyright 2008.

1.3.1 Fluorescence Recovery after Photobleaching

One of the oldest and most powerful methods for studying interfacial diffusion is fluorescence recovery after photobleaching (FRAP).[89] Basically, after bleaching a finite region of a fluorescently labeled interface, the recovery of fluorescence in that area due to the diffusive flux of fluorescent molecules from the surrounding unbleached areas can be monitored by microscopy. The apparent diffusion coefficient is proportional to the square of the radius of the bleached area divided by the time constant for the recovery process.[90] As shown in the example of Figure 1.11, FRAP has been used to characterize the fluidity of liquid interfaces, such as lipid bilayers. Indeed, the extensive knowledge of interfacial diffusion derived from study of liquid-liquid interfaces guided the development of methods to characterize the solid-liquid interface. Since FRAP measures diffusion over long timescales (seconds to minutes), the assumption of a single characteristic diffusion coefficient seems reasonable. The other typical variable measured is a "mobile fraction", reflecting the fact that the fluorescence often does not fully recover. This latter observations reflects that the interface is often more heterogeneous than implied by the assumption of a single characteristic diffusion coefficient.[91]

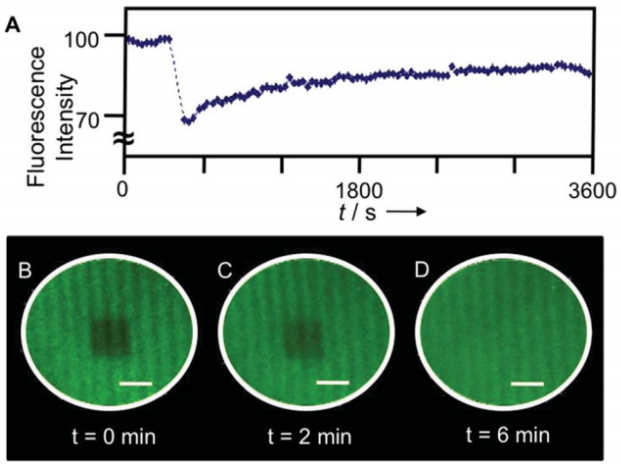

Figure 1.11: FRAP of lipid bilayer. Scale bar 500 µm. Adapted from Dutta, *et. al.*[88] Reprinted with permission from Royal Society of Chemistry: *Analyst.* Copyright 2014.

1.3.2 Fluorescence Correlation Spectroscopy

Early "single-molecule" studies of adsorbate dynamics at interfaces relied on fluorescence correlation spectroscopy (FCS).[92-94] FCS is based on measuring the temporal autocorrelation of fluorescence intensity arising from fluorescent molecules passing through a diffraction-limited volume, which can be centered at an interface.[95] A significant drawback of FCS measurement of molecular dynamics is that it requires the assumption of a model to extract kinetic parameters from the autocorrelation data. In practice, only one dynamic phenomena, such as surface diffusion, is usually included in the model to avoid overwhelming complexity. For example, by neglecting adsorption/desorption dynamics, surface diffusion can be characterized.[56,96] These types of limiting assumptions are valid under certain conditions (e.g. if all the molecules are strongly adsorbed to a fluid layer), but it is not generally clear which conditions apply, especially at the highly heterogeneous solid-liquid interfaces. As shown in Figure 1.12,

heterogeneity can be accounted for to an extent, by adjusting the size or position of the fluorescence detection volume. Indeed, Wirth and co-workers[56,93,96-98] recognized the heterogeneity of the silica-water interface and characterized it semi-quantitatively using FCS and low-resolution imaging methods. We have built off of much of their early work and the work of others[78,92,99-107] and bypassed the limitations of FCS by adopting a single-molecule imaging approach.

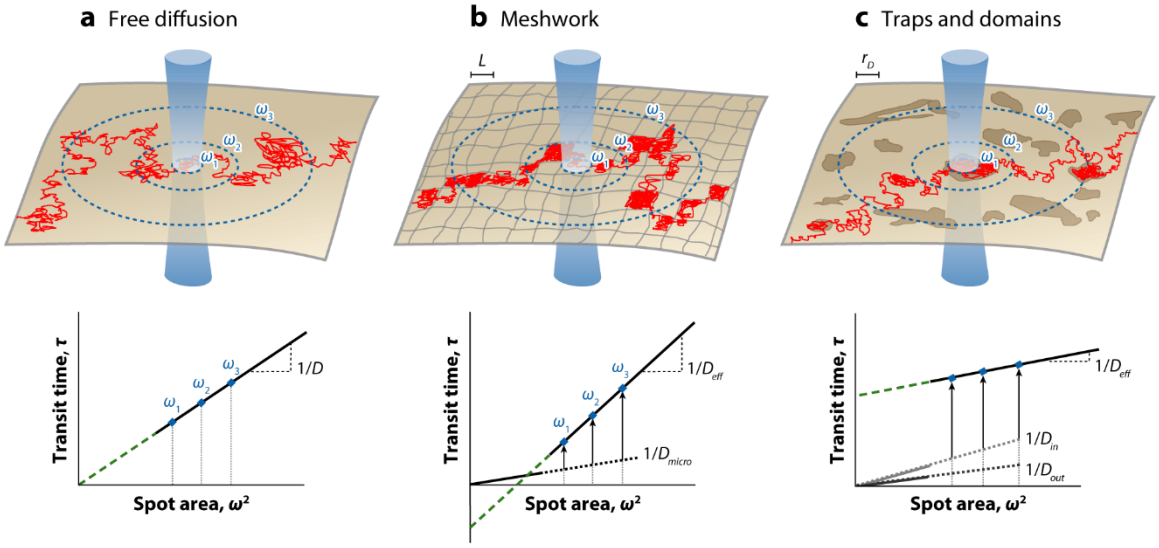

Figure 1.12: Detecting nanodomains in membranes using FCS. Adapted from He, *et. al.*[108] Reprinted with permission from Annual Reviews: *Annu. Rev. Phys. Chem.* Copyright 2011.

1.3.3 Total Internal Reflection Fluorescence Microscopy

Total internal reflection fluorescence microscopy (TIRFM) achieves single-molecule sensitivity by limiting excitation of fluorophores in solution to within about 100 nm of the solid surface.[109] The thin "evanescent field" is produced by an excitation light beam

encountering the solid-liquid interface at a high angle of incidence, greater than the "critical angle" derived from Snell's law.

$$\theta_c = sin^{-1}\left({}^{n_{liq}}/_{n_{sol}}\right) \quad (1.2)$$

where n_{liq} and n_{sol} are the refractive indices of the liquid and solid interfaces respectively. The evanescent wave decays exponentially with distance perpendicular to the interface. While there are several possible illumination geometries for TIRFM, the work reported here used a prism-based geometry as indicated in Figure 1.13.

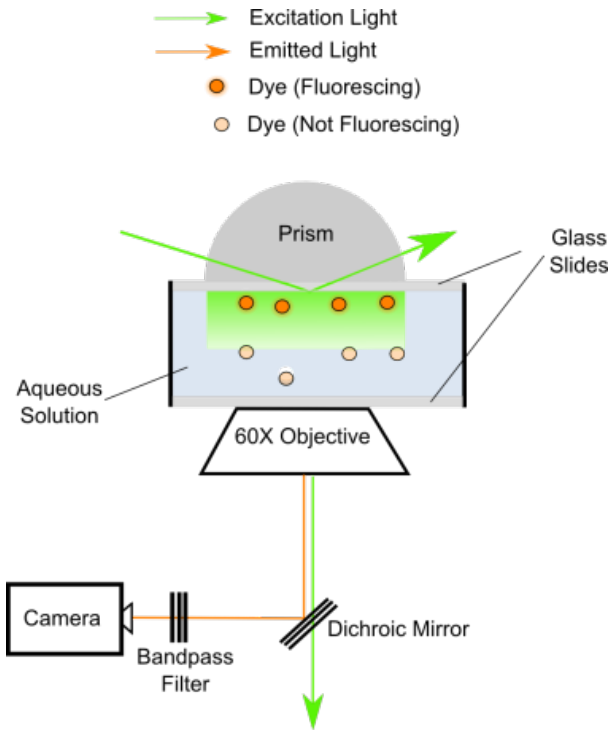

Figure 1.13: Prism-based TIRFM.

The surface sensitivity of the measurements arose because of the difference in diffusion coefficients for molecules in solution (~10^2 μm^2 s^{-1})[110] versus on the surface (< 1 μm^2 s^{-1}

).[111] To accumulate sufficient photons from adsorbed molecules to distinguish them from background fluorescence, acquisition times greater than ~10 ms were required. A field of view of ~20 microns in size was typically recorded, with up to about 10^2 molecules present. To capture spectroscopic phenomena such as energy transfer, the image could be split into two channels with separate filters and projected onto distinct regions of the CCD sensor. Adsorbed molecules were identified and tracked using computational image processing as described in the experimental methods for each subsequent chapter.

1.3.4 Förster Resonance Energy Transfer

Förster resonance energy transfer (FRET) has been termed a "spectroscopic ruler"[112] because it redirects energy absorbed by a low-wavelength "donor" fluorophore to a long-wavelength "acceptor" fluorophore over distances about 1–10 nm, the size range of many biomolecules. The efficiency of FRET, E_{FRET}, is readily predictable from the spectral properties of the fluorophores and obeys the following relation [113]

$$E_{FRET} = \left(1 + {}^{r}/_{R_0}\right)^{-1} \quad (1.3)$$

where r is the distance between donor and acceptor and R_0 is the Förster radius that depends on the donor/acceptor pair, orientation of fluorophores, and the solvent environment with typical values of ~5 nm.[113] FRET has been used previously in our group to monitor the conformation and aggregation of adsorbed biomolecules.[82,114-115]

Figure 1.14 shows an example of using FRET to monitor the conformational state of a DNA hairpin.

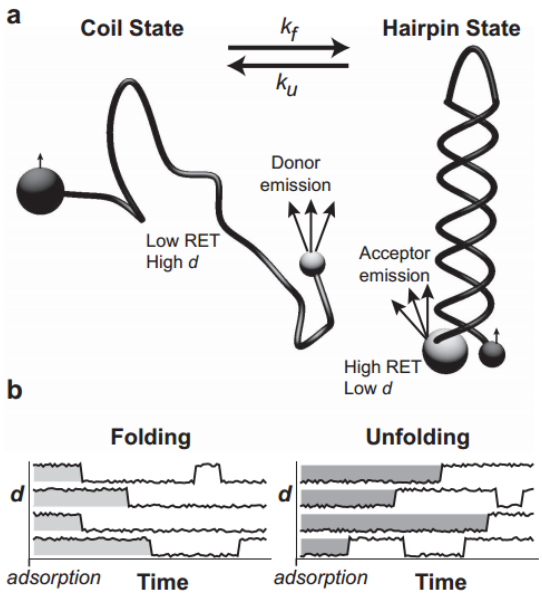

Figure 1.14: DNA hairpin conformation by FRET measurements. Small spheres represent donor florophores while acceptors are shown as large spheres. Light grey indicates strong fluorophore emission while dark grey indicates weak emission. The relative donor/acceptor distance is given by *d*. Adapted from Kastantin, *et. al.*[116] Reprinted with permission from John Wiley and Sons: *Small.* Copyright 2012.

1.4 OBJECTIVES

Our group has developed high-throughput single molecule imaging methods based on TIRFM that allow unambiguous characterization of interfacial dynamics[117] of fundamental importance to self-assembly, as well as separations, sensing, and catalysis. In this work, we studied adsorption, diffusion, and conformational changes of biomolecules on functionalized silica surfaces of significant technological interest. Our overall strategy was to use single-molecule tracking understand the behavior of adsorbed molecules, and we leveraged computational tools to create massive datasets capturing broad distributions of molecular kinetics and detailed information on surface lateral heterogeneity. We developed novel statistical approaches to learn about the molecular-level physical processes in unprecedented detail. The following three specific objective were pursued in this work.

1. Characterize *adsorption* on model reversed phase chromatography media and relate it to the macroscopic system performance.
2. Construct a new framework for understanding *surface diffusion* of molecules on hydrophobic surfaces and demonstrate the ability to tune interfacial transport.
3. Develop a mapping method to correlate peptide *conformation* and surface chemistry.

1.5 REFERENCES

1. Schwartz, D. K., Mechanisms and kinetics of self-assembled monolayer formation. *Annu. Rev. Phys. Chem.* **2001,** *52*, 107-137.
2. McCloskey, M. A.; Poo, M. M., Rates of membrane-associated reactions: reduction of dimensionality revisited. *The Journal of Cell Biology* **1986,** *102* (1), 88-96.
3. Nygren, P.; Lundqvist, M.; Broo, K.; Jonsson, B. H., Fundamental design principles that guide induction of helix upon formation of stable peptide-nanoparticle complexes. *Nano Lett.* **2008,** *8* (7), 1844-1852.
4. Thiruvengadathan, R.; Korampally, V.; Ghosh, A.; Chanda, N.; Gangopadhyay, K.; Gangopadhyay, S., Nanomaterial processing using self-assembly-bottom-up chemical and biological approaches. *Rep. Prog. Phys.* **2013,** *76* (6).
5. Whitesides, G. M.; Grzybowski, B., Self-Assembly at All Scales. *Science* **2002,** *295* (5564), 2418-2421.
6. Raghavachari, K.; Saha, A., Accurate Composite and Fragment-Based Quantum Chemical Models for Large Molecules. *Chem. Rev.* **2015**.
7. Han, D.; Pal, S.; Nangreave, J.; Deng, Z.; Liu, Y.; Yan, H., DNA Origami with Complex Curvatures in Three-Dimensional Space. *Science* **2011,** *332* (6027), 342-346.
8. Martins, S. A.; Sousa, S. F.; Ramos, M. J.; Fernandes, P. A., Prediction of Solvation Free Energies with Thermodynamic Integration Using the General Amber Force Field. *J. Chem. Theory Comput.* **2014,** *10* (8), 3570-3577.
9. Hansson, T.; Oostenbrink, C.; van Gunsteren, W., Molecular dynamics simulations. *Curr. Opin. Struct. Biol.* **2002,** *12* (2), 190-196.
10. Pierce, L. C. T.; Salomon-Ferrer, R.; Augusto F. de Oliveira, C.; McCammon, J. A.; Walker, R. C., Routine Access to Millisecond Time Scale Events with Accelerated Molecular Dynamics. *J. Chem. Theory Comput.* **2012,** *8* (9), 2997-3002.
11. Lindsey, R. K.; Rafferty, J. L.; Eggimann, B. L.; Siepmann, J. I.; Schure, M. R., Molecular simulation studies of reversed-phase liquid chromatography. *J. Chromatogr. A* **2013,** *1287*, 60-82.
12. Rimola, A.; Costa, D.; Sodupe, M.; Lambert, J.-F.; Ugliengo, P., Silica Surface Features and Their Role in the Adsorption of Biomolecules: Computational Modeling and Experiments. *Chem. Rev.* **2013,** *113* (6), 4216-4313.
13. Weisz, P. B.; Swegler, E. W., Catalytic Activity Induced by Neutron Irradiation of Inert Silica. *The Journal of Chemical Physics* **1955,** *23* (9), 1567-1568.
14. Peri, J. B.; Hensley, A. L., The surface structure of silica gel. *The Journal of Physical Chemistry* **1968,** *72* (8), 2926-2933.
15. Maschmeyer, T.; Rey, F.; Sankar, G.; Thomas, J. M., Heterogeneous catalysts obtained by grafting metallocene complexes onto mesoporous silica. *Nature* **1995,** *378* (6553), 159-162.
16. Gill, R. S.; Singh, S.; Singh, P. P., Design and development of desiccant seed dryer with airflow inversion and recirculation. *J. Food Sci. Technol.-Mysore* **2014,** *51* (11), 3418-3424.

17. Handbook of HPLC. In *Chromatogr. Sci. Ser.*, 2nd ed.; Taylor & Francis: Boca Raton, 2010.
18. Tong, H. M., MICROELECTRONICS PACKAGING - PRESENT AND FUTURE. *Mater. Chem. Phys.* **1995,** *40* (3), 147-161.
19. Kingon, A. I.; Maria, J.-P.; Streiffer, S. K., Alternative dielectrics to silicon dioxide for memory and logic devices. *Nature* **2000,** *406* (6799), 1032-1038.
20. Zhao, B.; Haasch, R. T.; MacLaren, S., Solvent-Induced Self-Assembly of Mixed Poly(methyl methacrylate)/Polystyrene Brushes on Planar Silica Substrates: Molecular Weight Effect. *J. Am. Chem. Soc.* **2004,** *126* (19), 6124-6134.
21. Cheng, J. Y.; Ross, C. A.; Smith, H. I.; Thomas, E. L., Templated Self-Assembly of Block Copolymers: Top-Down Helps Bottom-Up. *Adv. Mater.* **2006,** *18* (19), 2505-2521.
22. Bij, K. E.; Horvath, C.; Melander, W. R.; Nahum, A., Surface Silanols in Silica-Bonded Hydrocarbonaceous Stationary Phases .2. Irregular Retention Behavior and Effect of Silanol Masking. *J. Chromatogr.* **1981,** *203* (Jan), 65-84.
23. Spialter, L.; Pazdernik, L.; Bernstein, S.; Swansiger, W. A.; Buell, G. R.; Freeburger, M. E., Mechanism of the reaction of ozone with the silicon-hydrogen bond. *J. Am. Chem. Soc.* **1971,** *93* (22), 5682-5686.
24. Zhuravlev, N. D.; Siepmann, J. I.; Schure, M. R., Surface Coverages of Bonded-Phase Ligands on Silica: A Computational Study. *Anal. Chem.* **2001,** *73* (16), 4006-4011.
25. Rafferty, J. L.; Zhang, L.; Siepmann, J. I.; Schure, M. R., Retention mechanism in reversed-phase liquid chromatography: A molecular perspective. *Anal. Chem.* **2007,** *79* (17), 6551-6558.
26. Walba, D. M.; Liberko, C. A.; Korblova, E.; Farrow, M.; Furtak, T. E.; Chow, B. C.; Schwartz, D. K.; Freeman, A. S.; Douglas, K.; Williams, S. D.; Klittnick, A. F.; Clark, N. A., Self-assembled monolayers for liquid crystal alignment: simple preparation on glass using alkyltrialkoxysilanes. *Liq. Cryst.* **2004,** *31* (4), 481-489.
27. Zhuravlev, L. T., The surface chemistry of amorphous silica. Zhuravlev model. *Colloids Surf. Physicochem. Eng. Aspects* **2000,** *173* (1–3), 1-38.
28. Rafferty, J. L.; Siepmann, J. I.; Schure, M. R., Influence of bonded-phase coverage in reversed-phase liquid chromatography via molecular simulation: I. Effects on chain conformation and interfacial properties. *J. Chromatogr. A* **2008,** *1204* (1), 11-19.
29. Sandoval, J. E.; Pesek, J. J., Hydrolytically stable bonded chromatographic phases prepared through hydrosilylation of olefins on a hydride-modified silica intermediate. *Anal. Chem.* **1991,** *63* (22), 2634-2641.
30. Gritti, F.; Guiochon, G., Heterogeneity of the adsorption mechanism of low molecular weight compounds in reversed-phase liquid chromatography. *Anal. Chem.* **2006,** *78* (16), 5823-5834.
31. Felinger, A., Molecular dynamic theories in chromatography. *J. Chromatogr. A* **2008,** *1184* (1-2), 20-41.
32. Giddings, J. C., Kinetic Origin of Tailing in Chromatography. *Anal. Chem.* **1963,** *35* (13), 1999-&.

33. Giddings, J. C.; Eyring, H., A Molecular Dynamic Theory of Chromatography. *J. Phys. Chem.* **1955,** *59* (5), 416-421.
34. Rafferty, J. L.; Siepmann, J. I.; Schure, M. R., Influence of bonded-phase coverage in reversed-phase liquid chromatography via molecular simulation. II. Effects on solute retention. *J. Chromatogr. A* **2008,** *1204* (1), 20-27.
35. Woo, S.; Rothemund, P. W. K., Self-assembly of two-dimensional DNA origami lattices using cation-controlled surface diffusion. *Nat Commun* **2014,** *5*.
36. Rafferty, J. L.; Siepmann, J. I.; Schure, M. R., Molecular Simulations of Retention in Chromatographic Systems: Use of Biased Monte Carlo Techniques to Access Multiple Time and Length Scales. *Multiscale Molecular Methods in Applied Chemistry* **2012,** *307*, 181-200.
37. Denis, F. A.; Hanarp, P.; Sutherland, D. S.; Gold, J.; Mustin, C.; Rouxhet, P. G.; Dufrene, Y. F., Protein adsorption on model surfaces with controlled nanotopography and chemistry. *Langmuir* **2002,** *18* (3), 819-828.
38. Domke, K. F.; Pettinger, B., Studying Surface Chemistry beyond the Diffraction Limit: 10 Years of TERS. *Chemphyschem* **2010,** *11* (7), 1365-1373.
39. Muller, D. J.; Dufrene, Y. F., Atomic force microscopy as a multifunctional molecular toolbox in nanobiotechnology. *Nat Nano* **2008,** *3* (5), 261-269.
40. Dufrene, Y. F.; Martinez-Martin, D.; Medalsy, I.; Alsteens, D.; Muller, D. J., Multiparametric imaging of biological systems by force-distance curve-based AFM. *Nat Meth* **2013,** *10* (9), 847-854.
41. Tranchida, D.; Piccarolo, S.; Deblieck, R. A. C., Some experimental issues of AFM tip blind estimation: the effect of noise and resolution. *Meas. Sci. Technol.* **2006,** *17* (10), 2630-2636.
42. Huang, P.; Andersson, S. B., Fast scanning in AFM using non-raster sampling and time-optimal trajectories. *Ieee Decis Contr P* **2012**, 5073-5078.
43. Giessibl, F. J., Atomic Resolution of the Silicon (111)-(7x7) Surface by Atomic Force Microscopy. *Science* **1995,** *267* (5194), 68-71.
44. Atkin, J. M.; Berweger, S.; Jones, A. C.; Raschke, M. B., Nano-optical imaging and spectroscopy of order, phases, and domains in complex solids. *Adv. Phys.* **2012,** *61* (6), 745-842.
45. Soriaga, M. P., Ultra-high vacuum techniques in the study of single-crystal electrode surfaces. *Prog. Surf. Sci.* **1992,** *39* (4), 325-443.
46. Castner, D. G.; Ratner, B. D., Biomedical surface science: Foundations to frontiers. *Surf. Sci.* **2002,** *500* (1–3), 28-60.
47. Ferrin, P.; Kandoi, S.; Nilekar, A. U.; Mavrikakis, M., Hydrogen adsorption, absorption and diffusion on and in transition metal surfaces: A DFT study. *Surf. Sci.* **2012,** *606* (7–8), 679-689.
48. Williams, C. T.; Beattie, D. A., Probing buried interfaces with non-linear optical spectroscopy. *Surf. Sci.* **2002,** *500* (1–3), 545-576.
49. Bain, C. D., Sum-frequency vibrational spectroscopy of the solid/liquid interface. *J. Chem. Soc., Faraday Trans.* **1995,** *91* (9), 1281-1296.
50. Rafferty, J. L.; Siepmann, J. I.; Schure, M. R., Mobile phase effects in reversed-phase liquid chromatography: A comparison of acetonitrile/water and methanol/water

solvents as studied by molecular simulation. *J. Chromatogr. A* **2011,** *1218* (16), 2203-2213.
51. Kisley, L.; Chen, J.; Mansur, A. P.; Dominguez-Medina, S.; Kulla, E.; Kang, M. K.; Shuang, B.; Kourentzi, K.; Poongavanam, M. V.; Dhamane, S.; Willson, R. C.; Landes, C. F., High ionic strength narrows the population of sites participating in protein ion-exchange adsorption: a single-molecule study. *J. Chromatogr. A* **2014,** *1343*, 135-42.
52. Tswett, M., Physikalish-Chemische Studien ueber das Chlorophyll. Die Adsorption. *Berichte der Deutschen botanischen Gesellschaft* **1906,** *24*, 316-326.
53. Keil, F. J., Complexities in modeling of heterogeneous catalytic reactions. *Computers & Mathematics with Applications* **2013,** *65* (10), 1674-1697.
54. Satterfield, C. N.; Sherwood, T. K., *The role of diffusion in catalysis*. Addison-Wesley Pub. Co.: Reading, Mass.,, 1963; p vii, 118 p.
55. Miyabe, K.; Guiochon, G., Surface diffusion in reversed-phase liquid chromatography. *J. Chromatogr. A* **2010,** *1217* (11), 1713-1734.
56. Wirth, M. J.; Swinton, D. J.; Ludes, M. D., Adsorption and diffusion of single molecules at chromatographic interfaces. *J. Phys. Chem. B* **2003,** *107* (26), 6258-6268.
57. Chan, V.; Graves, D. J.; McKenzie, S. E., The biophysics of DNA hybridization with immobilized oligonucleotide probes. *Biophys. J.* **1995,** *69* (6), 2243-2255.
58. Squires, T. M.; Messinger, R. J.; Manalis, S. R., Making it stick: convection, reaction and diffusion in surface-based biosensors. *Nat. Biotechnol.* **2008,** *26* (4), 417-426.
59. Ulman, A., Formation and Structure of Self-Assembled Monolayers. *Chem. Rev.* **1996,** *96* (4), 1533-1554.
60. Doudevski, I.; Schwartz, D. K., Concentration dependence of self-assembled monolayer island nucleation and growth. *J. Am. Chem. Soc.* **2001,** *123* (28), 6867-6872.
61. Zhang, R.; Somasundaran, P., Advances in adsorption of surfactants and their mixtures at solid/solution interfaces. *Adv. Colloid Interface Sci.* **2006,** *123*, 213-229.
62. Honciuc, A.; Baptiste, D. J.; Campbell, I. P.; Schwartz, D. K., Solvent Dependence of the Activation Energy of Attachment Determined by Single Molecule Observations of Surfactant Adsorption. *Langmuir* **2009,** *25* (13), 7389-7392.
63. Mrksich, M.; Sigal, G. B.; Whitesides, G. M., Surface Plasmon Resonance Permits in Situ Measurement of Protein Adsorption on Self-Assembled Monolayers of Alkanethiolates on Gold. *Langmuir* **1995,** *11* (11), 4383-4385.
64. Silin, V.; Weetall, H.; Vanderah, D. J., SPR studies of the nonspecific adsorption kinetics of human IgG and BSA on gold surfaces modified by self-assembled monolayers (SAMs). *J. Colloid Interface Sci.* **1997,** *185* (1), 94-103.
65. Kastantin, M.; Langdon, B. B.; Schwartz, D. K., A bottom-up approach to understanding protein layer formation at solid–liquid interfaces. *Adv. Colloid Interface Sci.* **2014,** *207* (0).
66. Bychuk, O. V.; Oshaughnessy, B., Anomalous Surface-Diffusion - a Numerical Study. *J. Chem. Phys.* **1994,** *101* (1), 772-780.
67. Hlushkou, D.; Gritti, F.; Daneyko, A.; Guiochon, G.; Tallarek, U., How Microscopic Characteristics of the Adsorption Kinetics Impact Macroscale Transport in Chromatographic Beds. *J Phys Chem C* **2013,** *117* (44), 22974-22985.

68. Honciuc, A.; Howard, A. L.; Schwartz, D. K., Single Molecule Observations of Fatty Acid Adsorption at the Silica/Water Interface: Activation Energy of Attachment. *J Phys Chem C* **2009,** *113* (6), 2078-2081.
69. Ge, G.; Brus, L. E., Fast Surface Diffusion of Large Disk-Shaped Nanocrystal Aggregates. *Nano Lett.* **2001,** *1* (4), 219-222.
70. Benichou, O.; Loverdo, C.; Moreau, M.; Voituriez, R., Optimizing intermittent reaction paths. *PCCP* **2008,** *10* (47), 7059-7072.
71. Bénichou, O.; Loverdo, C.; Moreau, M.; Voituriez, R., Intermittent search strategies. *Rev. Mod. Phys.* **2011,** *83* (1), 81--129.
72. Bouchaud, J. P.; Georges, A., Anomalous diffusion in disordered media: Statistical mechanisms, models and physical applications. *Phys. Rep.* **1990,** *195* (4-5), 127-293.
73. Bychuk, O. V.; O'Shaughnessy, B., Anomalous diffusion at liquid surfaces. *Phys. Rev. Lett.* **1995,** *74* (10), 1795--1798.
74. Skaug, M. J.; Mabry, J.; Schwartz, D. K., Intermittent Molecular Hopping at the Solid-Liquid Interface. *Phys. Rev. Lett.* **2013,** *110* (25).
75. Skaug, M. J.; Mabry, J. N.; Schwartz, D. K., Single-Molecule Tracking of Polymer Surface Diffusion. *J. Am. Chem. Soc.* **2014,** *136* (4), 1327-1332.
76. Yu, C.; Guan, J.; Chen, K.; Bae, S. C.; Granick, S., Single-Molecule Observation of Long Jumps in Polymer Adsorption. *ACS Nano* **2013,** *7* (11), 9735-9742.
77. Wang, Y.; Rajagopalan, R.; Mattice, W., Kinetics of Detachment of Homopolymers from a Solid Surface. *Phys. Rev. Lett.* **1995,** *74* (13), 2503-2506.
78. Sukhishvili, S. A.; Chen, Y.; Muller, J. D.; Gratton, E.; Schweizer, K. S.; Granick, S., Materials science - Diffusion of a polymer 'pancake'. *Nature* **2000,** *406* (6792), 146-146.
79. Baugh, L.; Vogel, V., Structural changes of fibronectin adsorbed to model surfaces probed by fluorescence resonance energy transfer. *Journal of Biomedical Materials Research Part A* **2004,** *69A* (3), 525-534.
80. Maste, M. C. L.; Norde, W.; Visser, A. J. W. G., Adsorption-Induced Conformational Changes in the Serine Proteinase Savinase: A Tryptophan Fluorescence and Circular Dichroism Study. *J. Colloid Interface Sci.* **1997,** *196* (2), 224-230.
81. Kong, J.; Yu, S., Fourier Transform Infrared Spectroscopic Analysis of Protein Secondary Structures. *Acta Biochimica et Biophysica Sinica* **2007,** *39* (8), 549-559.
82. McLoughlin, S. Y.; Kastantin, M.; Schwartz, D. K.; Kaar, J. L., Single-molecule resolution of protein structure and interfacial dynamics on biomaterial surfaces. *Proc. Natl. Acad. Sci. U. S. A.* **2013,** *110* (48), 19396-19401.
83. Roach, P.; Farrar, D.; Perry, C. C., Interpretation of protein adsorption: Surface-induced conformational changes. *J. Am. Chem. Soc.* **2005,** *127* (22), 8168-8173.
84. Mermut, O.; Phillips, D. C.; York, R. L.; McCrea, K. R.; Ward, R. S.; Somorjai, G. A., In situ adsorption studies of a 14-amino acid leucine-lysine peptide onto hydrophobic polystyrene and hydrophilic silica surfaces using quartz crystal microbalance, atomic force microscopy, and sum frequency generation vibrational spectroscopy. *J. Am. Chem. Soc.* **2006,** *128* (11), 3598-3607.

85. Datta, S.; Christena, L. R.; Rajaram, Y. R. S., Enzyme immobilization: an overview on techniques and support materials. *3 Biotech* **2013,** *3* (1), 1-9.
86. Introduction to Fluorescence. In *Principles of Fluorescence Spectroscopy*, Lakowicz, J., Ed. Springer US: 2006; pp 1-26.
87. Weiss, S., Fluorescence Spectroscopy of Single Biomolecules. *Science* **1999,** *283* (5408), 1676-1683.
88. Lavis, L. D.; Raines, R. T., Bright Ideas for Chemical Biology. *ACS Chem. Biol.* **2008,** *3* (3), 142-155.
89. Meyvis, T. L.; De Smedt, S.; Van Oostveldt, P.; Demeester, J., Fluorescence Recovery After Photobleaching: A Versatile Tool for Mobility and Interaction Measurements in Pharmaceutical Research. *Pharm. Res.* **1999,** *16* (8), 1153-1162.
90. Walder, R. B.; Honciuc, A.; Schwartz, D. K., Phospholipid Diffusion at the Oil−Water Interface. *The Journal of Physical Chemistry B* **2010,** *114* (35), 11484-11488.
91. Malmsten, M., *Biopolymers at Interfaces* 2nd ed.; Marcel Dekker: New York, 2003; p xii, 908 p.
92. Hansen, R. L.; Harris, J. M., Measuring reversible adsorption kinetics of small molecules at solid/liquid interfaces by total internal reflection fluorescence correlation spectroscopy. *Anal. Chem.* **1998,** *70* (20), 4247-4256.
93. Wirth, M. J.; Swinton, D. J., Single-molecule probing of mixed-mode adsorption at a chromatographic interface. *Anal. Chem.* **1998,** *70* (24), 5264-5271.
94. Thompson, N., Fluorescence Correlation Spectroscopy. In *Top. Fluoresc. Spectrosc.*, Lakowicz, J., Ed. Springer US: 1999; Vol. 1, pp 337-378.
95. Fluorescence Correlation Spectroscopy. In *Principles of Fluorescence Spectroscopy*, Lakowicz, J. R., Ed. Springer US: 2006; pp 797-840.
96. Swinton, D. J.; Wirth, M. J., Lateral diffusion of 1,1 '-dioctadecyl-3,3,3 ' 3 '-tetramethylindocarbocyanine perchlorate at the interfaces of C-18 and chromatographic solvents. *Anal. Chem.* **2000,** *72* (16), 3725-3730.
97. Ludes, M. D.; Wirth, M. J., Single-molecule resolution and fluorescence imaging of mixed-mode sorption of a dye at the interface of C-18 and acetonitrile/water. *Anal. Chem.* **2002,** *74* (2), 386-393.
98. Wirth, M. J.; Legg, M. A., Single-molecule probing of adsorption and diffusion on silica surfaces. *Annu. Rev. Phys. Chem.* **2007,** *58*, 489-510.
99. Bae, S. C.; Granick, S., Molecular motion at soft and hard interfaces: from phospholipid bilayers to polymers and lubricants. *Annu. Rev. Phys. Chem.* **2007,** *58*, 353-374.
100. Desai, T. G.; Keblinski, P.; Kumar, S. K.; Granick, S., Modeling diffusion of adsorbed polymer with explicit solvent. *Phys. Rev. Lett.* **2007,** *98* (21).
101. Douglas, J. F.; Johnson, H. E.; Granick, S., A SIMPLE KINETIC-MODEL OF POLYMER ADSORPTION AND DESORPTION. *Science* **1993,** *262* (5142), 2010-2012.
102. Douglas, J. F.; Schneider, H. M.; Frantz, P.; Lipman, R.; Granick, S., The origin and characterization of conformational heterogeneity in adsorbed polymer layers. *Journal of Physics-Condensed Matter* **1997,** *9* (37), 7699-7718.

103. Frantz, P.; Granick, S., KINETICS OF POLYMER ADSORPTION AND DESORPTION. *Phys. Rev. Lett.* **1991,** *66* (7), 899-902.
104. Granick, S.; Bae, S. C., Open questions about polymer interfacial diffusion. *Journal of Polymer Science Part B-Polymer Physics* **2006,** *44* (24), 3434-3435.
105. Granick, S.; Kumar, S. K.; Amis, E. J.; Antonietti, M.; Balazs, A. C.; Chakraborty, A. K.; Grest, G. S.; Hawker, C. J.; Janmey, P.; Kramer, E. J.; Nuzzo, R.; Russell, T. P.; Safinya, C. R., Macromolecules at surfaces: Research challenges and opportunities from tribology to biology. *Journal of Polymer Science Part B-Polymer Physics* **2003,** *41* (22), 2755-2793.
106. Sukhishvili, S. A.; Chen, Y.; Muller, J. D.; Gratton, E.; Schweizer, K. S.; Granick, S., Surface diffusion of poly(ethylene glycol). *Macromolecules* **2002,** *35* (5), 1776-1784.
107. Harris, J. M.; Marshall, D. B., Direct measurement of sorption/desorption kinetics in reversed-phase chromatographic systems. *J. Microcolumn Sep.* **1997,** *9* (3), 185-191.
108. He, H.-T.; Marguet, D., Detecting Nanodomains in Living Cell Membrane by Fluorescence Correlation Spectroscopy. *Annu. Rev. Phys. Chem.* **2011,** *62* (1), 417-436.
109. Axelrod, D., Total Internal Reflection Fluorescence Microscopy in Cell Biology. *Traffic* **2001,** *2* (11), 764-774.
110. Horn, D.; Klingler, J.; Schorf, W.; Graf, K., Experimental progress in the characterization of colloidal systems. *Structure, Dynamics and Properties of Disperse Colloidal Systems* **1998,** *111*, 27-33.
111. Honciuc, A.; Harant, A. W.; Schwartz, D. K., Single-molecule observations of surfactant diffusion at the solution-solid interface. *Langmuir* **2008,** *24* (13), 6562-6566.
112. Stryer, L., Fluorescence Energy Transfer as a Spectroscopic Ruler. *Annu. Rev. Biochem* **1978,** *47* (1), 819-846.
113. Energy Transfer. In *Principles of Fluorescence Spectroscopy*, Lakowicz, J., Ed. Springer US: 2006; pp 443-475.
114. Langdon, B. B.; Kastantin, M.; Walder, R.; Schwartz, D. K., Interfacial Protein-Protein Associations. *Biomacromolecules* **2014,** *15* (1), 66-74.
115. Monserud, J. H.; Schwartz, D. K., Mechanisms of surface-mediated DNA hybridization. *ACS Nano* **2014,** *8* (5), 4488-99.
116. Kastantin, M.; Schwartz, D. K., DNA Hairpin Stabilization on a Hydrophobic Surface. *Small* **2013,** *9* (6), 933-941.
117. Walder, R.; Kastantin, M.; Schwartz, D. K., High throughput single molecule tracking for analysis of rare populations and events. *Analyst* **2012,** *137* (13), 2987-2996.

CHAPTER 2: SINGLE-MOLECULE INSIGHTS INTO RETENTION AT A REVERSED-PHASE CHROMATOGRAPHIC INTERFACE

Publication:

Mabry, J. N.; Skaug, M. J.; Schwartz, D. K., Single-Molecule Insights into Retention at a Reversed-Phase Chromatographic Interface. *Anal. Chem.* **2014,** *86* (19), 9451-9458.

2.1 ABSTRACT

The efficiency of chromatographic separations decreases markedly when peaks exhibit asymmetry (e.g. "peak tailing"). Theoretically, these effects can arise from heterogeneous adsorption kinetics. To investigate the nature and consequences of such heterogeneity, we used a combination of single-molecule imaging and reversed phase liquid chromatography (RPLC). In both single-molecule and macroscopic RPLC experiments, the stationary phase was hydrophobic end-capped (trimethylsilyl-functionalized) silica, which we exposed to different methanol/water solutions (50% - 62% methanol), containing a fluorescent fatty acid analyte. Super-resolution maps based on single-molecule observations revealed rare, strong adsorption sites with activity that varied significantly with methanol concentration. The adsorption and desorption kinetics on the strong sites were heterogeneous and positively correlated, suggesting a broad underlying distribution of site binding energies. Adsorption equilibrium on the strong sites was more sensitive to solution conditions than overall retention measured in RPLC

experiments, suggesting the effect of strong sites on the overall adsorption kinetics should change with solution conditions. Interestingly, in RPLC experiments, peak tailing had a non-monotonic dependence on methanol concentration within the range studied. Using the stochastic model of chromatography, we showed quantitatively that our single-molecule kinetic results were consistent with this macroscopic trend. This approach to identifying and quantifying adsorption sites should be useful for designing better chromatographic separations and for identifying the role of heterogeneous surface chemistry in molecular dynamics.

2.2 INTRODUCTION

Reversed phase liquid chromatography (RPLC) is used extensively for purification and analysis of food and pharmaceutical products, as well as metabolites and environmental toxins.[1] In an ideal system, the chromatographic elution peaks would be infinitely-sharp, but in real systems both transport and adsorption kinetics cause the peaks to have non-zero width.[2-3] When the adsorption kinetics are heterogeneous, peak tailing (i.e. asymmetry) can become a significant problem.[4-5] The stochastic model of chromatography, introduced by Giddings and Eyring[4] and recently reviewed by Felinger,[6] predicts the microscopic contribution of heterogeneous molecular adsorption kinetics to peak shape. The stochastic model of chromatography based on Lèvy processes directly incorporates single-molecule kinetics data for the prediction of theoretical chromatograms.[7] The stochastic modeling of adsorption kinetics was recently combined

with three-dimensional pore-scale simulations of mass transfer to describe the chromatographic process in a bed packed with solid spheres.[8] These simulations predicted that microscopic adsorption kinetics strongly affect peak shape. Therefore, in principle, single-molecule approaches that capture the full heterogeneous distribution of adsorption kinetics can provide the detailed statistical data needed for such simulations.

Early studies of adsorbate dynamics at chromatographic interfaces relied on fluorescence correlation spectroscopy (FCS).[9-11] Under conditions where lateral diffusion of adsorbed solutes (surface diffusion) can be neglected, adsorption and desorption rates can be measured using FCS.[9] On the other hand, under conditions where adsorption/desorption dynamics can be neglected, surface diffusion can be characterized using FCS.[12-13] These limiting assumptions are valid under certain conditions, but it is not generally clear which conditions apply in a given experimental realization. Our group has developed high-throughput tracking methods that allow unambiguous separation and characterization of interfacial adsorption, desorption, and surface diffusion.[14] This work is the first application of these methods to study adsorbate dynamics under conditions that directly mimic an RPLC experiment. In particular, we used organosilane-modified, planar fused silica as a model RPLC stationary phase, and systematically varied the concentration of methanol in the contacting aqueous "mobile phase".

It is generally expected that any RPLC stationary phase will exhibit heterogeneous adsorption sites. The silica support will typically have topographic defects, and the

functionalization of the surface with organic ligands is necessarily incomplete due to steric hindrance.[15] Single-molecule methods are exquisitely sensitive to rare strong sites. Fluorescence imaging has been combined with FCS to identify and focus on adsorption hot spots on planar surfaces that correlate with nanoscale topographic features similar to those found in high-quality silica gel.[13,16-19] These hot spots are the sites of long-lived binding events, which are attributed to strong interactions between the adsorbate and isolated silanols at these sites.[17] In FCS[18-19] and single-molecule tracking[20] studies of porous silica particles, typically used in commercial RPLC systems, long binding events were similarly observed. However, with either confocal or widefield fluorescence microscopy suitable for imaging in particles, the thickness of the imaging volume along the optical axis (~ 1μm) is significantly greater than the pore size of the particles (~10 nm), and so information on specific surface sites is not available. Thus, to study the effect of surface chemistry a planar geometry is preferred. A recent study of a planar ion-exchange chromatographic surface used super-resolution mapping to identify strong adsorption sites for kinetic characterization and predicted their contributions to theoretical chromatograms via the stochastic model.[21]

In RPLC, nonspecific hydrophobic interactions determine the average retention of a molecule in the column. Silanol activity has been widely associated with rare strong adsorption events that cause tailing.[10,16-17,22-26] In this work, our probe molecule was a fatty acid, capable of both non-specific hydrophobic interactions as well as of hydrogen bonding with the silanol groups.[27] We studied the chromatographic surface at the single-

molecule level in imaging experiments and at the ensemble level with RPLC experiments. In the single-molecule experiments, heterogeneous adsorption kinetics were observed and showed a significant dependence on solution conditions. In the macroscopic chromatography experiments, the peaks exhibited different amounts of tailing under different solution conditions. Using the stochastic model of chromatography, we demonstrated that the solution-dependence of the tailing was quantitatively consistent with our single-molecule data, suggesting that the adsorption sites rigorously characterized by single-molecule imaging experiments caused the tailing in RPLC. This approach to quantifying adsorption sites on surfaces should be useful not only for designing more effective separations but also for engineering surfaces with specific, molecular-level functionalities.

2.3 Experimental Section

2.3.1 Single-Molecule Experiments

A detailed description of the experiments is provided in the Supporting Information (SI). Using total internal reflection fluorescence microscopy (TIRFM), we collected movies of BODIPY C_{12} fatty acid (BFA) molecules at the planar interface of a highly polished, end-capped (trimethylsilyl- or TMS-functionalized) fused silica wafer and methanol-water solution. We studied a range of methanol-water solutions from 50% to 62% methanol by volume, where interfacial kinetics could be accurately measured as discussed in the SI.

In these experiments, molecules adsorbed to the interface and appeared as diffraction-limited spots; adsorbed molecules could be tracked from frame-to-frame prior to desorbing to bulk solution and disappearing from the field of view. Desorption could be confused with photobleaching or photoblinking if these photophysical effects occurred on the same timescale. To check for photophysical effects, we characterized the desorption kinetics at different incident laser intensities as shown in the SI. Finding no difference in the kinetics under the different conditions, we ruled out the presence of photophysical artifacts.

2.3.2 Single-Molecule Data Analysis

Our analysis made extensive use of previously reported equations, and the conventional symbols sometimes conflicted. We defined original notation as needed to minimize conflicts in notation, but we encourage the reader to consult the cited literature in the case of any uncertainty.

2.3.2.1 Correlation Analysis of Adsorption Event Positions

At the 75 ms exposure times of the imaging experiments, molecules could be localized only when bound to the surface; molecules diffusing quickly in solution contributed to background fluorescence. On functionalized silica, adsorbed molecules are immobilized

and move to different adsorption sites by executing hops through bulk solution.[28-29] (We show in the SI that the 1D step size distributions are consistent with a hopping mechanism for surface transport.) If the surface is homogeneous, the positions of adsorption events will be uncorrelated. We tested for correlation by calculating a pair radial auto-correlation function $g(r)$ of adsorption event positions.

$$g(r) = \langle \frac{A}{N^2} \sum_{i,j} \delta(\vec{r}_i - \vec{r}_j - \vec{r}) \rangle_{angle} \qquad (2.1)$$

This function is defined for a set of N adsorption events at positions $\vec{r}_i$ for $1 < i < N$ in a total area A, with the brackets indicating averaging and δ indicating the Kronecker delta function. It is normalized such that $g(r) = 1$ for a random distribution of adsorption sites. (We calculated $g(r)$ and analyzed the resulting data using the procedures of Veatch et. al.[30]) If each adsorption site can be occupied more than once and the spatial distribution of sites is random, then the following function describes the correlation

$$g_{fit}(r) = (4\pi\sigma_{loc}^2\rho_{app})^{-1} \exp\left[{-r^2}\Big/{4\sigma_{loc}^2}\right] + 1 \qquad (2.2)$$

where σ_{loc} is the resolution for localizing the adsorption sites. In the case where the sampling of sites is well described by a Poisson distribution, ρ_{app} is the apparent density of sites (i.e. the density of sites actually measured in a given experiment as opposed to the actual density of strong binding sites on the surface).

2.3.2.2 Super-Resolution Imaging and Adsorption Site Analysis

We generated super-resolution maps of BFA adsorption events and identified adsorption sites using a variation of the localization technique termed "motion blur" point accumulation for imaging in nanoscale topography (mbPAINT) by Landes and co-workers.[21,31-32] To generate the super-resolution maps, we first placed the adsorption event position centers on a high-resolution pseudo image (15 nm pixels). We blurred these images such that each adsorption center was converted to a Gaussian peak with standard deviation σ_{loc} and amplitude of 1 adsorption event. The blurred pseudo images were summed to generate the super-resolution maps of adsorption events. We identified sites with 1 or more adsorption events by binarizing the maps and grouping connected pixels above the threshold. Each contiguous region comprised an adsorption site; the maximum pixel value for the site was recorded as that site's adsorption events count, x. The probability histogram for x was fit to a multicomponent Poisson distribution $f_{ads}(x)$ normalized for $x > 0$

$$f_{ads}(x) = \sum_{i=1}^{n} p_i \frac{{\lambda_i}^x \, e^{-\lambda_i}}{x!\,(1 - e^{-\lambda_i})} \qquad (2.3)$$

where for the i^{th} population of sites, λ_i is the mean number of adsorption events per site and p_i is the fraction of total sites with $\sum p_i = 1$. The average site has $\bar{\lambda} = \sum p_i \lambda_i$ adsorption events. If N molecules adsorb, the total number of sites S is given by $S = N/\bar{\lambda}$.

2.3.2.3 Adsorption/Desorption Kinetics and Adsorption Equilibrium Calculations

The observed attachment rate was $k_{ads}\,c$ where c was the concentration of BFA in solution. The adsorption rate constant for each condition was defined as k_{ads} (nm s^{-1}). To quantify the desorption kinetics, the adsorption site residence time of a single molecule was recorded as the time interval between adsorption and desorption. We then determined the complementary cumulative distribution $F(\tau_S)$ of observed residence times τ_S, which represented the fraction of objects with a residence time ≥ τ_S. This distribution was then fit using an exponential mixture model.[33]

$$F(\tau_S) = \sum_{i=1}^{n} p_i\, e^{-\tau_S/\tau_i} \qquad (4)$$

Each component distribution of the mixture model had a characteristic residence time τ_i and represented a fraction p_i of the adsorption events. The most common physical interpretation of this model is that the surface adsorption sites have n possible binding energies, giving rise to n characteristic times for first-order desorption. The distribution of binding energies can arise from having physically different surface sites or from the adsorbed molecule having different binding configurations. The average residence time $\overline{\tau_S}$ was given by $\overline{\tau_S} = \sum p_i \tau_i$ with the desorption rate constant $k_{des} = 1/\overline{\tau_S}$. The equilibrium adsorption coefficient (K) was calculated according to its canonical definition.

$$K = k_{ads}/k_{des} \qquad (2.5)$$

We note that *K* has units of distance and represents the adsorption depth, which is the thickness of a slice of solution containing the number of molecules necessary to populate the surface. The rate constants were calculated for three subsets of data, and the uncertainty was quantified using the *t*-distribution and displayed as standard error.

2.3.3 Reversed Phase Liquid Chromatography

2.3.3.1 Experiments

We conducted chromatography experiments with a trimethylsilyl analytical column (Waters #PSS832611, particle size 5 μm, pore size 80 Å, carbon content 2.38%, surface area 193 m^2/g) using a Waters HPLC system with a Gradient Module (#2545), Sample Manager (#2762), and UV/Vis Detector (#2489). Stock solutions for RPLC were made with BFA (180 μM) and uracil (340 μM) in a methanol-water solution of the same composition as the mobile phase. 20 μL of stock solution was injected into the column at a mobile phase flow rate of 8 mL min^{-1}, and elution was monitored using UV/Vis absorbance measurements at 260 nm for uracil and 530 nm for BFA. The capacity factor *k'* was calculated using the expression

$$k' = \frac{M_1 - t_0}{t_0} \qquad (2.6)$$

where M_1 is the position of the peak centroid of BFA and t_0 is the elution time for uracil (also measured at peak centroid). Uracil is commonly assumed to not bind to RPLC columns, and so its elution time equals the column dead time.[34-35]

2.3.3.2 Stochastic Model of Chromatography

The stochastic model of chromatography, introduced by Gidding and Erying[4] and refined further by Felinger, Dondi, and co-workers,[6-7,36] views chromatography as a Poisson process, where the number of adsorption events and duration of individual adsorption events (residence times) are randomly distributed. We provide a more detailed discussion of the theory and our modeling in the SI. In brief, if the true residence time distribution $f_S(\tau_S)$ and mean number of adsorption events $\overline{r_M}$ are known, the chromatographic process can be represented by a characteristic function ϕ_{τ_S} in the frequency (ω) domain for molecules spending time t_M in the mobile phase.[7]

$$\phi_{\tau_S}(t_S;\omega|t_M) = \exp\left[\overline{r_M}\int_0^{\infty}(\exp[i\omega\tau_S]-1)f_S(\tau_S)d\tau_S\right] \qquad (2.7)$$

The chromatographic peak is obtained by transforming ϕ_{τ_S} to the time domain. We note that in our calculations $\overline{r_M}$ was obtained by dividing the adjusted experimental chromatographic retention time ($M_1 - t_0$) by the estimated mean residence time. We detail in the following paragraph how we estimated the distribution of residence times. To account for mobile phase effects, such as axial diffusion and eddy diffusion, we convoluted the peak obtained after the transformation with the experimental uracil peak, making the assumption that solution-phase transport of BFA and uracil is similar.[36]

Using current techniques, the whole spectrum of adsorption site residence times cannot be directly observed.[7,10,33] To demonstrate the conceptual link between peak tailing and

adsorption on strong sites, it was necessary to adopt a consistent way to estimate the full residence time distribution $f_S(\tau_S)$ under different solution conditions. Single-molecule imaging characterizes adsorption events in which the surface residence time is long enough to reach signal-to-noise levels that allow fluorescent molecules to be distinguished from the background.[21,33] Using model RPLC stationary phase materials, single-molecule experiments typically measure molecular residence times on rare, strong "specific" (SP) adsorption sites over millisecond to second timescales.[7,18-19] However, in chromatography experiments, the average retention of the analyte is presumably determined by more abundant, weaker interactions with "nonspecific" (NS) adsorption sites, while adsorption onto the SP sites (comprising a fraction p_{SP} of the total adsorption events) contributes to peak tailing.[7,37-38] Pasti et. al.[7] suggested that the true residence time distribution can be modeled as a linear combination of these two processes, and so we adopted the following estimate of $f_S(\tau_S)$.

$$f_S(\tau_S) = p_{SP} f_{SP}(\tau_S) + (1 - p_{SP}) f_{NS}(\tau_S) \qquad (2.8)$$

In our calculations, $f_{SP}(\tau_S)$ was the distribution of residence times fit to our single-molecule data (using Eq 2.4) with mean $\overline{\tau_{SP}}$, and $f_{NS}(\tau_S)$ was an exponential distribution with a mean residence time $\overline{\tau_{NS}}$, which was set to be one order of magnitude lower than residence times measured by single-molecule experiments. (In the SI, we present a sensitivity study with different estimates of $\overline{\tau_{NS}}$, showing that the trends predicted by the model were insensitive to the specific value of $\overline{\tau_{NS}}$.) To estimate how the fraction of strong sites, p_{SP}, changed with solution conditions in our chromatography experiments, we derived the following expression (see SI).

$$p_{SP} = \varphi/\delta \qquad (2.9)$$

where $\varphi = \frac{K}{k'}\frac{\overline{\tau_{NS}}}{\overline{\tau_{SP}}}$ and δ is a fitting parameter inversely proportional to both the concentration of analyte and area of the stationary phase in a theoretical plate that is assumed to be independent of solution conditions. The critical assumption is that average retention on the chromatography column is primarily determined by NS sites, while average retention in the single-molecule experiments is determined by SP sites. In our modeling of experimental chromatograms, we adjusted δ as shown graphically in Fig A10 such that the experimental and theoretical measures of peak asymmetry agreed.

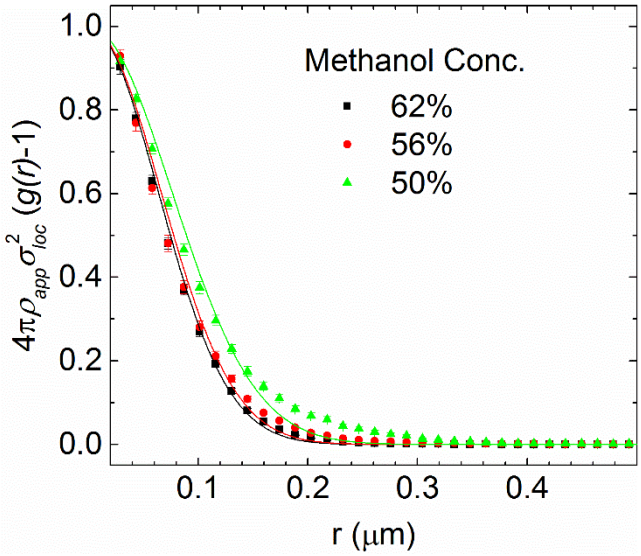

Figure 2.1: Pair autocorrelation function of molecule adsorption positions, where ordinate values > 0 signify correlation. Significant correlation was detected at distances < 300 nm. The data came from experiments with solution compositions as indicated in the legend in terms of percent methanol by volume. We modeled the data with Eq 2.2, which applies when randomly distributed adsorption sites can be occupied more than one time and are resolved with precision σloc. Solid lines show fits of Eq 2.2 with σloc of 45 nm, 47 nm, and 54 nm and ρ_{app} of 0.07 μm-2, 0.20 μm-2, and 0.09 μm-2 for 62%, 56%, and 50% (v/v) methanol respectively. Ordinate values were normalized by the height of the fitted peaks. The error bars represent standard error.

2.4 RESULTS AND DISCUSSION

2.4.1 Mapping Adsorption Sites

The silica surfaces imaged in the current study were highly polished and functionalized with a small modifier (TMS), and so one might reasonably expect them to appear relatively homogeneous to an adsorbate molecule. To test this hypothesis, we calculated a pair autocorrelation function of molecule adsorption positions (Fig 2.1). The function $g(r)$ would have a constant value of one if the adsorption positions were uncorrelated. Adsorption events were spatially correlated at distances less than 300 nm, and we were able to model this correlation with Eq 2.2, which applies when adsorption sites are randomly distributed and can be localized with a precision of σ_{loc} (~50 nm in our experiments). [30] Based on this modeling, we concluded that many of the observed adsorption events occurred on strongly binding, discrete sites smaller than our resolution limit.

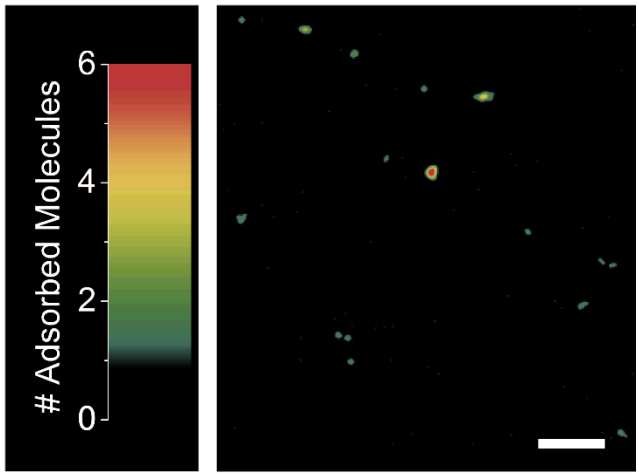

Figure 2.2: Super-resolution map of BFA adsorption events in 62% methanol from a dataset with 2.3 molecules μm^{-2}. Scale bar 1 μm.

To visualize the adsorption sites, we created super-resolution maps of adsorption events (Fig 2.2). Sites with a large number of adsorption events are emphasized in these maps, and previous work focused on characterizing the kinetics of these sites exclusively, since they are clearly anomalous.[21,32] However, the absolute density of strong sites will remain unknown if a threshold based on the number of adsorption events is used to identify strong sites because the number of observations is finite. We observed about 2 adsorption events per square micron on average over the course of our movies (using very low adsorbate concentrations), but we expect the density of molecular-scale adsorption sites to be much higher. We set out to estimate the number of adsorption sites and to determine if the adsorption sites could be approximated as a single type of site, for which simple Poisson statistics should describe the number of adsorption events.

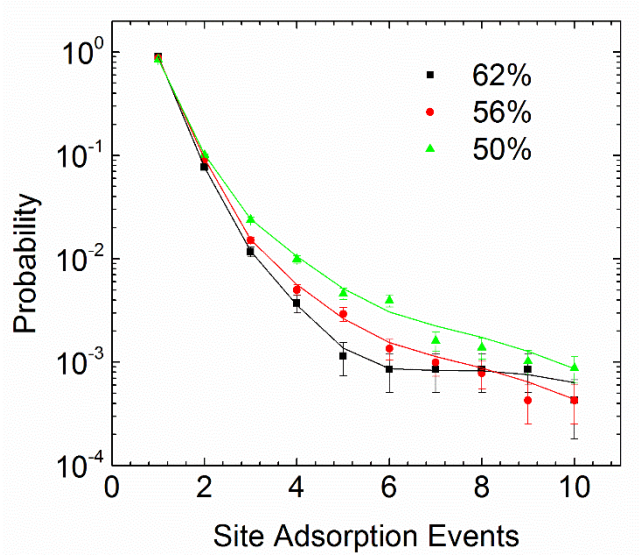

Figure 2.3: Probability histogram of site adsorption events. Fits to multicomponent Poisson distributions (Eq 2.3) are shown with solid lines. Based on the fit parameters (Table A1), we calculated site densities of 15 ± 2 μm^{-2}, 18 ± 2 μm^{-2}, and 10 ± 2 μm^{-2} in 50%, 56%, and 62% methanol, respectively. Percent methanol in solution as annotated. The error bars represent standard error.

We constructed a probability histogram of the site adsorption event counts (Fig 2.3) and found that the distribution was heavy-tailed. We then fit the histogram with a Poisson mixture model (Eq 2.3), assuming that the adsorption kinetics were due to several different types of sites exhibiting first-order kinetics. Previous studies have shown that kinetics on individual sites are indeed first-order.[21,32] Three populations were required to fit the data (Fig A1), meaning that adsorption was observed on some sites significantly more often than would be expected for a single population of sites obeying Poisson statistics. The model parameters are reported in full detail in Table A1. Approximately 90% of the adsorption sites were of the weakest type with 0.1 adsorption events, 10% of the intermediate type with 1 adsorption event, and 1% of the strongest type with 10 adsorption events. The site adsorption rates were heterogeneous, suggesting that the

adsorption sites had a distribution of characteristic binding energies. We calculated average site densities of 15 ± 2 μm^{-2}, 18 ± 2 μm^{-2}, and 10 ± 1 μm^{-2} for 50%, 56%, and 62% methanol, respectively. Thus, these sites, which we classify as specific (SP) sites, were rare on the scale of a nanometer-sized BFA molecule and displayed a range of adsorption rates. To the best of our knowledge, we are the first investigators to introduce Poisson mixture modeling of adsorption site kinetics in the context of single-molecule imaging and to report adsorption site densities. By extracting an absolute strong site density for a given surface, we provide a new quantitative method for comparing different surfaces.

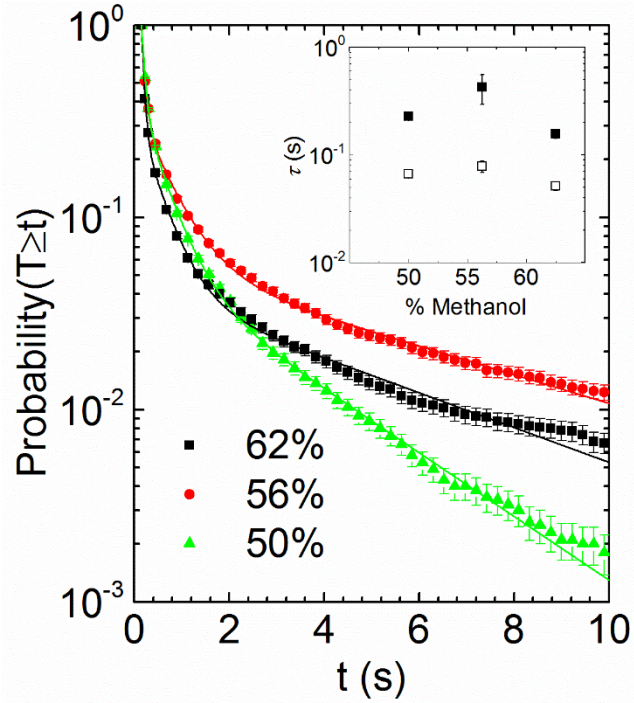

Figure 2.4: Adsorption site residence time distributions. Main Figure: complementary cumulative residence time distributions for all sites. Experimental data are shown with standard error for percent methanol in solution as annotated. Fits using Eq 2.4 are shown with solid lines. Inset: Average residence times for sites with adsorption event count x =1 (□) and sites with x > 1 (■), showing that sites exhibiting faster adsorption kinetics also displayed longer site residence times. An average of 2.3 adsorption events μm-2 were observed at each condition. Average residence times were calculated from fits reported in Table A3.

Table 2.1: Eq 2.4 fit parameters for site residence time distributions. The parameter values are for the fits shown in Fig 2.4. The numbers in parentheses represents the uncertainty in the last significant digit of each value (standard error).

Percent Methanol	$\overline{\tau_S}$	p_i	τ_i
50	0.13(1)	0.915(3)	0.071(1)
		0.075(2)	0.50(9)
		0.010(1)	2.8(5)
56	0.16(3)	0.932(2)	0.070(6)
		0.058(2)	0.7(1)
		0.009(1)	6.3(7)
62	0.08(1)	0.969(4)	0.055(4)
		0.028(3)	0.47(3)
		0.004(1)	5.0(5)

2.4.2 Heterogeneous Adsorption Site Residence Time Distributions

Desorption kinetics were characterized under each solution condition by analysis of ~10^4 molecular trajectories. The residence times from all adsorption sites are presented in Fig 2.4. The presence of multiple types of adsorption sites led to heavy-tailed distributions of residence times. Specifically, long residence times were observed at a higher frequency than would be expected for data from a single exponential distribution (originating from a single type of site), as demonstrated graphically in Fig A2. For each solution condition, we fit the adsorption site residence distributions with an exponential mixture model (Eq 2.4) with three populations (the minimum number of components that fully described the residence time distributions), as discussed in the SI. Table 2.1 shows the parameter values for the fits to the residence time distributions. The fastest-desorbing population

had a characteristic residence time close to the 75 ms frame time and its prevalence (92% - 97%) increased as the amount of methanol in solution increased. Interestingly, the characteristic times for the two slower populations had maximum values at the intermediate 56% methanol condition. Thus, the probability of observing long residence times (> 1 s) was significantly higher in 56% methanol. We note that the values of the population fractions (p_i values) shifted slightly in the different solution conditions, indicating that the exact composition of the active adsorption sites may have had a weak solution dependence.

Methanol-water mixtures exhibit nonideal properties at chromatographic interfaces;[39] for example, excess adsorption of methanol peaks at about 40% methanol by volume.[40-41] Molecular simulations have also shown that polar molecules form the most hydrogen bonds with silanol groups and adsorbed solvent molecules at intermediate methanol concentration.[39] Such nonideal thermodynamics may contribute to the non-monotonic dependence of the observed residence time distributions on solution conditions.

The average residence times of 0.13 s ± 0.01 s and 0.16 s ± 0.03 s in 50% and 56% methanol respectively were not significantly different, while the average residence time in 62% methanol condition, 0.08 s ± 0.01 s, was significantly lower (Table 2.1). Extending these results to retention in RPLC, we expect that the solution conditions dictate what types of surface sites significantly contribute to retention. For example, the two-site (strong-site/weak-site) model has previously been used to model RPLC elution

curves for phenol in different methanol/water solutions;[36] the characteristic residence times for the strong sites increased as the methanol content decreased, with larger increases at lower methanol concentrations. Our averaged single-molecule residence times represent the behavior on the strong sites and exhibit a similar dependence of residence times on methanol concentration.

2.4.3 Correlation of Adsorption and Desorption Kinetics

Both the adsorption and desorption kinetics for a single adsorption site should be related to the site binding strength.[42] In principle, the three populations identified in the desorption kinetics data (site residence time data) and the adsorption kinetics data (adsorption site event counts) could have arisen from three distinct types of sites, with the sites with the fastest adsorption kinetics having the slowest desorption kinetics. However, the mean number of adsorption events for a given site was low (~0.3 events/site), and so definitively assigning an individual site to a given population based on adsorption kinetics was not possible. If there were distinctly different types of sites, then sites with larger numbers of adsorption events should have been more likely to have longer site residence times. To test this hypothesis, we analyzed residence times for sites with only one adsorption event ($x = 1$) and sites with larger numbers of adsorption events. We fit the residence time distributions as shown in the SI (Table A3) with exponential mixture models and calculated average residence times shown in the Fig 2.4 inset. The phenomenon of faster adsorption kinetics (higher numbers of adsorption events x) being

correlated with slower desorption kinetics (longer residence times) was observed in all the solution conditions. Thus, we can infer that sites with different binding strengths affect the kinetics in the expected way for a reversible process.

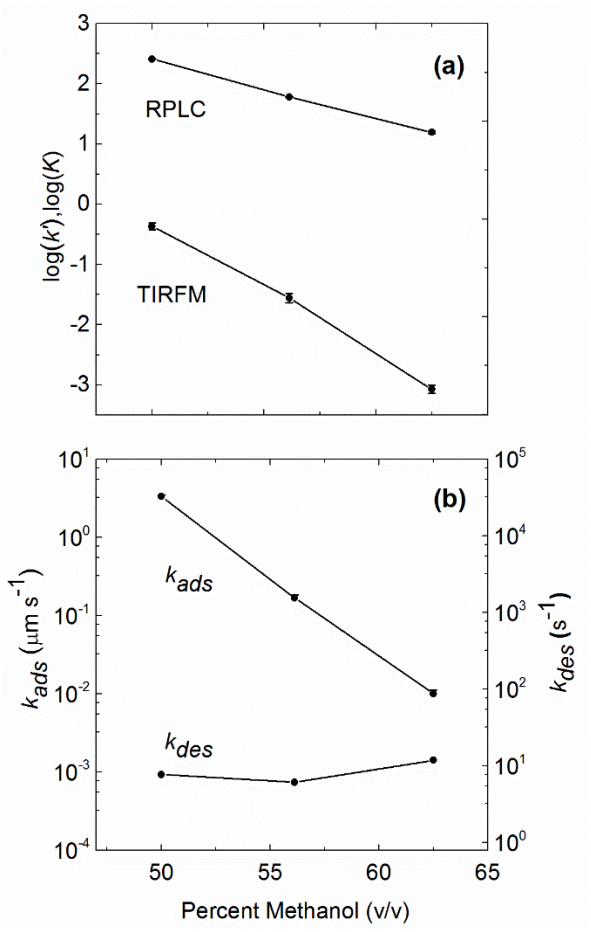

Figure 2.5: Dependence of average solute behavior on methanol concentration. (a) Measurements of retention: log(*k'*) from chromatography experiments and log(*K*) from single-molecule TIRFM. *K* in units of μm. (b) Single-molecule adsorption rate kads and desorption rate kdes constants on logarithmic scales.

2.4.4 Retention in Single-Molecule and Macroscopic RPLC Experiments

It is well known that retention of a hydrophobic solute on a hydrophobic surface such as TMS decreases with increasing methanol concentration as the solvent becomes more nonpolar.[43-45] We characterized retention of BFA, which is largely hydrophobic, under different solution conditions with both single-molecule and ensemble methods, calculating the single-molecule adsorption equilibrium coefficient K (Eq 2.5) and RPLC capacity factor k' (Eq 2.6), respectively, which relate to the adsorption free energy ΔG_{ads} as follows[43-45]

$$\log(k') = \log(K/d_t) + \log(\Phi) \qquad (2.6a)$$

$$\Delta G_{ads} = -RTln(K/d_t) \qquad (2.6b)$$

where Φ is the phase ratio (the volumetric ratio of the stationary and mobile phases), d_t is the effective thickness of the stationary phase, R is the gas constant, and T is temperature.

Fig 2.5(a) shows that log(k') and log(K) values had a qualitatively similar monotonic dependence on the solution conditions as expected for hydrophobic interactions. However, log(K) values, calculated from single-molecule data, reflected adsorption only on rare, strong SP sites and were more sensitive to methanol concentration than log(k') values, which were measured with macroscopic RPLC and presumably determined by the more abundant, weak NS sites. Similar trends were seen in macroscopic RPLC

experiments with amphiphilic phenol, when the two-site stochastic model was used to fit experimental chromatograms (i.e. the strong sites were more sensitive to solution conditions).[36] We note that the changes in retention on the SP sites were almost entirely due to changes in the adsorption rate constant as shown in Fig 2.5(b). We speculate that the strong SP sites were areas with unreacted silanols with which the carboxylic acid moiety of BFA can form hydrogen bonds.[46] Molecular simulations suggest that nonpolar solutes also prefer to adsorb to these sites due to steric effects.[24] Adsorption of amphiphilic solute molecules can then be viewed as a competition between the solute and solvent molecules for these strong adsorption sites.[27] Due to the hydrophobic nature of the stationary phase, it is more highly solvated by methanol than by water,[47] and isotherm measurements of solvent adsorption seem to indicate that within bonded stationary phases methanol interacts with silanols more strongly than does water.[40-41] Thus, the enhanced sensitivity of SP site adsorption to solution conditions could be a consequence of the solvent and solute competing for these unreacted adsorption sites.

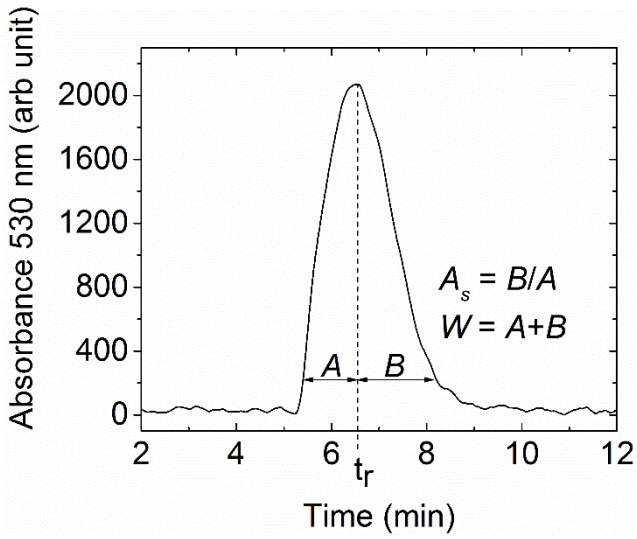

Figure 2.6: Experimental chromatogram for BFA with 56% methanol mobile phase. *A* and *B* measured at 10 % peak height.

Table 2.2: Chromatographic figures of merit: peak position (tr), centroid (M1), width (W), and asymmetry factor (As) for different methanol/water mobile phase compositions. Model data for $\alpha = 10$ and $\delta^{-1} = 33\ \mu m^{-1}$.

	Experimental				**Theoretical Model**	
Percent Methanol (v/v)	t_r **(min)**	M_1 **(min)**	W **(min)**	A_s	W **(min)**	A_s
50	28.4(4)	28.5(3)	8.3(3)	1.38(4)	0.77	1.42
56	6.60(5)	6.76(8)	2.7(1)	1.6(1)	0.26	1.67
62	1.86(7)	1.86(1)	0.80(4)	1.1(2)	0.09	1.01

2.4.4 Chromatographic Peak Tailing

Chromatographic peaks can exhibit tailing when the analyte interacts with a heterogeneous stationary phase (kinetic effect) or when the concentration of the analyte reaches the nonlinear regime of the adsorption isotherm (overloading effect).[22,48] Our peak shapes did not exhibit a dependence on concentration (Fig A9) and therefore reflected kinetic effects. The simplest model for a heterogeneous surface is the two-site model. When a chromatographic surface has weak NS and strong SP sites, peak asymmetry is maximized when the fraction of strong-site adsorption events p_{SP} is relatively small; the asymmetry increases as the difference in the residence times on the two types of sites becomes greater.[37] Our experimental chromatograms had asymmetry factors (A_s, as defined in Fig 2.6 and reported in Table 2.2) that correlated with average residence times for SP sites ($\bar{\tau}_S$ in Table 2.1). So if the fraction of adsorption events onto SP sites remained constant and the residence time on the NS sites was constant, we would expect peak asymmetry to be correlated simply with SP site residence times. However, the adsorption rate constants for the SP sites were particularly sensitive to solution conditions, and so a more complex analysis was required. Specifically, using Eq 2.9, we determined that p_{SP} was increasing as methanol concentration decreased. The change in p_{SP} is primarily due to the ratio K/k' changing with solution conditions, as can be seen in Fig 2.5. We relied on Eq 2.9 and our empirical SP-site residence time data from

single-molecule experiments to approximate the overall residence time distribution (Eq 2.8).

We generated theoretical chromatograms by the stochastic model of chromatography (see SI). Since this simple model does not fully account for mass transfer effects in the stationary phase, which contribute significantly to experimental peak widths.[3,8,48-50] we focused our efforts on matching the peak asymmetry data that depend directly on the adsorption/desorption kinetics.[6,38] We show in Table 2.2 and Fig A10 that, with proper choice of a single fitting parameter δ, our theoretical peaks had the same asymmetry as the experimental peaks and that the widths scaled as expected. The peak asymmetry depends on two factors: (1) the difference in NS and SP site residence times and (2) the fraction of adsorption events onto SP sites. Both of these factors depended on solution conditions and were accounted for in our modeling of chromatographic peaks that properly accounted for peak asymmetry. These results demonstrate that the SP sites identified in our single-molecule experiments are likely responsible for tailing in the chromatographic system.

2.5 CONCLUSIONS

Single-molecule tracking provided a detailed view of kinetics on rare strong adsorption sites on an end-capped silica surface. The dynamics were extremely sensitive to changes in the composition of the overlying methanol-water solution, in agreement with the

viewpoint that adsorption represents a competition between the adsorbate and solvent molecules. These strong sites exhibited heterogeneous adsorption and desorption kinetics that were correlated, suggesting a common energy landscape for the forward and reverse adsorption process. Using single-molecule data to represent the detailed molecular behavior on strong binding sites, we approximated the overall adsorption site residence time distribution in the context of a model that included both weak and strong binding sites. By incorporating this approach into the standard stochastic model of the chromatographic process, we were able to reproduce the solvent dependence of chromatographic peak asymmetry. With the ability to directly resolve and characterize strong sites, advanced stationary phase chemistries, such as embedded polar groups, can be evaluated based on their ability to decrease strong site adsorption events. These measurements can be conducted with small samples and without convoluting effects such as mass transfer, which should greatly simplify the design process for new separation media. More generally, we have demonstrated a robust statistical approach to characterizing adsorption kinetics on a functionalized surface, which can be applied to other surface-based technologies such as biosensing and heterogeneous catalysis.

2.7 REFERENCES

1. *Handbook of HPLC*. 2nd ed.; Taylor & Francis: Boca Raton, 2010.
2. Vandeemter, J. J.; Zuiderweg, F. J.; Klinkenberg, A., Longitudinal Diffusion and Resistance to Mass Transfer as Causes of Nonideality in Chromatography. *Chem. Eng. Sci.* **1956,** *5* (6), 271-289.
3. Gritti, F.; Guiochon, G., Mass transfer kinetics, band broadening and column efficiency. *J. Chromatogr. A* **2012,** *1221*, 2-40.
4. Giddings, J. C.; Eyring, H., A Molecular Dynamic Theory of Chromatography. *J. Phys. Chem.* **1955,** *59* (5), 416-421.
5. Giddings, J. C., Kinetic Origin of Tailing in Chromatography. *Anal. Chem.* **1963,** *35* (13), 1999-&.
6. Felinger, A., Molecular dynamic theories in chromatography. *J. Chromatogr. A* **2008,** *1184* (1-2), 20-41.
7. Pasti, L.; Cavazzini, A.; Felinger, A.; Martin, M.; Dondi, F., Single-molecule observation and chromatography unified by levy process representation. *Anal. Chem.* **2005,** *77* (8), 2524-2535.
8. Hlushkou, D.; Gritti, F.; Daneyko, A.; Guiochon, G.; Tallarek, U., How Microscopic Characteristics of the Adsorption Kinetics Impact Macroscale Transport in Chromatographic Beds. *J Phys Chem C* **2013,** *117* (44), 22974-22985.
9. Hansen, R. L.; Harris, J. M., Measuring reversible adsorption kinetics of small molecules at solid/liquid interfaces by total internal reflection fluorescence correlation spectroscopy. *Anal. Chem.* **1998,** *70* (20), 4247-4256.
10. Wirth, M. J.; Swinton, D. J., Single-molecule probing of mixed-mode adsorption at a chromatographic interface. *Anal. Chem.* **1998,** *70* (24), 5264-5271.
11. Thompson, N., Fluorescence Correlation Spectroscopy. In *Top. Fluoresc. Spectrosc.*, Lakowicz, J., Ed. Springer US: 1999; Vol. 1, pp 337-378.
12. Swinton, D. J.; Wirth, M. J., Lateral diffusion of 1,1 '-dioctadecyl-3,3,3 ' 3 '-tetramethylindocarbocyanine perchlorate at the interfaces of C-18 and chromatographic solvents. *Anal. Chem.* **2000,** *72* (16), 3725-3730.
13. Wirth, M. J.; Swinton, D. J.; Ludes, M. D., Adsorption and diffusion of single molecules at chromatographic interfaces. *J. Phys. Chem. B* **2003,** *107* (26), 6258-6268.
14. Walder, R.; Kastantin, M.; Schwartz, D. K., High throughput single molecule tracking for analysis of rare populations and events. *Analyst* **2012,** *137* (13), 2987-2996.
15. Gritti, F.; Guiochon, G., Heterogeneity of the adsorption mechanism of low molecular weight compounds in reversed-phase liquid chromatography. *Anal. Chem.* **2006,** *78* (16), 5823-5834.
16. Ludes, M. D.; Wirth, M. J., Single-molecule resolution and fluorescence imaging of mixed-mode sorption of a dye at the interface of C-18 and acetonitrile/water. *Anal. Chem.* **2002,** *74* (2), 386-393.

17. Wirth, M. J.; Legg, M. A., Single-molecule probing of adsorption and diffusion on silica surfaces. *Annu. Rev. Phys. Chem.* **2007,** *58*, 489-510.
18. Zhong, Z. M.; Lowry, M.; Wang, G. F.; Geng, L., Probing strong adsorption of solute onto cis-silica gel by fluorescence correlation imaging and single-molecule spectroscopy under RPLC conditions. *Anal. Chem.* **2005,** *77* (8), 2303-2310.
19. Zhong, Z. M.; Wang, G. F.; Geng, M. L., Probing strong adsorption of individual solute molecules at solid/liquid interfaces with model-based statistical two-dimensional correlation analysis. *J. Mol. Struct.* **2006,** *799* (1-3), 204-210.
20. Cooper, J. T.; Peterson, E. M.; Harris, J. M., Fluorescence imaging of single-molecule retention trajectories in reversed-phase chromatographic particles. *Anal. Chem.* **2013,** *85* (19), 9363-70.
21. Kisley, L.; Chen, J.; Mansur, A. P.; Shuang, B.; Kourentzi, K.; Poongavanam, M. V.; Chen, W. H.; Dhamane, S.; Willson, R. C.; Landes, C. F., Unified superresolution experiments and stochastic theory provide mechanistic insight into protein ion-exchange adsorptive separations. *Proc. Natl. Acad. Sci. U. S. A.* **2014,** *111* (6), 2075-80.
22. Wirth, M. J.; Smith, E. A.; Anthony, S. R., Measurement and simulation of tailing zones of a cationic dye in analytical-scale reversed phase chromatography. *J. Chromatogr. A* **2004,** *1034* (1-2), 69-75.
23. Rafferty, J. L.; Siepmann, J. I.; Schure, M. R., Understanding the Retention Mechanism in Reversed-Phase Liquid Chromatography: Insights from Molecular Simulation. *Advances in Chromatography, Vol 48* **2010,** *48*, 1-55.
24. Rafferty, J. L.; Siepmann, J. I.; Schure, M. R., Influence of bonded-phase coverage in reversed-phase liquid chromatography via molecular simulation. II. Effects on solute retention. *J. Chromatogr. A* **2008,** *1204* (1), 20-27.
25. Lindsey, R. K.; Rafferty, J. L.; Eggimann, B. L.; Siepmann, J. I.; Schure, M. R., Molecular simulation studies of reversed-phase liquid chromatography. *J. Chromatogr. A* **2013,** *1287*, 60-82.
26. Kohler, J.; Chase, D. B.; Farlee, R. D.; Vega, A. J.; Kirkland, J. J., Comprehensive Characterization of Some Silica-Based Stationary Phases for High-Performance Liquid-Chromatography. *J. Chromatogr.* **1986,** *352*, 275-305.
27. Honciuc, A.; Baptiste, D. J.; Campbell, I. P.; Schwartz, D. K., Solvent Dependence of the Activation Energy of Attachment Determined by Single Molecule Observations of Surfactant Adsorption. *Langmuir* **2009,** *25* (13), 7389-7392.
28. Skaug, M. J.; Mabry, J.; Schwartz, D. K., Intermittent Molecular Hopping at the Solid-Liquid Interface. *Phys. Rev. Lett.* **2013,** *110* (25), 256101
29. Skaug, M. J.; Mabry, J. N.; Schwartz, D. K., Single-Molecule Tracking of Polymer Surface Diffusion. *J. Am. Chem. Soc.* **2014,** *136* (4), 1327-1332.
30. Veatch, S. L.; Machta, B. B.; Shelby, S. A.; Chiang, E. N.; Holowka, D. A.; Baird, B. A., Correlation Functions Quantify Super-Resolution Images and Estimate Apparent Clustering Due to Over-Counting. *Plos One* **2012,** *7* (2).
31. Chen, J. X.; Bremauntz, A.; Kisley, L.; Shuang, B.; Landes, C. F., Super-Resolution mbPAINT for Optical Localization of Single-Stranded DNA. *Acs Applied Materials & Interfaces* **2013,** *5* (19), 9338-9343.

32. Kisley, L.; Chen, J.; Mansur, A. P.; Dominguez-Medina, S.; Kulla, E.; Kang, M. K.; Shuang, B.; Kourentzi, K.; Poongavanam, M. V.; Dhamane, S.; Willson, R. C.; Landes, C. F., High ionic strength narrows the population of sites participating in protein ion-exchange adsorption: a single-molecule study. *J. Chromatogr. A* **2014,** *1343*, 135-42.
33. Kastantin, M.; Schwartz, D. K., Identifying Multiple Populations from Single-Molecule Lifetime Distributions. *Chemphyschem* **2013,** *14* (2), 374-380.
34. Poole, C. F.; Poole, S. K., Foundations of retention in partition chromatography. *J. Chromatogr. A* **2009,** *1216* (10), 1530-1550.
35. Gritti, F.; Guiochon, G., Effect of the mobile phase composition on the isotherm parameters and the high concentration band profiles in reversed-phase liquid chromatography. *J. Chromatogr. A* **2003,** *995* (1-2), 37-54.
36. Felinger, A., Determination of rate constants for heterogeneous mass transfer kinetics in liquid chromatography. *J. Chromatogr. A* **2006,** *1126* (1-2), 120-128.
37. Felinger, A.; Cavazzini, A.; Remelli, M.; Dondi, F., Stochastic-dispersive theory of chromatography. *Anal. Chem.* **1999,** *71* (20), 4472-4479.
38. Bacskay, I.; Felinger, A., Macroscopic and microscopic analysis of mass transfer in reversed phase liquid chromatography. *J. Chromatogr. A* **2009,** *1216* (8), 1253-1262.
39. Rafferty, J. L.; Siepmann, J. I.; Schure, M. R., Mobile phase effects in reversed-phase liquid chromatography: A comparison of acetonitrile/water and methanol/water solvents as studied by molecular simulation. *J. Chromatogr. A* **2011,** *1218* (16), 2203-2213.
40. Bocian, S.; Vajda, P.; Felinger, A.; Buszewski, B., Effect of End-Capping and Surface Coverage on the Mechanism of Solvent Adsorption. *Chromatographia* **2010,** *71*, S5-S11.
41. Gritti, F.; Kazakevich, Y. V.; Guiochon, G., Effect of the surface coverage of endcapped C-18-silica on the excess adsorption isotherms of commonly used organic solvents from water in reversed phase liquid chromatography. *J. Chromatogr. A* **2007,** *1169* (1-2), 111-124.
42. Masel, R. I., *Principles of Adsorption and Reaction on Solid Surfaces*. Wiley: New York, 1996; p xiv, 804 p.
43. Horvath, C.; Melander, W.; Molnar, I., Solvophobic Interactions in Liquid-Chromatography with Nonpolar Stationary Phases. *J. Chromatogr.* **1976,** *125* (1), 129-156.
44. Dorsey, J. G.; Dill, K. A., The Molecular Mechanism of Retention in Reversed-Phase Liquid-Chromatography. *Chem. Rev.* **1989,** *89* (2), 331-346.
45. Rafferty, J. L.; Zhang, L.; Siepmann, J. I.; Schure, M. R., Retention mechanism in reversed-phase liquid chromatography: A molecular perspective. *Anal. Chem.* **2007,** *79* (17), 6551-6558.
46. Honciuc, A.; Harant, A. W.; Schwartz, D. K., Single-Molecule Observations of Surfactant Diffusion at the Solution- Solid Interface. *Langmuir* **2008,** *24* (13), 6562-6566.
47. Zhang, L.; Rafferty, J. L.; Siepmann, J. I.; Chen, B.; Schure, M. R., Chain conformation and solvent partitioning in reversed-phase liquid chromatography: Monte Carlo simulations for various water/methanol concentrations. *J. Chromatogr. A* **2006,** *1126* (1-2), 219-231.

48. Fornstedt, T.; Zhong, G. M.; Guiochon, G., Peak tailing and slow mass transfer kinetics in nonlinear chromatography. *J. Chromatogr. A* **1996,** *742* (1-2), 55-68.
49. Miyabe, K.; Guiochon, G., Surface diffusion in reversed-phase liquid chromatography. *J. Chromatogr. A* **2010,** *1217* (11), 1713-1734.
50. Miyabe, K.; Guiochon, G., Comparison of the Characteristics of Adsorption Equilibrium and Surface Diffusion in Liquid−Solid and Gas−Solid Adsorption on C18-Silica Gels. *J. Phys. Chem. B* **2004,** *108* (9), 2987-2997.

CHAPTER 3: TUNING THE FLIGHT LENGTH OF MOLECULES DIFFUSING ON A HYDROPHOBIC SURFACE

Publication:

Mabry, J. N.; Schwartz, D. K. Tuning the Flight Length of Molecules Diffusing on a Hydrophobic Surface. Submitted.

3.1 ABSTRACT

Transport at solid-liquid interfaces is critical to self-assembly, biosensing, and heterogeneous catalysis, but surface diffusion remain difficult to characterize and rationally manipulate, due to the inherent heterogeneity of adsorption on solid surfaces. Using single-molecule tracking, we characterized the diffusion of a fluorescent long-chain surfactant on a hydrophobic surface, which involved periods of confinement alternating with bulk-mediated "flights". The concentration of methanol in solution was varied to tune the strength of the hydrophobic surface-molecule interaction. The frequency of confinement had a non-monotonic dependence on methanol concentration that reflected the relative influence of anomalously strong adsorption sites. By carefully accounting for the effect of this surface heterogeneity, we demonstrated that flight lengths increased monotonically as the hydrophobic attraction decreased, in agreement

with theoretical predictions for bulk-mediated surface diffusion. The theory provided an accurate description of surface diffusion, despite the system being heterogeneous, and can be leveraged to optimize molecular search and assembly processes.

3.2 INTRODUCTION

Stepwise control of surface diffusion can enable the precise assembly of molecular building blocks, such as DNA origami, on solid substrates.[1] While surface diffusion is an activated, temperature-sensitive process,[2-3] many molecules, such as proteins, are stable only over a narrow temperature range, and so other isothermal control strategies for surface diffusion are needed. The exact mechanism of surface diffusion determines how the overall molecular mobility is affected by environmental conditions and drastically affects the efficiency of molecular search processes,[4-8] important in heterogeneous catalysis,[9] surface-based biosensing,[10] and self-assembly of organic monolayers and complex hierarchical structures.[11] In the simplest model of interfacial transport,[12-14] molecules are hypothesized to adsorb to the interface, undergo Gaussian diffusion, and then desorb from the interface. This model can describe behavior at liquid-liquid interfaces,[15] but the frozen, heterogeneous nature of a solid surface makes this scenario less likely.[16-18] At solid-liquid interfaces, the energy landscape is typically more complex, and multiple modes of diffusion may contribute to the overall transport of molecules at the interface.[19]

After molecules adsorb from solution to a solid surface, they typically remain confined to nanoscale surface sites prior to desorption.[20-22] Once a molecule desorbs, it diffuses through solution, but is not necessarily "lost to the bulk". Under strongly adsorbing conditions, a molecule may quickly reabsorb, executing a "flight" though solution.[23-25] This bulk-mediated surface diffusion controls the rate at which inhomogeneous surface density perturbations *relax* when the timescale for re-adsorption is much less than for desorption.[23-25] This mode of surface diffusion dominates the *effective* interfacial transport of hydrophilic polymers,[26-27] DNA origami,[1] small fluorescent dyes,[28] and proteins[20] at solid-aqueous interfaces. Both the frequency and the length of flights influence exactly how a molecule explores the surface, and independent control of these variables would enable optimization of search and assembly processes.

The frequency of bulk-mediated displacements, i.e. flights, is very sensitive to the strength of adsorbate-surface interactions and is directly proportional to the desorption rate. For polyethylene glycol (PEG) polymers on silica, flights are more frequent at high pH when hydrogen bonding interactions between the polymer and surface are weaker. For PEG on a hydrophobic surface, more flights are observed as PEG chain length decreases and desorption becomes faster.[29] Bulk-mediated diffusion is a significant mode of surface diffusion only when the probability for fast re-adsorption is significant. Because of this phenomenon, flights were observed on a polyelectrolyte surface only when there was a strong electrostatic attraction between the small-molecule probes and the surface.[28] The frequency of flights is not the only contributor to the overall mobility

of the molecules, however. The distribution of flight lengths is also critically important.[4,30] Surface topography can influence the length of flights; on a surface decorated with pillars 3 nm – 7 nm in height, surface diffusion was slowed as pillar height increased, presumably due to flights being obstructed by the pillars.[27] At a strictly planar interface, the theoretical behavior of an adsorbate flying across a surface has been carefully examined,[23-25,30] and the expected behavior is remarkably simple: flight lengths should increase as the re-adsorption probability decreases. However, this simple relationship has not been tested or demonstrated experimentally. Flight lengths are difficult to examine in isolation, because in practice, the flight length distribution is convoluted with the apparent step-size distribution for confined (i.e. adsorbed) molecules. Further complicating the picture, the frequency of flights is particularly sensitive to experimental parameters that might shift the distribution of flight lengths. We present here a careful analysis of single-molecule mobility under a broad range of solution conditions, accounting separately for the contribution of confined and flying motion to the mobility of the ensemble. For the case of a hydrophobic surface, we examine how changing the solvent polarity affects interfacial transport.

3.3 Results and Discussion

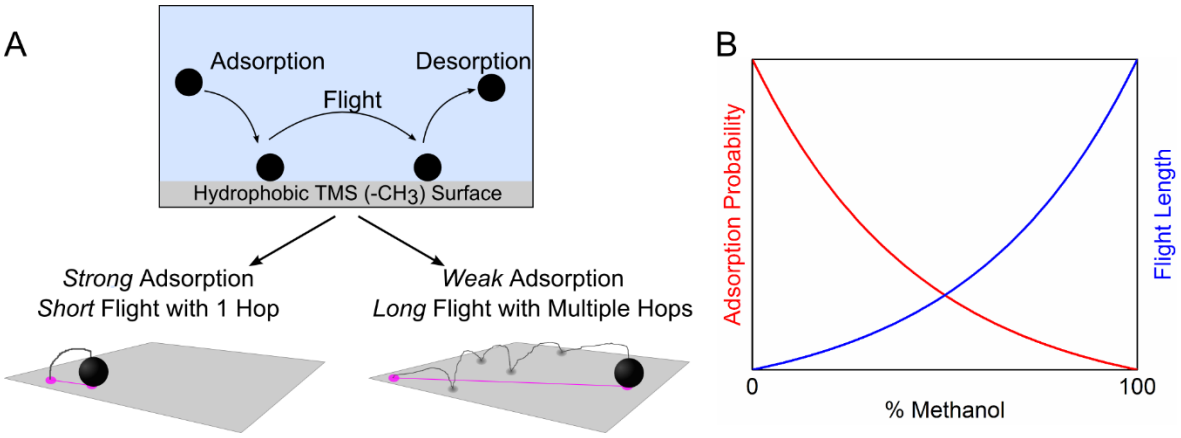

Figure 3.1: Schematic depiction of surface diffusion. (A) Molecules undergoing bulk-mediated surface diffusion and (B) the expected sensitivity of adsorption probability and flight length to the methanol content of an aqueous solution. These qualitative relationships apply to a nonpolar adsorbate molecule undergoing bulk-mediated diffusion on a hydrophobic solid surface.

We depict the mechanistic relationship between adsorption kinetics and flight lengths in Figure 3.1 If the (re-)adsorption probability is unity, flights are short in length because a flight is terminated the first time the molecule, diffusing in bulk solution, encounters the surface. When the adsorption probability is less than unity, the diffusing molecule may encounter the surface without re-adsorbing, thus executing a *hop* across the surface. When multiple *hops* can comprise a single *flight*, the flight lengths increase. At the solid-liquid interface, the adsorption probability is orders of magnitude less than unity, so that a diffusing molecule may have many interactions with the surface prior to adsorption.[31-32] The system studied here was comprised of a largely nonpolar fluorescent BODIPY C_{12} fatty acid (BFA) probe molecule and a hydrophobic trimethylsilane (TMS) surface in methanol-water solutions. Methanol is commonly added to modify the polarity of

aqueous solutions, especially for liquid chromatography,[33] and the adsorption rate constant of nonpolar adsorbates to hydrophobic surfaces is known to decrease logarithmically with the volumetric concentration of methanol.[34-35] In this work, we studied the molecular mobility of molecules over the range 0% to 50% methanol by volume, over which re-adsorption rates were high enough for bulk-mediated diffusion to be significant. At these methanol concentrations, the attachment rate was so high that the bulk solution actually became depleted of molecules; without knowledge of the bulk adsorbate concentration, the adsorption rate constant cannot be simply calculated.[21] However, extrapolating from previous measurements,[21] we could be confident that the adsorption rate constants varied by several orders of magnitude over the range of conditions studied.

The adsorbed molecules switched between two qualitatively different behaviors: confinement and mobility (Figure 3.2A). As the methanol content of the solution was varied, the frequency of confinement and characteristic step sizes both appeared to change. When the frequency of confinement was high, molecules often remained confined the duration of the trajectory and had small radii of gyration. These types of trajectories (far left side of the plots in Figure 3.2A) were common in 0% and 50% methanol but were not observed in 25% methanol. We verified that the molecules were actually physically confined, and not simply diffusing slowly, by examining the lag-time dependence of the step-size distributions (Figure 3.2B). The statistical signature of confinement was a peak in the step-size distribution, at small r as annotated in Figure

3.2B, that did not broaden at longer lag times. Not all trajectories contained long periods of confinement, however; these trajectories, with larger radii of gyration, were placed at the bottom of the plots in Figure 3.2A. The steps composing these trajectories increased in length monotonically from 0% to 50% methanol, consistent with the expectation that flight lengths increase as the re-adsorption probability decreases, as depicted in Figure 3.1B. Further evidence of flying motion was apparent in the step-size distributions, which exhibited a power law tail at the shortest lag time (0.115 s) that transformed to a Gaussian tail at longer lag times (Figure 3.2B). This feature of the step-size distributions was consistent with previous observations and modeling of desorption-mediated diffusion i.e. flying motion.[20,29]

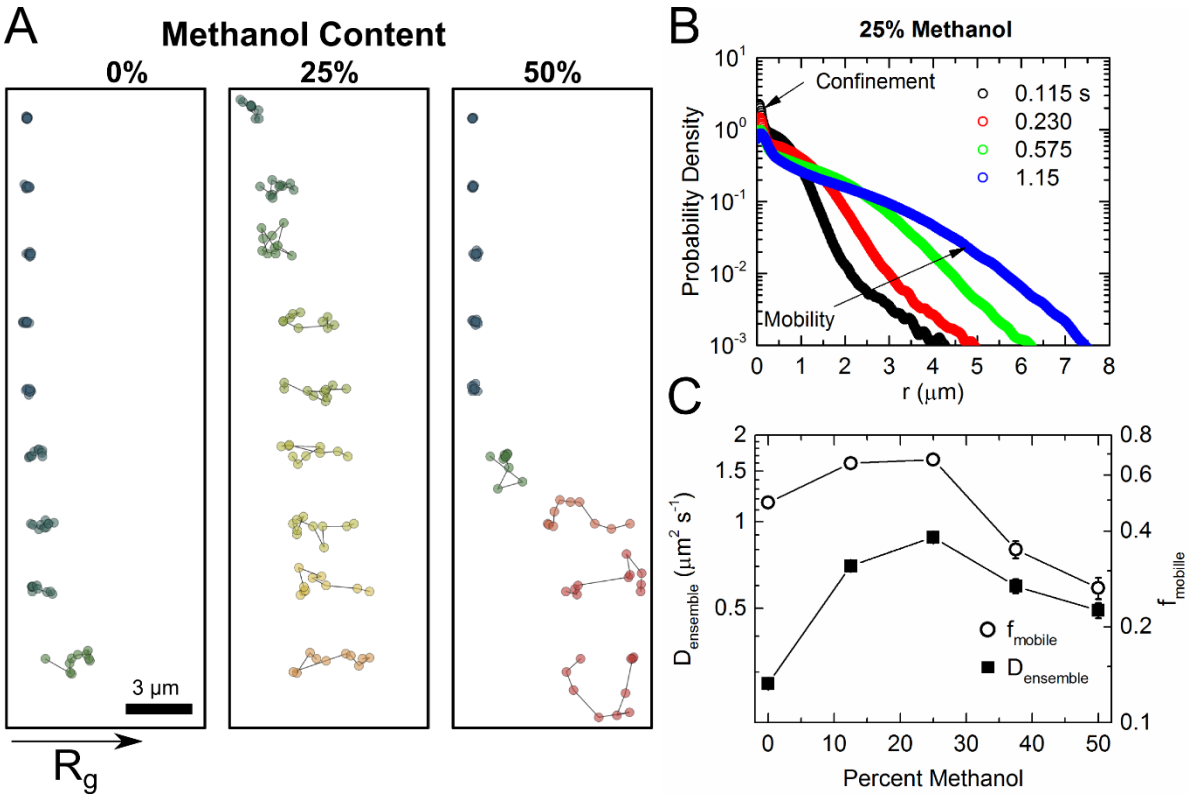

Figure 3.2: Selected trajectories and detailed statistics of surface diffusion in different solutions. (A) Randomly selected trajectories (each 10 frames or 1.15 s in length) in aqueous solutions with indicated percent methanol by volume. The trajectories were colored and positioned on the x-axis based on their respective radii of gyration (R_g). (B) Step-size distributions in 25% methanol, measured at the indicated lag time and (C) ensemble-averaged diffusion coefficients and fraction of steps characteristic of mobility (flying), from trajectories exhibiting mobility (end-to-end distance > 200 nm).

Fitting the step-size distributions by Equation 3.3 provided the fraction of steps representing mobility (f_{mobile}) (Figure 3.2C) and confinement ($1 - f_{mobile}$). The detailed fitting procedure is presented in the SI (Figure B1–B5 and Tables B2–B2). The fraction of time molecules spent confined ($1 - f_{mobile}$) had the same non-monotonic dependence on solution methanol content apparent in the representative trajectories of Figure 3.2A. In general, adsorbate-surface interactions are very sensitive to the fine chemical environment, and the chemical properties of methanol-water solutions near alkyl-coated

silica are very non-ideal.[34] For example, the excess adsorption of methanol varies non-monotonically with concentration, with a maximum at about 40% methanol by volume.[36-37] It was expected, therefore, that anomalous adsorbate-surface interactions might peak at intermediate methanol concentrations, leading to increased confinement on anomalous surface sites. Indeed, the frequency of confinement correlated strongly with the probability of molecular adsorption onto anomalously strong surface sites (Figure B7–B8, Table B3). We previously observed that molecules remained bound for longer times on these anomalous sites on TMS and that the frequency of adsorption onto these sites varied strongly with solution conditions.[21-22] The long periods of confinement evident in the trajectories were clearly associated with specific areas of the surface, which was noted in other studies of surface diffusion, as well.[18,32] The consequence of confinement at the macroscopic level was slower overall transport. Interestingly, when confinement increased, the scaling exponent of the mean squared displacement as a function of time decreased (Figure B6), from a maximum of 0.97(2) at 25% methanol to 0.72(3) at 50% methanol. The average diffusion coefficient $D_{ensemble}$ also decreased from ~0.8 $\mu m^2 s^{-1}$ at 25% methanol to ~0.3 $\mu m^2 s^{-1}$ at 50% methanol.

Clearly, the confinement arising from microscopic surface heterogeneity affected the average mobility of molecules. The variation in $D_{ensemble}$ was strongly correlated with f_{mobile} (Figure 3.2C). However, this correlation explained only some of the variability of $D_{ensemble}$ (Pearson correlation coefficient = 0.56), suggesting that the flight length distribution was also changing with solution polarity. The shift in flight lengths with

solution condition was visually evident in the 27 representative trajectories (Figure 3.2A) as previously discussed. To provide quantitative evidence of the increase in flight length with increasing methanol concentration, we fit the broad tails of the step-size distributions using a mixture of Gaussian distributions and then found the weighted average diffusion coefficient, D_{mobile}. D_{mobile} scales with the flight lengths, and as expected from theory presented in Figure 3.1, we found that D_{mobile} increased monotonically as the methanol content of the aqueous solutions increased and the adsorption probability decreased (Figure 3.3A). The rate of increase in D_{mobile} diminished at higher methanol concentrations, indicating that the characteristic flight lengths were approaching the maximum measurable displacement r_{max}. The finite field of view and nearest-neighbor tracking algorithm (see Experimental Methods) limited the maximum displacement that could be measured by single-molecule tracking, and so the apparent changes in D_{mobile} may not have fully reflected increases in characteristic flight length at higher methanol concentrations. Nonetheless, the mobility of the molecules showed the expected dependence on adsorption probability.

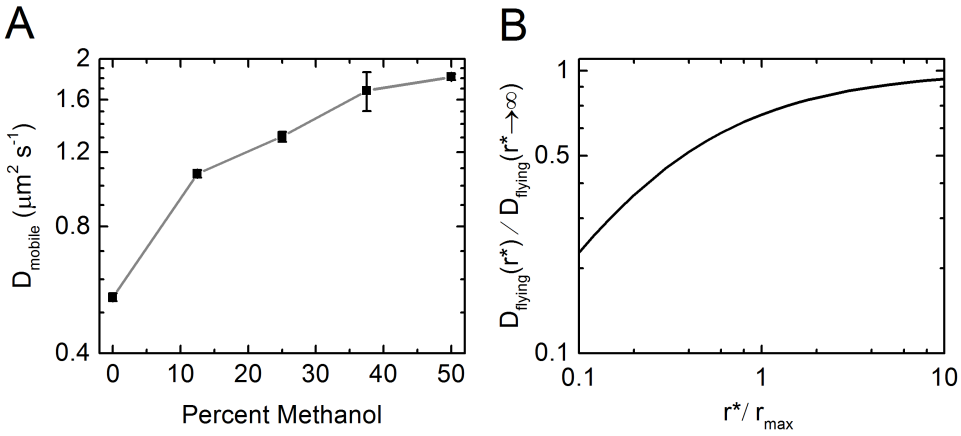

Figure 3.3 Flying mode diffusion coefficients. (A) Weighted average diffusion coefficient from fitting the tails of the step-size distributions of mobile molecules in various methanol-water solutions (see Figure B5 and Table B2). (B) Scaling of diffusion coefficient from the theoretical description (Equation B4) of bulk-mediated diffusion (flying) as a function of adsorption probability~ $(r^*)^{-1}$.

Since the flight length distribution has been derived analytically (Equation B3),[30] we are able to compare the experimental results to theory. The theoretical step-size distribution for flying molecules is expressed in terms of a characteristic length scale $r^* \sim$ (*adsorption probability)*$^{-1}$. In Figure 3.3B, we show how the diffusion coefficient for flying motion D_{flying} depends on r^*, when steps can be measured up to a finite tracking radius (r_{max}) (Equation B4). Basically, D_{flying} increases as r^* increases ultimately saturates for $r^* >> r_{max}$. The theoretical dependence of the flying mode diffusion coefficient on the adsorption probability is quite similar to that observed experimentally (characterized by D_{mobile}). This agreement between experiment and theory provides further evidence that bulk-mediated surface diffusion dominates interfacial diffusion at solid-liquid interfaces when there is a significant driving force for re-adsorption, such as hydrophobic[21,29] or electrostatic effects.[28]

In summary, we have developed a robust statistical approach to characterize diffusion on heterogeneous surfaces when molecules exhibit both confined and bulk-mediated (flying) surface diffusion modes. The presence of anomalous surface binding sites primarily determined the relative frequencies of the two modes, with confinement increasing as the surface adsorption became more heterogeneous. Flying molecules likely encountered the surface many times prior to re-adsorption, and so the average surface interaction determined the flight lengths. In this system dominated by hydrophobic interactions, flight lengths increased as the solvent polarity and adsorption probability decreased, and the measured surface diffusion coefficients for flying molecules agreed with theoretical predictions. This strategy of altering solution conditions to control adsorption probabilities and the rate of desorption-mediated surface diffusion can be applied quite generally. We expect our improved understanding of surface diffusion to enable the stepwise, isothermal control of molecular self-assembly at solid surfaces and the optimization of molecular searching processes.

3.3 EXPERIMENTAL METHODS

The experimental system was recently described in detail in Mabry, *et. al.*[21] Using total internal reflection fluorescence microscopy, we collected image sequences of BFA (Invitrogen) molecules adsorbed to the planar interface of a water-methanol solution and a fused silica wafer coated with a TMS monolayer to render it hydrophobic (water contact angle 91° ± 1°). Molecules in solution underwent diffusion that was much faster

($D \sim 10^2$ μm^2 s^{-1})[38] than for molecules on the surface, and so only adsorbed molecules were distinguished from background fluorescence in these images with 0.115s acquisition times. The bulk concentration of BFA was chosen to achieve extremely dilute surface coverage of adsorbed molecules (~0.01 molecules μm^{-2}) and ranged from 0.1 pM to 1 nM. Low surface coverage was necessary so that individual molecular trajectories did not overlap. Using custom Mathematica programs, we identified the positions of individual adsorbed molecules in each image and then tracked the molecules from frame-to-frame by connecting nearest-neighbor objects within a radius r_{max} = 5.8 μm. Trajectories greater than 10 frames in length were selected for subsequent analysis to minimize the effects of falsely identified molecules[20] and to allow us to distinguish molecules that remained confined for their entire trajectory by end-to-end distance (Figure B1). For each solution condition, we analyzed >10^3 molecular trajectories and could gain detailed insight into the statistics of surface diffusion.

At short timescales, the statistics of molecular motion are sensitive to the underlying mechanism, and the spatial position evolves over time according to the relevant distribution.[23] For heterogeneous systems, one of the simplest descriptions of the molecular motion comes from assuming that a molecule can exhibit multiple modes of Gaussian diffusion. The distribution of displacements of length R observed over time Δt can be described by a Gaussian mixture distribution that is simply the weighted sum of the component distributions.

$$p(R,\Delta t) = \frac{R}{2\Delta t}\sum_{i=1}^{n} f_i D_i^{-1} e^{-\frac{R^2}{4D_i\Delta t}} \quad (3-1)$$

Fitting to a complementary cumulative distributions of squared displacements minimizes fitting error, and the relevant form of the Gaussian mixture model is given by

$$p(R^2 \geq r^2,\Delta t) = \sum_{i=1}^{n} f_i e^{-r^2/(4D_i\Delta t)} \quad (3-2)$$

Each mode of diffusion has a characteristic diffusion coefficient D_i and is responsible for a fraction f_i of all observed steps. The average diffusion coefficient $\overline{D}$ is given by $\sum_i f_i D_i$. In this work, the model was fit to steps observed over lag time Δt = 0.115 s. Because molecules switched between periods of confinement and mobility, we fit the step size distributions using a more sophisticated model that accounted for both behaviors.

$$p_{ensemble}(R,\Delta t) = f_{confined} p_{confined}(R,\Delta t) + f_{mobile} p_{mobile}(R,\Delta t) \quad (3-3)$$

The constraint was imposed that $f_{confined}$ and f_{mobile} sum to unity. The step-size distributions of confined molecules $p_{confined}$ and mobile molecules p_{mobile} were of the form of Equation 3.1. The function $p_{confined}$ was determined by fitting the step-size distributions of molecules with end-to-end distances less than 50 nm (Figure B2–B4 and Table B1) for each condition. Because these molecules were confined and the apparent diffusion coefficient was not independent of lag time, the relevant descriptor of them was the length scale of confinement $\ell_{confined} = \sqrt{4D_{confined}\Delta t}$. To characterize molecular mobility, the step-size distributions of molecules with end-to-end distance > 200 nm (see Fig B1 for details on selection of this subset) were then fit to Equation 3.3 with $P_{confined}$

fixed as described. The weighted average diffusion coefficient determined from fitting of p_{mobile} was referred to as D_{mobile}. The apparent ensemble-averaged diffusion coefficient was given by $D_{ensemble} = f_{confined}D_{confined} + f_{mobile}D_{mobile}$.

3.4 REFERENCES

1. Woo, S.; Rothemund, P. W. K., Self-assembly of two-dimensional DNA origami lattices using cation-controlled surface diffusion. *Nat Commun* **2014,** *5*.
2. Schunack, M.; Linderoth, T. R.; Rosei, F.; Lægsgaard, E.; Stensgaard, I.; Besenbacher, F., Long Jumps in the Surface Diffusion of Large Molecules. *Phys. Rev. Lett.* **2002,** *88* (15), 156102.
3. Honciuc, A.; Harant, A. W.; Schwartz, D. K., Single-molecule observations of surfactant diffusion at the solution-solid interface. *Langmuir* **2008,** *24* (13), 6562-6566.
4. Lomholt, M. A.; Koren, T.; Metzler, R.; Klafter, J., Levy strategies in intermittent search processes are advantageous. *Proc. Natl. Acad. Sci. U. S. A.* **2008,** *105* (32), 11055-11059.
5. Calandre, T.; Bénichou, O.; Grebenkov, D. S.; Voituriez, R., Splitting probabilities and interfacial territory covered by two-dimensional and three-dimensional surface-mediated diffusion. *Physical Review E* **2014,** *89* (1), 012149.
6. Bénichou, O.; Loverdo, C.; Moreau, M.; Voituriez, R., Intermittent search strategies. *Rev. Mod. Phys.* **2011,** *83* (1), 81--129.
7. Benichou, O.; Loverdo, C.; Moreau, M.; Voituriez, R., Optimizing intermittent reaction paths. *PCCP* **2008,** *10* (47), 7059-7072.
8. Loverdo, C.; Benichou, O.; Moreau, M.; Voituriez, R., Enhanced reaction kinetics in biological cells. *Nature Physics* **2008,** *4* (2), 134-137.
9. Krapivsky, P. L., Kinetics of monomer-monomer surface catalytic reactions. *Phys. Rev. A* **1992,** *45* (2), 1067-1072.
10. Chan, V.; Graves, D. J.; McKenzie, S. E., The biophysics of DNA hybridization with immobilized oligonucleotide probes. *Biophys. J.* **1995,** *69* (6), 2243-2255.
11. Ulman, A., Formation and Structure of Self-Assembled Monolayers. *Chem. Rev.* **1996,** *96* (4), 1533-1554.
12. Bae, S. C.; Granick, S., Molecular motion at soft and hard interfaces: from phospholipid bilayers to polymers and lubricants. *Annu. Rev. Phys. Chem.* **2007,** *58*, 353-374.
13. Sukhishvili, S. A.; Chen, Y.; Muller, J. D.; Gratton, E.; Schweizer, K. S.; Granick, S., Materials science - Diffusion of a polymer 'pancake'. *Nature* **2000,** *406* (6792), 146-146.

14. Sukhishvili, S. A.; Chen, Y.; Muller, J. D.; Gratton, E.; Schweizer, K. S.; Granick, S., Surface diffusion of poly(ethylene glycol). *Macromolecules* **2002,** *35* (5), 1776-1784.
15. Sriram, I.; Walder, R.; Schwartz, D. K., Stokes-Einstein and desorption-mediated diffusion of protein molecules at the oil-water interface. *Soft Matter* **2012,** *8* (22), 6000-6003.
16. Swinton, D. J.; Wirth, M. J., Lateral diffusion of 1,1 '-dioctadecyl-3,3,3 ' 3 '-tetramethylindocarbocyanine perchlorate at the interfaces of C-18 and chromatographic solvents. *Anal. Chem.* **2000,** *72* (16), 3725-3730.
17. Wirth, M. J.; Legg, M. A., Single-molecule probing of adsorption and diffusion on silica surfaces. *Annu. Rev. Phys. Chem.* **2007,** *58*, 489-510.
18. Wirth, M. J.; Swinton, D. J.; Ludes, M. D., Adsorption and diffusion of single molecules at chromatographic interfaces. *J. Phys. Chem. B* **2003,** *107* (26), 6258-6268.
19. Wang, B.; Kuo, J.; Bae, S. C.; Granick, S., When Brownian diffusion is not Gaussian. *Nature Materials* **2012,** *11* (6), 481-485.
20. Skaug, M. J.; Mabry, J.; Schwartz, D. K., Intermittent Molecular Hopping at the Solid-Liquid Interface. *Phys. Rev. Lett.* **2013,** *110* (25).
21. Mabry, J. N.; Skaug, M. J.; Schwartz, D. K., Single-Molecule Insights into Retention at a Reversed-Phase Chromatographic Interface. *Anal. Chem.* **2014,** *86* (19), 9451-9458.
22. Langdon, B. B.; Mirhossaini, R. B.; Mabry, J. N.; Sriram, I.; Lajmi, A.; Zhang, Y.; Rojas, O. J.; Schwartz, D. K., Single-Molecule Resolution of Protein Dynamics on Polymeric Membrane Surfaces: The Roles of Spatial and Population Heterogeneity. *ACS Applied Materials & Interfaces* **2015,** *7* (6), 3607-3617.
23. Bychuk, O. V.; O'Shaughnessy, B., Anomalous diffusion at liquid surfaces. *Phys. Rev. Lett.* **1995,** *74* (10), 1795--1798.
24. Bychuk, O. V.; O'Shaughnessy, B., Anomalous diffusion of surface-active species at liquid-fluid and liquid-solid interfaces. *J. Phys. II France* **1994,** *4*, 1135-1156.
25. Bychuk, O. V.; Oshaughnessy, B., Anomalous Surface-Diffusion - a Numerical Study. *J. Chem. Phys.* **1994,** *101* (1), 772-780.
26. Yu, C.; Guan, J.; Chen, K.; Bae, S. C.; Granick, S., Single-Molecule Observation of Long Jumps in Polymer Adsorption. *ACS Nano* **2013,** *7* (11), 9735-9742.
27. Wang, D.; He, C.; Stoykovich, M. P.; Schwartz, D. K., Nanoscale Topography Influences Polymer Surface Diffusion. *ACS nano* **2015,** *9* (2), 1656-1664.
28. Tauzin, L. J.; Shuang, B.; Kisley, L.; Mansur, A. P.; Chen, J. X.; de Leon, A.; Advincula, R. C.; Landes, C. F., Charge-Dependent Transport Switching of Single Molecular Ions in a Weak Polyelectrolyte Multilayer. *Langmuir* **2014,** *30* (28), 8391-8399.
29. Skaug, M. J.; Mabry, J. N.; Schwartz, D. K., Single-Molecule Tracking of Polymer Surface Diffusion. *J. Am. Chem. Soc.* **2014,** *136* (4), 1327-1332.
30. Chechkin, A. V.; Zaid, I. M.; Lomholt, M. A.; Sokolov, I. M.; Metzler, R., Bulk-mediated diffusion on a planar surface: Full solution. *Physical Review E* **2012,** *86* (4).
31. Jung, L. S.; Campbell, C. T., Sticking Probabilities in Adsorption from Liquid Solutions: Alkylthiols on Gold. *Phys. Rev. Lett.* **2000,** *84* (22), 5164-5167.

32. Cooper, J. T.; Harris, J. M., Imaging Fluorescence-Correlation Spectroscopy for Measuring Fast Surface Diffusion at Liquid/Solid Interfaces. *Anal. Chem.* **2014,** *86* (15), 7618-7626.
33. Handbook of HPLC. In *Chromatogr. Sci. Ser.*, 2nd ed.; Taylor & Francis: Boca Raton, 2010.
34. Rafferty, J. L.; Siepmann, J. I.; Schure, M. R., Mobile phase effects in reversed-phase liquid chromatography: A comparison of acetonitrile/water and methanol/water solvents as studied by molecular simulation. *J. Chromatogr. A* **2011,** *1218* (16), 2203-2213.
35. Horvath, C.; Melander, W.; Molnar, I., Solvophobic Interactions in Liquid-Chromatography with Nonpolar Stationary Phases. *J. Chromatogr.* **1976,** *125* (1), 129-156.
36. Bocian, S.; Vajda, P.; Felinger, A.; Buszewski, B., Effect of End-Capping and Surface Coverage on the Mechanism of Solvent Adsorption. *Chromatographia* **2010,** *71*, S5-S11.
37. Gritti, F.; Kazakevich, Y. V.; Guiochon, G., Effect of the surface coverage of endcapped C-18-silica on the excess adsorption isotherms of commonly used organic solvents from water in reversed phase liquid chromatography. *J. Chromatogr. A* **2007,** *1169* (1-2), 111-124.
38. Horn, D.; Klingler, J.; Schorf, W.; Graf, K., Experimental progress in the characterization of colloidal systems. *Structure, Dynamics and Properties of Disperse Colloidal Systems* **1998,** *111*, 27-33.

CHAPTER 4: CAPTURING CONFORMATION-DEPENDENT MOLECULE-SURFACE INTERACTIONS WHEN SURFACE CHEMISTRY IS HETEROGENEOUS

Publication:

Mabry, J. N.; Kastantin, M.; Schwartz, D. K. Capturing Conformation-Dependent Molecule-Surface Interactions when Surface Chemistry Is Heterogeneous. Submitted.

4.1 ABSTRACT

Molecular building blocks, such as carbon nanotubes and DNA origami, can be fully integrated into electronic and optical devices if they can be assembled on solid surfaces using biomolecular interactions. However, the conformation and functionality of biomolecules depend strongly on the local chemical environment, which is highly heterogeneous near a surface. To help realize the potential of biomolecular self-assembly, we introduce here a technique to spatially map molecular conformations and adsorption,

based on single-molecule fluorescence microscopy. On a deliberately patterned surface, with regions of varying hydrophobicity, we characterized the conformations of adsorbed helicogenic alanine-lysine co-peptides using Förster Resonance Energy Transfer. The peptides adopted helical conformations on hydrophilic regions of the surface more often than on hydrophobic regions, consistent with previous ensemble-averaged observations of α-helix surface stability. Interestingly, this dependence on surface chemistry was not due to surface-induced unfolding, as the apparent folding and unfolding dynamics were usually much slower than desorption. The most significant effect of surface chemistry was on the adsorption rate of molecules as a function of their initial conformational state. In particular, regions with higher adsorption rates attracted more molecules in compact, disordered coil states, and this difference in adsorption rates dominated the average conformation of the ensemble. The correlation between adsorption rate and average conformation was also observed on nominally uniform surfaces. Spatial variations in the functional state of adsorbed molecules would strongly affect the success rates of surface-based molecular assembly and can be fully understood using the approach developed in this work.

4.2 INTRODUCTION

Biological recognition mechanisms, such as DNA hybridization and antibody-antigen binding, can be exquisitely selective and enable facile assembly of nanodevices[1-3] and programmable materials.[4-6] The specificity of the biomolecular interactions arises

because the interacting molecules adopt well-defined secondary structures, such as α-helices in the case of coiled-coil peptide interactions.[7] If biomolecule secondary structure can be retained in the vicinity of a surface, then device building blocks can be reliably positioned and oriented on solid planar substrates via biomolecular recognition.[8-9] Many important sensing mechanisms also rely on biomolecular interactions at interfaces, for example in DNA and peptide microarrays.[10-11] However, the structure of biological macromolecules near interfaces can be different from the bulk structure due to confinement effects and also can be sensitive to surface chemistry.[12-15] Surface-induced effects on biomolecule conformation present a challenge to the bottom-up assembly of hierarchical devices on solid substrates because most of our understanding of biomolecular interactions is based on solution measurements.[16-17] Furthermore, while solutions are relatively homogeneous, solid surfaces are very heterogeneous chemical environments due to variations in local surface chemistry[18-19] and interfacial structuring of the solvent environment.[20-22] Lateral heterogeneity of surface chemistry presents a particularly difficult challenge to the self-assembly of large-scale devices.

The detailed chemical microenvironment in technologically and biologically important systems is generally unknown *a priori*, and so there is an acute need for methods that can study the dynamics of molecules while properly accounting for environmental heterogeneity.[23] For surfaces, a variety of chemical imaging techniques exist,[24] and low-throughput scanning probe measurements can examine the conformations of relatively static molecular species.[8,25-26] Here, we present a unified technique, based on single-

molecule total internal reflection fluorescence microscopy (smTIRFM), for simultaneously mapping a surface and extracting thousands of highly dynamic, single-molecule observations from distinct regions that are identified. This approach is an extension of the previously developed technique, known as Mapping using Accumulated Probe Trajectories (MAPT). MAPT can distinguish different regions of a surface based on the dynamics of probe molecules, including adsorption, desorption, and interfacial diffusion.[27] We have extended MAPT imaging to use molecular conformation (specifically molecular end-to-end distance) as a measure of surface functionality, both for the purpose of surface characterization and as a way to study conformational dynamics of adsorbed macromolecules on heterogeneous surfaces. We measured relative end-to-end distances for adsorbed molecules using Förster Resonance Energy Transfer (FRET), which is sensitive to distance changes over the 1 – 10 nm range.[28] To validate our approach, we correlated observations on a deliberately patterned surface with uniform surfaces of the same surface chemistry. The molecular probe was a helicogenic peptide, which freely adsorbed onto hydrophilic fused silica (FS) and hydrophobic trimethylsilyl (TMS) surfaces. This particular combination of surface chemistries can be patterned with e-beam lithography and has been used to direct interfacial assembly of biomolecular building blocks, including DNA origami.[8,29-30] More generally, by developing a new spatially resolved, single-molecule technique to study molecular conformation, we can better understand the effect of surface heterogeneity on the structure of freely adsorbing molecules.

4.3 RESULTS AND DISCUSSION

4.3.1 Peptide Conformation in Solution and on the Surface

We examined the conformation of short adsorbed peptides, rich in alanine with lysine residues included to confer solubility (specific sequence given in Methods). Peptides with such sequences are known to be strong α-helix formers in solution.[31-32] As depicted in Figure 1, the peptide was end-labeled with donor dye (HiLyte Fluor 488) on the N-terminus and acceptor dye (HiLyte Fluor 594) on the C-terminus so that, upon excitation of the donor dye, the end-to-end distance could be monitored with FRET. To characterize the solution conformation of the peptide, we performed circular dichroism (CD) spectroscopy of the peptide solution and found that the spectra could be fit reasonably well using a linear combination of helix and coil reference spectra (Figure C1). Based on this fit, we estimated that the ensemble-averaged α-helical content of the peptides in solution was ~40% at room temperature. The conformational heterogeneity of alanine-rich helical peptides has been an active area of both theoretical and experimental research over the last two decades.[31-41] A broad distribution of conformations exist at intermediate fractional helicities for peptides that are approximately 20 residues in length, and the kinetics of the conformational state transitions are strongly sequence-dependent.[36,40-41] However, the two-state approximation of single-helix structures in equilibrium with coil structures is widely accepted.[33,36,38] Importantly, atomistic simulations show that the average end-to-end distance for the single-helix population is significantly longer than the average-end-to-end distance for the coil population, even

with some fraying of the helix ends, at temperatures where the overall helical content is approximately 40%.[33]

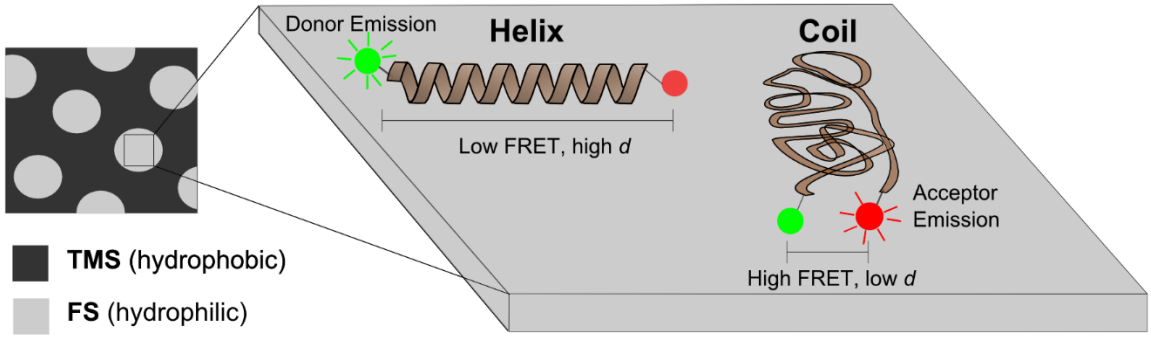

Figure 4.1: Schematic of mapping technique. On a heterogeneous surface — hydrophobic trimethylsilyl (TMS) with defined hydrophilic fused silica (FS) regions — single molecule observations were accumulated in specific regions (pixels). Peptide end-to-end distance d was identified by Förster Resonance Energy Transfer (FRET) between a donor dye at the N-terminus and an acceptor dye at the C-terminus. The end-to-end distance was large for a peptide in the helix state, resulting in low FRET efficiency; for the majority of possible coil conformations, the end-to-end distance was shorter, resulting in high FRET efficiency. The conformations of adsorbed peptides depicted in this scheme are idealized representations for illustrative purposes.

Adsorption of a peptide to a solid surface changes the free energy landscape with respect to molecular conformation. For example, hydrophilic silica surfaces, which are negatively charged at neutral pH,[19] can stabilize helical conformations of peptides containing positively-charged residues such as lysine through electrostatic interactions.[42-43] In contrast, the helical content of peptides generally decreases upon adsorption to hydrophobic materials, such as carbon nanotubes,[16,44-45] unless the peptide has been carefully designed to be amphiphilic.[46-47] For many proteins, including bovine serum albumin and fibrinogen, more secondary structure is lost upon adsorption to hydrophobic surfaces than to hydrophilic surfaces.[48-49] Thus, based on previous literature, we

expected a hydrophilic silica surface to favor helical peptide conformations and a hydrophobic surface to destabilize the helix.

Using smTIRFM, we acquired image sequences at room temperature for each surface studied, in which $>10^6$ peptides were observed to adsorb to the surface, and after finite surface residence times, desorb from the surface. We recorded in separate channels the fluorescence intensity of the FRET donor and acceptor dyes, which were spectrally well-separated. Single-molecule FRET measurements were converted to relative end-to-end distance, *d*, for peptides adsorbed on hydrophilic FS, hydrophobic TMS, and patterned TMS/FS surfaces. In the Methods section we detail the theoretical relationship between *d* and absolute end-to-end distance. In short, *d* equals the absolute end-to-end distance divided by a distance on the order of the Förster radius (~5 nm). The probability distributions of all of observed *d*-values (Figure 4.2A) had similar features on all the surfaces studied. While many molecules had intermediate *d*-values between 0.4 and 1.8 (i.e. the fluorescence intensity of both the donor and acceptor dye was significant), some molecules had extremely high or extremely low apparent *d*-values, as represented by rectangular bins at the ends of the distributions in Figure 4.2A. This measurement artifact largely stemmed from the difficulty of quantifying single-molecule FRET when fluorescence intensity in one channel was very. Thus, the most salient information available from these *d*-distributions was the frequency of low *d*-values compared to the frequency of high *d*-values, i.e. the height of the low *d* peak (centered at d=0.8) and the height of the high *d* peak (centered at d=1.5). The low *d* and high *d* peaks were well-

separated by a threshold of d=1.14 so that two conformational states were readily distinguished. This general approach has previously been applied to understand the conformational states of DNA and proteins.[50-51] The only drawback to this approach was that the fraction of molecules observed in the high d state may have been increased slightly by the presence of molecules labeled with only the donor dye, but this this artifact would not have changed the overall trends reported below with respect to surface chemistry and the kinetics of molecules that changed conformational state.

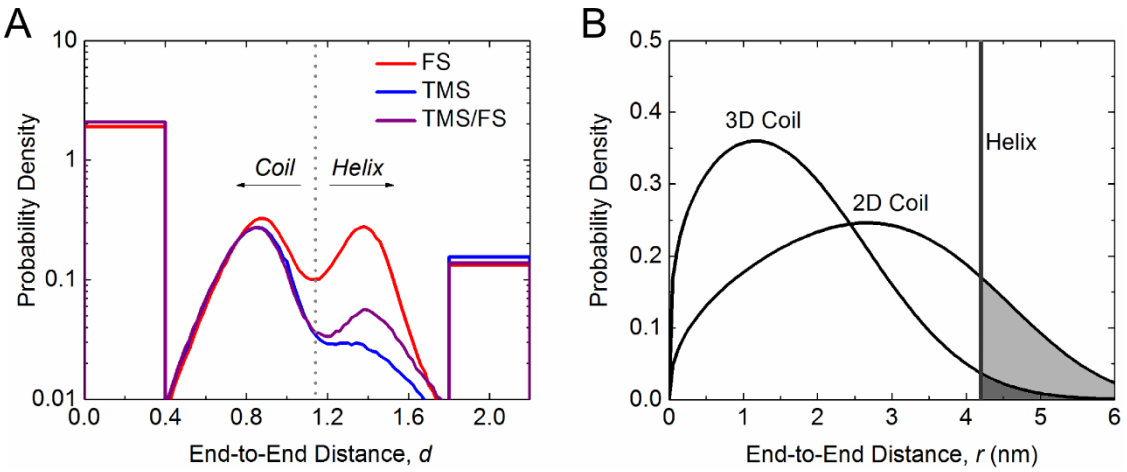

Figure 4.2: Peptide end-to-end distance distributions. (A) Peptide conformation on hydrophobic trimethylsilyl (TMS), hydrophilic fused silica (FS), and a patterned TMS/FS surface. The distributions describe the probability of observing a given relative end-to-end distance, d. The boxes from d = 0 to 0.2 and from d = 1.8 to 2.2 represent adsorbed peptides with negligible intensity in either the acceptor or donor channel, respectively. The area of each box is proportional to the number of molecules in these extreme states. The cumulative area under the boxes and curve integrates to unity. Note that probability is reported on a logarithmic axis to highlight the minima at approximately d = 1.14, which are marked with a dashed vertical line. This value of d was used as a threshold to classify a given observation of peptide conformation as either "coil" (d < 1.14) or "helix" (d > 1.14). (B) Absolute end-to-end distance probability distributions (black curves) for disordered peptide based on a self-avoiding random walk in 2D and in 3D as described in the SI (Equation C2) and the end-to-end distance for the fully helical peptide (gray vertical line).

To assign low *d* and high *d* "states" identified by these distributions to physical molecular conformations, we carefully considered the potential conformations that an adsorbed peptide can adopt. Using NMR spectroscopy, Burkett and Read[52] found that peptides that were strongly helical in solution adopted conformations that, when adsorbed on silica, retained significant helical character, with some helical loss at the peptide termini. Similarly, using molecular dynamics simulations, Gnanakaran[35] and co-workers characterized the conformations of a 20-residue alanine-lysine helical peptide and found that at intermediate temperatures, in the helix-coil transition regime, helical loss was also most significant at the peptide termini. Peptides with significant helical content were considerably longer than the disordered peptides, which had an end-to-end distance distribution resembling that of a compact random coil. Thus, with respect to our experiments, while the adsorbed peptides potentially had a range of fractional helicities, the end-to-end distances were expected to be systematically larger for molecules with more helical structure. For simplicity we refer to more-extended structures as being in the "helix" state, and to less-extended structures as being in the "coil" state throughout the rest of the paper.

If the adsorbed peptides lacked all secondary structure, then the conformation could have resembled either the structure of a disordered a peptide in solution (a three-dimensional coil) or the structure of a two-dimensional "pancake," with longer end end-to-end distances.[53] Using sum frequency generation (SFG) vibrational spectroscopy to investigate adsorbed peptide conformations, Mermut and co-workers found that only

certain side chains (charged, polar side chains on hydrophilic silica and alkyl side chains on hydrophobic polystyrene) had significant interactions with the surface,[54] suggesting that the adsorbed coil conformations of our alanine-lysine peptide were largely three-dimensional in nature. In Figure 4.2B, we present theoretical distributions of the end-to-end distance for two-dimensional and three-dimensional statistical coils and for a fully helical peptide. (The details of these idealized calculations are in the SI.) Fewer than 17% of the two-dimensional coils and 2% of the three-dimensional coils had end-to-end distances greater than the end-to-end distance for a fully helical peptide, as shown graphically in Figure 4.2B by the light and dark gray shaded areas respectively. Thus, it seemed reasonable that helix-rich and coil states could be distinguished by end-to-end distance for the majority of expected conformations, which likely were between the extremes of being purely two-dimensional or purely three-dimensional.

Based on a longstanding model of polymer adsorption, one could also view the adsorbed peptide as a sequence of adsorbed "trains" (finite, continuous sections of the amino acid chain in contact with the surface) and unbound "loops."[55-59] In this picture, the end-to-end distance increases as the number and length of adsorbed trains increases, causing the adsorbed polymer to become more two-dimensional in shape, or when the stiffness of loops increases, causing the spacing between trains to increase. In the special case of amino acid chains, helical structure would cause the stiffness of the chain to increase, increasing the distance between adsorbed segments. Therefore, for helix-rich peptides,

we would again expect the end-to-end distance to be greater than for disordered peptides, in the adsorbed state.

4.3.2 Identifying Distinct Regions of a Heterogeneous Surface

As discussed above, ensemble-averaged measurements have shown that peptides and proteins typically exhibit less secondary structure upon adsorption to more hydrophobic surfaces.[16,44-45,48-49] In our experiments, the measured conformations of the adsorbed peptides were very sensitive to surface chemistry. In particular, the extended helix state (identified in Figure 4.2A) was more strongly favored on hydrophilic FS than on hydrophobic TMS, in qualitative agreement with the previous literature on the impact of surface chemistry on helix stability.[16,42-45,48] The strong effect of surface chemistry on peptide conformation suggested that our single-molecule observations could be used to identify different surface chemistries in a heterogeneous environment based on peptide conformation.

We have adopted the approach of accumulating multivariate, single-molecule observations in spatial bins ("pixels") to construct maps of surface properties. We previously used adsorption, desorption, and diffusion data to construct surface maps,[27,60] and we extended the approach here to FRET data to examine the spatial dependence of molecular conformation. Figure 4.3 shows MAPT images of a photo-patterned surface containing circular FS holes within a TMS matrix. This patterning approach was

independently validated by creating FS circles within a patterned amine-terminated organosilane monolayer to which dye molecules were covalently bound (Figure C2). The MAPT images were assembled based on the adsorption rate and average peptide conformation in individual pixels (760 nm × 760 nm in size). The pixel size was set so that a significant number of molecules were observed in nearly all pixels (pixels with fewer than 3 observations of molecules are shaded grey in Figure 4.3).

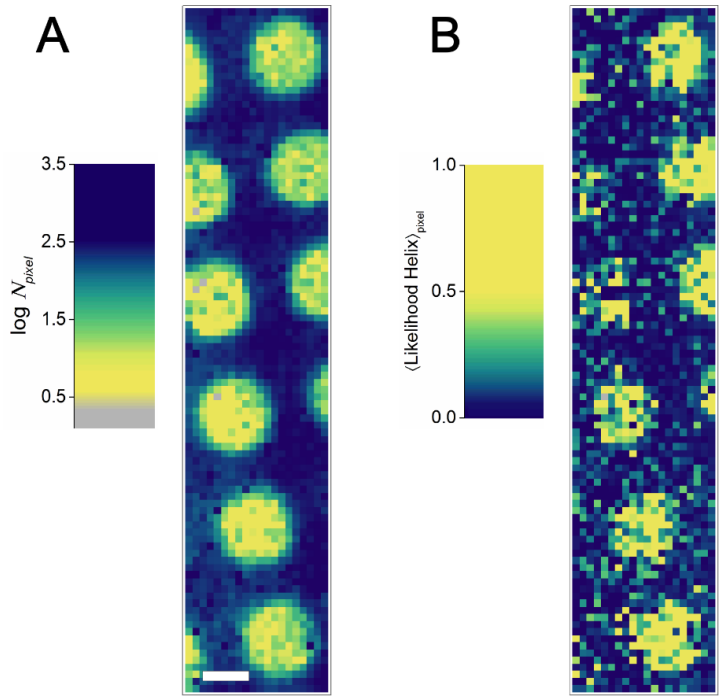

Figure 4.3: MAPT Images. A TMS-coated surface was photo-patterned as described in the Supporting Information (SI), such that circular holes of FS were created in the TMS coating. (A) Map showing the number of molecules that adsorbed in each pixel (N_{pixel}), which was higher on TMS than on FS regions. (B) Map of the likelihood of observing peptides in the helix state in each pixel. Peptides were more commonly found in the helix state on FS than on TMS regions. The scale bar represents 5 µm. The pixel size is 760 nm × 760 nm.

Both images were assembled from the same set of ~300,000 molecular trajectories, and the spatial locations of the underlying surface chemistries were clearly distinguished via the peptide adsorption rate and average conformation. On the TMS regions (blue area), the number of adsorbed molecules (Figure 4.3A) was approximately 100 times greater than on the circular FS regions (yellow area). At the boundaries between the two regions (green area), where the ozone removal of the TMS was likely incomplete, the number of adsorbed molecules was about 10 times greater than on FS. These results agreed qualitatively with previous observations of fatty acid adsorption on TMS/FS surfaces, where more fatty acid adsorption was observed on hydrophobic TMS than on hydrophilic FS regions.[27] The difference in adsorption rates was explained by viewing adsorption as a competition between the adsorbate and solvent to attach to the surface.[61] Because attachment of polar solvent molecules to the surface is less favorable on hydrophobic surfaces, adsorption of the peptide was more favorable on these areas.

Since each spatially resolved peptide observation was classified as either helix or coil on the basis of its FRET signal, the likelihood of observing the helix state was calculated for each pixel individually. The likelihood of observing the helix was the fraction of all observations that were helical. As shown in Figure 4.3B, the likelihood of observing the helix was higher overall in the circular FS regions than in the TMS regions. Compared to the spatial variation of the adsorption behavior on a given surface chemistry, the conformational behavior was more heterogeneous, both on the patterned surface (Figure 4.3) and on the nominally uniform control surfaces (Figures S-3 and S-4). For example,

in Figure 4.3B, some pixels (blue, green) in the circular FS regions had fewer observations of helical peptides than the more typical pixels (yellow) whereas FS regions in the adsorption maps (Figure 4.3A) were much more uniform. Therefore, for purposes of comparing the different surfaces chemistries, we used the more homogeneous adsorption MAPT image (Figure 4.3A) to select regions for comparison to unpatterned (control) FS and TMS surfaces.

Qualitatively, regions of low, intermediate, and high adsorption were distinguished in Figure 4.3A, corresponding to regions with hydrophilic, intermediate, and hydrophobic surface chemistry. We constructed a probability distribution of the number of adsorption events per pixel (Figure 4.4A) and used this distribution to set thresholds for distinguishing these different surface regions of low, medium, and high adsorption rate.

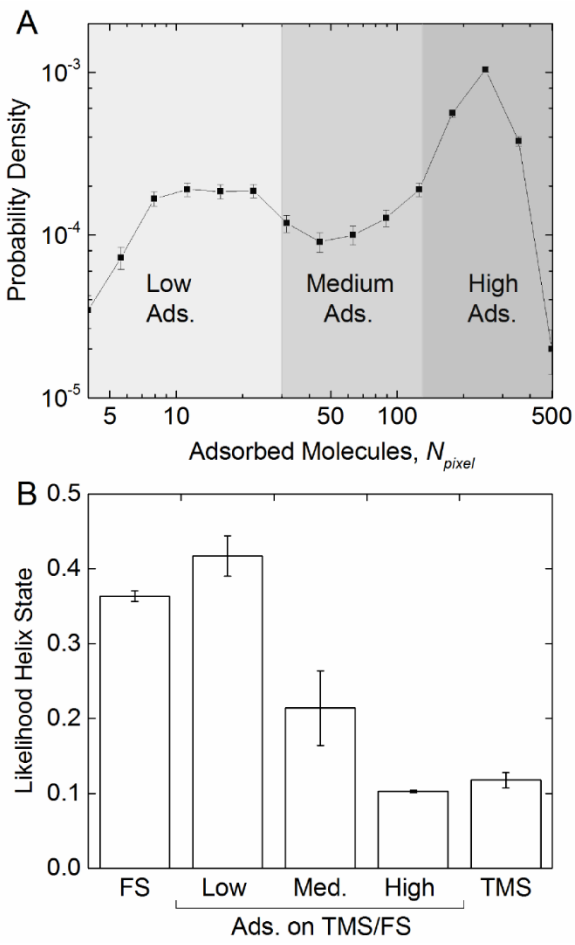

Figure 4.4: Spatial dependence of adsorption and conformational states. (A) Probability distribution of the number of adsorbed molecules per pixel (N_{pixel}) on a patterned TMS/FS surface. The shading indicates subsets of data selected for subsequent analysis corresponding to regions of low, medium, and high adsorption (appearing as yellow, green, and blue in Figure 4.3A), which cover 26%, 16%, and 58% of the total surface area respectively. The low and high adsorption regions were patterned regions of FS and TMS, respectively. The medium adsorption regions were located at the interface between the TMS and FS regions. (B) Likelihood of observing peptides in the helix state on control FS and TMS surfaces and in the regions of the patterned TMS/FS surface with low, medium, and high adsorption. Error bars denote standard error of the mean.

For each of these regions, we calculated the likelihood of observing the helical state, and compared the identified regions of the patterned surface to the control TMS and FS surfaces (Figure 4.4B). We found that the conformations on the high adsorption regions were statistically similar to the control TMS surface and that the low adsorption regions

were similar to the control FS surface. These results demonstrated that statistically meaningful comparisons could be made of molecular conformations on microscopic regions of a heterogeneous surface using the MAPT technique. This validation of the MAPT approach also suggested that the heterogeneity in conformational behavior seen in the circular FS regions of the photo-patterned surface and also seen on the control FS surface (Figure C4) resulted from meaningful differences in surface chemistry, as opposed to having been a statistical artifact.

4.3.3 Contributions of Adsorption/Desorption and Folding/Unfolding Processes to Average Conformation

The difference in conformation (likelihood of the helix state) on the FS and TMS surfaces could potentially have resulted from a number of different physical mechanisms. For example, single-molecule imaging of an adsorbed enzyme, organophosphorus hydrolase, revealed that most proteins that adsorbed in the folded state quickly unfolded prior to desorption.[51] Thus, the initial conformation (measured immediately after adsorption) favored the folded state when compared to the final conformation (measured in the frame prior to desorption). We performed a similar analysis here, comparing the likelihood of observing the helix state immediately after adsorption and immediately prior to desorption (Figure 4.5A). Interestingly, we did not see significant differences between the initial and final conformations of peptides adsorbed to either the TMS or FS surface (Figure 4.5A). This implied that most peptides remained in the same conformation in

which they adsorbed or relaxed to the most favorable conformational state within 100 ms (one frame time) of adsorbing to the surface and then remained in a stable conformation. The prevalence of unfolding processes probably depends on how exactly the molecules become immobilized on the surface. Comparing our current results with peptides to the previous results with proteins,[51] for a large protein, there were many points of potential attachment, which might not have affected the ability of the molecule to unfold, whereas for a small peptide the points of attachment were much more limited, leading to the molecule becoming pinned on the surface and rarely changing conformational state without desorbing.

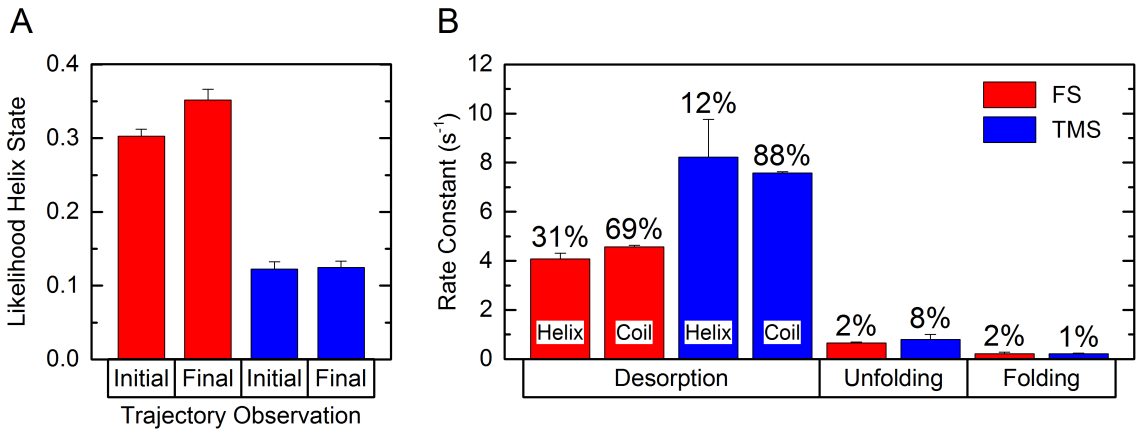

Figure 4.5: Conformational state dynamics. (A) Likelihood of observing the helix state in the "initial" observation for a given trajectory (i.e. the first image after adsorption) and in the "final" observation (i.e. the last image prior to desorption). (B) Mean rate constants of desorption, unfolding from the helix to coil state, and folding from the coil to helix state. Mean rate constants were obtained by fitting the distributions of surface residence times (desorption rate), initial helix states (unfolding rate), and initial coil states (folding rate) as shown in Figure C5 with mixtures of exponential distributions (Eq. 2). The desorption rate constants were calculated separately for molecules initially in the helix state and the coil state, as labeled on the bars. The percentage of molecules undergoing each process is given above the applicable bar. Error bars represent standard error of different subsets of the data.

The average conformational state was not noticeably affected by folding/unfolding processes, which were rare, but it could have been affected by desorption if the average kinetics for desorption depended on the conformation of the molecule, e.g. if coil peptides had longer residence times than helix peptides. In fact, we did not find a significant difference between the average desorption rate constants for molecules that adsorbed in the helix state and molecules that adsorbed in the coil state on either TMS or FS (Figure 4.5B). So the higher likelihood of observing the helix state on FS than on TMS could not be attributed to a large difference in average surface residence times of different conformations. Having eliminated the effects of conformational change and desorption, we therefore concluded that the average likelihood of observing peptides in the helix state was mostly determined by a bias in the initial conformation adopted upon adsorption. In other words, the difference in adsorption rates of the helix and coil peptides determined the average surface conformation, and these adsorption rates had a strong dependence on the surface hydrophobicity. We cannot discern to what extent fast sub-millisecond relaxation processes of the adsorbed peptide contributed to these observations, but the conformations were relatively stable and most of the molecules (~90%) desorbed without changing conformation and followed approximately the same average desorption kinetics regardless of conformation.

4.3.4 Heterogeneous Peptide Behavior on Nominally Uniform Surfaces

The unique advantage of the single-molecule approach is access to the full distribution of molecular behaviors, which can give insight into the effects of fine spatial differences on nominally uniform surfaces. Surface residence time distributions are especially sensitive to surface heterogeneity, and the presence of distinctly different types of surface sites can lead to broadly distributed residence times.[62-64] Therefore, to assess the chemical heterogeneity of nominally uniform surfaces, we fit the surface residence time distribution to mixture models, as described in the Methods section, and examined the populations of surface residence times. While residence time distributions on both TMS and FS surfaces required three populations for an accurate fit, the fraction of molecules exhibiting anomalously long residence times (i.e. belonging to the two longer-lived populations) was ~10% on TMS and greater than 20% on FS (Table C S-1). This agreed with our initial assessment, based on visual inspection of the maps of adsorption and conformation, that FS might be intrinsically more heterogeneous than TMS. Interestingly, the increased presence of long-lived species on FS compared to TMS is supported by previous atomic force microscopy (AFM) measurements.[8] Adsorbed DNA could be observed directly on FS, but remained AFM-invisible on TMS due to fast desorption kinetics. While AFM is undeniably a powerful tool, in an actual molecular device, all species present will contribute to overall performance; clearly, single-molecule imaging can supplement characterization techniques, such as AFM, that are sensitive to different timescales.

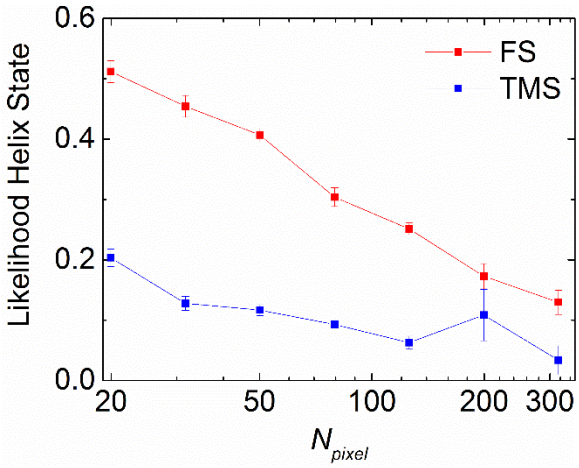

Figure 4.6: Likelihood of helical peptide conformation for observations in adsorption map pixels with N_{pixel} adsorption events. Equivalent surface maps of adsorption were constructed for both surfaces with an average N_{pixel} of 52. Error bars denote standard error.

Surface heterogeneity will have an important effect on surface-based assembly if it alters the spatial distribution of adsorbed, *functional* building block materials (e.g. peptides in the helical state rather than the disordered coil state). While the residence time distributions suggested that the uniform surfaces were chemically heterogeneous, mapping the surface quantified the length-scale of that heterogeneity. In this work, we validated our mapping technique using the patterned TMS/FS surface and showed that adsorption rates and conformational states were sensitive to variations in surface chemistry over microscopic length scales. This approach could be applied with confidence to quantify heterogeneity on the nominally uniform TMS and FS surfaces and to examine the mechanistic effects of surface heterogeneity. To determine if the heterogeneity in the adsorption and conformational behavior was correlated, we calculated the likelihood of the helix state in surface map pixels with different numbers of adsorption events (Figure 4.6). Interestingly, we found that

helical conformations were more likely to be observed than coil conformations on regions with weaker adsorption (lower values of N_{pixel}) on both TMS and FS. We observed a stronger correlation between adsorption rate and conformational state on FS than on TMS, suggesting that FS was less chemically uniform. The chemical heterogeneity of FS might have been due the presence of silanol groups with different characteristic acidities (e.g. isolated, vicinal, or germinal silanols), and this would have affected the behavior of adsorbate molecules because more acidic silanols form stronger hydrogen bonds.[19,65] It is worth noting that this type of chemical heterogeneity often accompanies physical heterogeneity (i.e. topographic features like pits and scratches); on crystalline silica surfaces, different crystal planes are "cut" at these topographic defects, resulting in different characteristic silanol species at the surface.[19] In agreement with this picture, strong adsorption of polar molecules is often correlated with topographic features at the nanoscale, as combined atomic force microscopy and fluorescence imaging have shown.[66] In our system, the TMS coating of FS had the effect of introducing hydrophobic ligands, which capped many of the diverse silanol species. Nevertheless, the same phenomena of helical conformations being more favorable on regions with weaker adsorption was observed on TMS and FS. So while "passivating" layers such as TMS can help reduce spatial heterogeneity, the effect of spatial heterogeneity on conformation and adsorption of macromolecule seems to be quite general in nature.

4.4 CONCLUSION

Using a helical peptide and surfaces with varying hydrophobicity, we have demonstrated the ability to correlate molecular conformation with microscopic regions of a surface. Extended peptide conformations, likely more helical in nature, were more favorable on hydrophilic FS than on hydrophobic TMS at the single-molecule level on patterned surfaces and on uniform control surfaces. The FS surface captured more molecules in the helix state than did TMS, and these conformational states were stable, such that most peptides did not undergo a conformational change prior to desorption from the surface. On FS, extremely long surface residence times were observed relatively often; these rare molecular populations could dominate measurements made over longer time-scales and were indirect evidence of the heterogeneity of the surface. Quantifying the observations made on the surface maps revealed that the helical conformation was more favorable on regions with low adsorption rates. These types of local variations in surface chemistry could strongly affect the ability of adsorbed biomolecules to recognize other biomolecules through specific interactions and cold be important in determining the final structure of self-assembled materials or devices. This type of analysis should prove valuable in characterizing surface coatings designed to promote biomolecular recognition not only for the assembly of molecular building blocks but also for surface-based sensors. Typically, the primary role of the coating is to control adsorption phenomena, but surface-induced denaturation of the molecular building blocks or analytes of interest

is clearly undesirable and seemingly correlated with the adsorption kinetics on the surface. Spatial heterogeneity is an important feature of such coatings, and we have provided a new, rigorous method for fine spatial characterization of surface chemistry. This work demonstrates the importance of considering spatial heterogeneity at microscopic length-scales when interpreting ensemble-averaged experiments and especially when making comparisons to molecular simulations. With this technique in hand, we can harness the unique capabilities of single-molecule imaging for characterizing molecular conformation in diverse biological and functional materials systems.

4.5 METHODS

4.5.1 Solutions of End-Labeled Peptide

A fluorescently labeled peptide (purity >95% by reversed phase high performance liquid chromatography) was purchased from Anaspec (Fremont, CA). The amino acid sequence was AAAKAAKAKAAKAAAAKAAKKAAAAKAK, with an amidated C-terminus, HiLyte Fluor 488 conjugated to the N-terminus and HiLyte Fluor 594 conjugated to the side chain of the C-terminal lysine. For single-molecule imaging experiments, the peptide was dissolved in phosphate buffered saline (Gibco, calcium and magnesium free, pH 7.4, ionic strength 162 mM, Debye length 0.8 nm) to 10^{-9} to 10^{-11} M. Prior to acquiring images, the solution concentration was increased until the field of view had

sufficient densities of adsorbed molecules to provide robust statistics (~10^{-3} molecules μm^{-2}).

4.5.2 Surface Preparation and Characterization

Two-inch diameter fused silica (FS) wafers (Mark Optics) were washed with detergent (Micro 90, International Product Corp) and thoroughly rinsed with ultrapure water with 18 MΩ-cm resistivity (Milli-Q UV Plus, EMD Millipore). Wafers were immediately immersed in a 70% sulfuric acid, 30% hydrogen peroxide, piranha solution (warning: hazardous corrosive, strongly oxidizing solution) for 1 hour, rinsed with ultrapure water, dried with nitrogen, and further cleaned in a UV/ozone cleaner (Novascan) for 1 hour, as previously described.[67] The cleaned wafers were then used as cleaned for experiments with uniform FS. To create a trimethylsilyl (TMS) monolayer, the cleaned wafers were placed in the lid of a sealed 2 inch diameter jar with 5 mL of hexamethyldisilazane in the bottom of the jar for 18 hours at room tempeature. After this deposition, the TMS surface had a static water contact angle of 91° ± 1°, measured with a custom-built goniometer, using an ~1 μL sessile drop on three different positions on the wafer.[68] Using a contact photomask and an ultraviolet light source, the TMS was patterned as described in the SI to create a TMS/FS patterned surface with ~6 μm diameter FS holes every ~13 μm on a square grid.

4.5.3 Single-Molecule Total Internal Reflection Fluorescence Microscopy (TIRFM)

Our TIRF microscope has been described in detail elsewhere.[69-70] Briefly, it consisted of an inverted Nikon TE-2000 microscope with 60X objective with 1.5X auxiliary magnification, prism-based illumination provided by a 491 nm laser, flow cell, an Optosplit III Image Splitter (Cairn Research) and an electron multiplied CCD-camera (Andor). The microscope was focused at the interface between the surface of interest and a stagnant peptide solution, which was held at room temperature. The image was split by a 580 nm dichroic mirror (Chroma) into donor and acceptor channels, which were each projected onto different regions of the CCD sensor. The donor channel was filtered with a bandpass filter with a 95% transmission interval, centered at 525 nm, with a width of 39 nm (Semrock), and the acceptor channel was filtered with a 591 nm longpass filter (Semrock). The channels were aligned and molecules identified as described previously (using an image processing routine where the raw images were convolved with a disk matrix and then thresholded to identify distinct objects).[63,70] Only molecules adsorbed to the interface were localized during image processing because diffusion in solution was too fast to allow localization at the 100 ms frame acquisition times used in these experiments. Previous studies of FS and TMS surfaces have shown that adsorbed molecules are typically confined to regions smaller than the localization precision (~100 nm).[60,71] Molecular trajectories were formed by tracking the closest objects in sequential frames that were less than 445 nm (3 pixels) apart. (The finite tracking radius accounted

for uncertainty in the channel alignment and object localization.) All image processing and object tracking was performed in Mathematica 9 (Wolfram).

4.5.4 Quantification of Förster Resonance Energy Transfer (FRET)

FRET is the nonradiative transfer of energy from a donor to acceptor fluorophore across a distance r with an efficiency that is proportional to r^{-6} and equals 50% at the Förster radius (R_o).[28] For the HiLyte Fluor 488/594 dye pair, we calculated R_o to be 5.1 nm using standard Förster theory (assuming unhindered dye rotation, orientation factor of 2/3) and the published absorption and emission spectra.[72] The absolute donor-acceptor distance is given by

$$r = \mu d = \mu \left({}^{F_D}/_{F_A} \right)^{1/6} \qquad (4.1)$$

where F_D is the fluorescence intensity of the molecule in the donor channel and F_A is the fluorescence intensity in the acceptor channel. The factor $\mu = R_o \left(\frac{F_A|r \to 0}{F_D|r \to \infty} \right)$ depends on the Förster radius and the fluorescence intensities of the donor and acceptor at known separation distances. While the donor fluorescence in the absence of acceptor, $F_D|r \to \infty$, can be empirically measured, the fluorescence of the acceptor in the limit of 100% efficient energy transfer, $F_A|r \to 0$ can be derived only by fixing the dyes with sub-nanometer precision and assuming no donor quenching by non-FRET collisional processes. The efficiency of the resonance energy transfer may also be strongly affected by the presence of the solid surface, which can hinder dye rotation or interact with the

dyes electronically. The absolute values of F_A may also have been slightly increased by bleeding of the donor emission into the acceptor channel; however, this bleed-through effect was found to be minor for spectrally similar donor and acceptor dyes.[73] Due to the significant uncertainty in the parameter μ and the absolute fluorescence intensities, we reported our data using the relative end-to-end distance $d = r/\mu = \left({F_D}/{F_A}\right)^{1/6}$ as in previous single-molecule FRET studies of freely adsorbing molecules.[50-51,70,74]

4.5.5 Calculation of Likelihood of Conformational States

For a dataset with *N* total observations, the likelihood of observing a helix is $n(helix)/N$, where $n(helix)$ is the number of observations of the helix state. For the MAPT images (e.g. Figure 4.3B), we used the notation $\langle Likelihood\ Helix \rangle_{pixel}$ to denote that the likelihood was calculated for observations in each pixel separately. For all other calculations, the data was pooled from either the whole image or pixels with a specific number of adsorption events or from trajectories with specific surface residence times. When comparing the initial and final observations in a trajectory, only trajectories at least 0.2 s (two frames) long were considered.

4.5.6 Characterization of Desorption and Folding/Unfolding Kinetics

For each molecule, the time interval between adsorption and desorption was recorded as the surface residence time t. For each dataset considered, we compiled a complementary cumulative distribution $F(t)$ of residence times. We fit these distributions using an exponential mixture model, where each component distribution represents a distinct first-order kinetic pathway.[75]

$$F(\tau) = \sum_{i=1}^{n} p_i \, e^{-t/\tau_i} \qquad (4.2)$$

Each component distribution of the mixture model had a characteristic residence time τ_i and represented a fraction p_i of the molecules. The distribution was constrained so that $\sum pi = 1$. For a more detailed discussion of the significance of the model and fitting procedure, see Mabry, et. al.[63] We fit the distributions using the minimum number of components necessary for good fits (R-squared > 0.99) to find the average surface residence time, given by $\langle\tau\rangle = \sum p_i \tau_i$. The desorption rate constant was given by $\langle\tau\rangle^{-1}$. To characterize the folding and unfolding kinetics, we measured the initial state residence time of the coil and helix conformational states respectively. We ignored subsequent conformational changes because the probability of observing a subsequent conformational change depends on the length of the trajectory and the previous state residence times, such that the data cannot easily be normalized.[50] We utilized a previously outlined strategy to construct probability distributions of initial state residence times (Eq S-5) , which were corrected for observation bias (the bias to only observe state

residence times shorter than the surface residence times).[50] We fit the initial state residence time distributions to a mixture of exponential distributions in the same manner as the surface residence times and reported the average rate constants derived from these fits. To decrease the effect of anomalously bright, one-frame "noise" objects, we included only surface residence times and initial conformational state times that were 0.2 s or longer. The percentages of molecules undergoing the associated processes of desorption and folding/unfolding were calculated based on the subset of trajectories that could possibly exhibit these phenomena (specifically 0.2 s or longer in the case of desorption and 0.3 s or longer in the case of folding/unfolding).

4.6 REFERENCES

1. Maune, H. T.; Han, S.-p.; Barish, R. D.; Bockrath, M.; Goddard, W. A.; Rothemund, P. W. K.; Winfree, E., Self-assembly of carbon nanotubes into two-dimensional geometries using DNA origami templates. *Nat Nano* **2010,** *5* (1), 61-66.
2. Kuzyk, A.; Schreiber, R.; Fan, Z.; Pardatscher, G.; Roller, E.-M.; Hogele, A.; Simmel, F. C.; Govorov, A. O.; Liedl, T., DNA-based self-assembly of chiral plasmonic nanostructures with tailored optical response. *Nature* **2012,** *483* (7389), 311-314.
3. Hyman, P.; Valluzzi, R.; Goldberg, E., Design of protein struts for self-assembling nanoconstructs. *Proceedings of the National Academy of Sciences* **2002,** *99* (13), 8488-8493.
4. Park, S. Y.; Lytton-Jean, K. R. A.; Lee, B.; Weigand, S.; Schatz, G. C.; Mirkin, C. A., DNA programmable nanoparticle crystallization. *Nature* **2008,** *451*, 553-556.
5. Jones, M. R.; Macfarlane, R. J.; Lee, B.; Zhang, J. A.; Young, K. L.; Senesi, A. J.; Mirkin, C. A., DNA-nanoparticle superlattices formed from anisotropic building blocks. *Nature Materials* **2010,** *9* (11), 913-917.
6. Merzlyak, A.; Lee, S.-W., Phage as templates for hybrid materials and mediators for nanomaterial synthesis. *Curr. Opin. Chem. Biol.* **2006,** *10* (3), 246-252.

7. Oshea, E. K.; Rutkowski, R.; Kim, P. S., Evidence That the Leucine Zipper Is a Coiled Coil. *Science* **1989,** *243* (4890), 538-542.
8. Gopinath, A.; Rothemund, P. W. K., Optimized Assembly and Covalent Coupling of Single-Molecule DNA Origami Nanoarrays. *ACS Nano* **2014,** *8* (12), 12030-12040.
9. Nuraje, N.; Banerjee, I. A.; MacCuspie, R. I.; Yu, L. T.; Matsui, H., Biological bottom-up assembly of antibody nanotubes on patterned antigen arrays. *J. Am. Chem. Soc.* **2004,** *126* (26), 8088-8089.
10. Heller, M. J., DNA MICROARRAY TECHNOLOGY: Devices, Systems, and Applications. *Annu. Rev. Biomed. Eng.* **2002,** *4* (1), 129-153.
11. Cretich, M.; Damin, F.; Pirri, G.; Chiari, M., Protein and peptide arrays: Recent trends and new directions. *Biomol. Eng* **2006,** *23* (2–3), 77-88.
12. Jamadagni, S. N.; Godawat, R.; Dordick, J. S.; Garde, S., How Interfaces Affect Hydrophobically Driven Polymer Folding. *Journal of Physical Chemistry B* **2009,** *113* (13), 4093-4101.
13. Claesson, P. M.; Blomberg, E.; Froberg, J. C.; Nylander, T.; Arnebrant, T., PROTEIN INTERACTIONS AT SOLID-SURFACES. *Advances in Colloid and Interface Science* **1995,** *57*, 161-227.
14. Raffaini, G.; Ganazzoli, F., Protein adsorption on biomaterial and nanomaterial surfaces: a molecular modeling approach to study non-covalent interactions. *Journal of Applied Biomaterials & Biomechanics* **2010,** *8* (3), 135-145.
15. Jones, R. A. L.; Richards, R. W., *Polymers at Surfaces and Interfaces*. Cambridge University Press 1999.
16. Balamurugan, K.; Gopalakrishnan, R.; Raman, S. S.; Subramanian, V., Exploring the Changes in the Structure of α-Helical Peptides Adsorbed onto a Single Walled Carbon Nanotube Using Classical Molecular Dynamics Simulation. *The Journal of Physical Chemistry B* **2010,** *114* (44), 14048-14058.
17. Gong, P.; Levicky, R., DNA surface hybridization regimes. *Proceedings of the National Academy of Sciences of the United States of America* **2008,** *105* (14), 5301-5306.
18. Rafferty, J. L.; Siepmann, J. I.; Schure, M. R., Influence of bonded-phase coverage in reversed-phase liquid chromatography via molecular simulation. II. Effects on solute retention. *J. Chromatogr. A* **2008,** *1204* (1), 20-27.
19. Rimola, A.; Costa, D.; Sodupe, M.; Lambert, J.-F.; Ugliengo, P., Silica Surface Features and Their Role in the Adsorption of Biomolecules: Computational Modeling and Experiments. *Chem. Rev.* **2013,** *113* (6), 4216-4313.
20. Doshi, D. A.; Watkins, E. B.; Israelachvili, J. N.; Majewski, J., Reduced water density at hydrophobic surfaces: Effect of dissolved gases. *Proceedings of the National Academy of Sciences of the United States of America* **2005,** *102* (27), 9458-9462.
21. Scatena, L. F.; Brown, M. G.; Richmond, G. L., Water at hydrophobic surfaces: Weak hydrogen bonding and strong orientation effects. *Science* **2001,** *292* (5518), 908-912.
22. Patel, A. J.; Varilly, P.; Chandler, D.; Garde, S., Quantifying Density Fluctuations in Volumes of All Shapes and Sizes Using Indirect Umbrella Sampling. *Journal of Statistical Physics* **2011,** *145* (2), 265-275.

23. Mrksich, M.; Whitesides, G. M., Using self-assembled monolayers to understand the interactions of man-made surfaces with proteins and cells. *Annu. Rev. Biophys. Biomol. Struct.* **1996,** *25*, 55-78.
24. Ramos, R.; Gordon, M. J., Reflection-mode, confocal, tip-enhanced Raman spectroscopy system for scanning chemical microscopy of surfaces. *Rev. Sci. Instrum.* **2012,** *83* (9), -.
25. Mazzola, L. T.; Frank, C. W.; Fodor, S. P.; Mosher, C.; Lartius, R.; Henderson, E., Discrimination of DNA hybridization using chemical force microscopy. *Biophys. J.* **1999,** *76* (6), 2922-2933.
26. Woo, S.; Rothemund, P. W. K., Self-assembly of two-dimensional DNA origamilattices using cation-controlled surface diffusion. *Nature Communications* **2014,** *5*, 4889.
27. Walder, R.; Nelson, N.; Schwartz, D. K., Super-resolution surface mapping using the trajectories of molecular probes. *Nature Communications* **2011,** *2*.
28. Lakowicz, J. R., Energy Transfer. In *Principles of Fluorescence Spectroscopy*, 3rd ed.; Lakowicz, J., Ed. Springer: New York, 2006; pp 443-475.
29. Huang, Y.; Duan, X.; Wei, Q.; Lieber, C. M., Directed Assembly of One-Dimensional Nanostructures into Functional Networks. *Science* **2001,** *291* (5504), 630-633.
30. Penzo, E.; Wang, R.; Palma, M.; Wind, S. J., Selective placement of DNA origami on substrates patterned by nanoimprint lithography. *Journal of Vacuum Science & Technology B* **2011,** *29* (6), 06F205.
31. Marqusee, S.; Robbins, V. H.; Baldwin, R. L., Unusually Stable Helix Formation in Short Alanine-Based Peptides. *Proc. Natl. Acad. Sci. U. S. A.* **1989,** *86* (14), 5286-5290.
32. Scholtz, J. M.; Baldwin, R. L., The Mechanism of Alpha-Helix Formation by Peptides. *Annu. Rev. Biophys. Biomol. Struct.* **1992,** *21*, 95-118.
33. Jas, G. S.; Hegefeld, W. A.; Middaugh, C. R.; Johnson, C. K.; Kuczera, K., Detailed Microscopic Unfolding Pathways of an alpha-Helix and a beta-Hairpin: Direct Observation and Molecular Dynamics. *J. Phys. Chem. B* **2014,** *118* (26), 7233-7246.
34. Zagrovic, B.; Jayachandran, G.; Millett, I. S.; Doniach, S.; Pande, V. S., How large is an alpha-helix? Studies of the radii of gyration of helical peptides by small-angle X-ray scattering and molecular dynamics. *J. Mol. Biol.* **2005,** *353* (2), 232-241.
35. Gnanakaran, S.; Hochstrasser, R. M.; Garcia, A. E., Nature of structural inhomogeneities on folding a helix and their influence on spectral measurements. *Proc. Natl. Acad. Sci. U. S. A.* **2004,** *101* (25), 9229-9234.
36. Thompson, P. A.; Munoz, V.; Jas, G. S.; Henry, E. R.; Eaton, W. A.; Hofrichter, J., The helix-coil kinetics of a heteropeptide. *J. Phys. Chem. B* **2000,** *104* (2), 378-389.
37. Wang, T.; Zhu, Y.; Getahun, Z.; Du, D.; Huang, C. Y.; Degrado, W. F.; Gai, F., Length Dependent Helix-Coil Transition Kinetics of Nine Alanine-Based Peptides. *J. Phys. Chem. B* **2004,** *108* (39).
38. Sorin, E. J.; Pande, V. S., Exploring the helix-coil transition via all-atom equilibrium ensemble simulations. *Biophys. J.* **2005,** *88* (4), 2472-2493.

39. Nymeyer, H.; Garcia, A. E., Simulation of the folding equilibrium of alpha-helical peptides: A comparison of the generalized born approximation with explicit solvent. *Proc. Natl. Acad. Sci. U. S. A.* **2003,** *100* (24), 13934-13939.
40. Chakrabartty, A.; Kortemme, T.; Baldwin, R. L., HELIX PROPENSITIES OF THE AMINO-ACIDS MEASURED IN ALANINE-BASED PEPTIDES WITHOUT HELIX-STABILIZING SIDE-CHAIN INTERACTIONS. *Protein Sci.* **1994,** *3* (5), 843-852.
41. Doig, A. J.; Chakrabartty, A.; Klingler, T. M.; Baldwin, R. L., Determination of Free Energies of N-Capping in .alpha.-Helixes by Modification of the Lifson-Roig Helix-Coil Theory To Include N- and C-Capping. *Biochemistry* **1994,** *33* (11), 3396-3403.
42. Lundqvist, M.; Nygren, P.; Jonsson, B. H.; Broo, K., Induction of structure and function in a designed peptide upon adsorption on a silica nanoparticle. *Angew. Chem.-Int. Edit.* **2006,** *45* (48), 8169-8173.
43. Nygren, P.; Lundqvist, M.; Broo, K.; Jonsson, B. H., Fundamental design principles that guide induction of helix upon formation of stable peptide-nanoparticle complexes. *Nano Lett.* **2008,** *8* (7), 1844-1852.
44. Zhao, X.; Liu, R.; Chi, Z.; Teng, Y.; Qin, P., New Insights into the Behavior of Bovine Serum Albumin Adsorbed onto Carbon Nanotubes: Comprehensive Spectroscopic Studies. *The Journal of Physical Chemistry B* **2010,** *114* (16), 5625-5631.
45. Matsuura, K.; Saito, T.; Okazaki, T.; Ohshima, S.; Yumura, M.; Iijima, S., Selectivity of water-soluble proteins in single-walled carbon nanotube dispersions. *Chem. Phys. Lett.* **2006,** *429* (4–6), 497-502.
46. Wang, S.; Humphreys, E. S.; Chung, S.-Y.; Delduco, D. F.; Lustig, S. R.; Wang, H.; Parker, K. N.; Rizzo, N. W.; Subramoney, S.; Chiang, Y.-M.; Jagota, A., Peptides with selective affinity for carbon nanotubes. *Nat Mater* **2003,** *2* (3), 196-200.
47. Dieckmann, G. R.; Dalton, A. B.; Johnson, P. A.; Razal, J.; Chen, J.; Giordano, G. M.; Muñoz, E.; Musselman, I. H.; Baughman, R. H.; Draper, R. K., Controlled Assembly of Carbon Nanotubes by Designed Amphiphilic Peptide Helices. *J. Am. Chem. Soc.* **2003,** *125* (7), 1770-1777.
48. Roach, P.; Farrar, D.; Perry, C. C., Interpretation of protein adsorption: Surface-induced conformational changes. *J. Am. Chem. Soc.* **2005,** *127* (22), 8168-8173.
49. Lu, D. R.; Park, K., Effect of Surface Hydrophobicity on the Conformational-Changes of Adsorbed Fibrinogen. *J. Colloid Interface Sci.* **1991,** *144* (1), 271-281.
50. Kastantin, M.; Schwartz, D. K., DNA Hairpin Stabilization on a Hydrophobic Surface. *Small* **2013,** *9* (6), 933-941.
51. McLoughlin, S. Y.; Kastantin, M.; Schwartz, D. K.; Kaar, J. L., Single-molecule resolution of protein structure and interfacial dynamics on biomaterial surfaces. *Proc. Natl. Acad. Sci. U. S. A.* **2013,** *110* (48), 19396-19401.
52. Burkett, S. L.; Read, M. J., Adsorption-Induced Conformational Changes of α-Helical Peptides. *Langmuir* **2001,** *17* (16), 5059-5065.
53. Sukhishvili, S. A.; Chen, Y.; Muller, J. D.; Gratton, E.; Schweizer, K. S.; Granick, S., Surface diffusion of poly(ethylene glycol). *Macromolecules* **2002,** *35* (5), 1776-1784.
54. Mermut, O.; Phillips, D. C.; York, R. L.; McCrea, K. R.; Ward, R. S.; Somorjai, G. A., In situ adsorption studies of a 14-amino acid leucine-lysine peptide onto

hydrophobic polystyrene and hydrophilic silica surfaces using quartz crystal microbalance, atomic force microscopy, and sum frequency generation vibrational spectroscopy. *J. Am. Chem. Soc.* **2006,** *128* (11), 3598-3607.
55. Lai, P. Y., STATICS AND DYNAMICS OF A POLYMER-CHAIN ADSORBED ON A SURFACE - MONTE-CARLO SIMULATION USING THE BOND-FLUCTUATION MODEL. *Physical Review E* **1994,** *49* (6), 5420-5430.
56. Eisenriegler, E.; Kremer, K.; Binder, K., Adsorption of polymer chains at surfaces: Scaling and Monte Carlo analyses. *The Journal of Chemical Physics* **1982,** *77* (12), 6296-6320.
57. Skaug, M. J.; Mabry, J. N.; Schwartz, D. K., Single-Molecule Tracking of Polymer Surface Diffusion. *J. Am. Chem. Soc.* **2014,** *136* (4), 1327-1332.
58. Sukhishvili, S. A.; Chen, Y.; Muller, J. D.; Gratton, E.; Schweizer, K. S.; Granick, S., Materials science - Diffusion of a polymer 'pancake'. *Nature* **2000,** *406* (6792), 146-146.
59. Wong, J. S. S.; Hong, L.; Bae, S. C.; Granick, S., Polymer Surface Diffusion in the Dilute Limit. *Macromolecules* **2011,** *44* (8), 3073-3076.
60. Skaug, M. J.; Schwartz, D. K., Using the dynamics of fluorescent cations to probe and map charged surfaces. *Soft Matter* **2012,** *8* (48), 12017-12024.
61. Honciuc, A.; Baptiste, D. J.; Campbell, I. P.; Schwartz, D. K., Solvent Dependence of the Activation Energy of Attachment Determined by Single Molecule Observations of Surfactant Adsorption. *Langmuir* **2009,** *25* (13), 7389-7392.
62. Langdon, B. B.; Mirhossaini, R. B.; Mabry, J. N.; Sriram, I.; Lajmi, A.; Zhang, Y.; Rojas, O. J.; Schwartz, D. K., Single-Molecule Resolution of Protein Dynamics on Polymeric Membrane Surfaces: The Roles of Spatial and Population Heterogeneity. *ACS Applied Materials & Interfaces* **2015,** *7* (6), 3607-3617.
63. Mabry, J. N.; Skaug, M. J.; Schwartz, D. K., Single-Molecule Insights into Retention at a Reversed-Phase Chromatographic Interface. *Anal. Chem.* **2014,** *86* (19), 9451-9458.
64. Kisley, L.; Chen, J.; Mansur, A. P.; Shuang, B.; Kourentzi, K.; Poongavanam, M. V.; Chen, W. H.; Dhamane, S.; Willson, R. C.; Landes, C. F., Unified superresolution experiments and stochastic theory provide mechanistic insight into protein ion-exchange adsorptive separations. *Proc. Natl. Acad. Sci. U. S. A.* **2014,** *111* (6), 2075-80.
65. Sulpizi, M.; Gaigeot, M.-P.; Sprik, M., The Silica–Water Interface: How the Silanols Determine the Surface Acidity and Modulate the Water Properties. *J. Chem. Theory Comput.* **2012,** *8* (3), 1037-1047.
66. Wirth, M. J.; Swinton, D. J.; Ludes, M. D., Adsorption and diffusion of single molecules at chromatographic interfaces. *J. Phys. Chem. B* **2003,** *107* (26), 6258-6268.
67. Kastantin, M.; Langdon, B. B.; Chang, E. L.; Schwartz, D. K., Single-Molecule Resolution of Interfacial Fibrinogen Behavior: Effects of Oligomer Populations and Surface Chemistry. *J. Am. Chem. Soc.* **2011,** *133* (13), 4975-4983.
68. Skaug, M. J.; Schwartz, D. K., Using the dynamics of fluorescent cations to probe and map charged surfaces. *Soft Matter* **2012,** *8*, 12017-12024.
69. Honciuc, A.; Harant, A. W.; Schwartz, D. K., Single-Molecule Observations of Surfactant Diffusion at the Solution- Solid Interface. *Langmuir* **2008,** *24* (13), 6562-6566.

70. Kastantin, M.; Schwartz, D. K., Connecting Rare DNA Conformations and Surface Dynamics Using Single-Molecule Resonance Energy Transfer. *ACS Nano* **2011,** *5* (12), 9861-9869.
71. Skaug, M. J.; Mabry, J.; Schwartz, D. K., Intermittent Molecular Hopping at the Solid-Liquid Interface. *Phys. Rev. Lett.* **2013,** *110* (25).
72. HiLyte Fluor. http://www.anaspec.com/content/pdfs/c_literature168.pdf (accessed March 1, 2015).
73. Mukhopadhyay, S.; Krishnan, R.; Lemke, E. A.; Lindquist, S.; Deniz, A. A., A natively unfolded yeast prion monomer adopts an ensemble of collapsed and rapidly fluctuating structures. *Proceedings of the National Academy of Sciences* **2007,** *104* (8), 2649-2654.
74. Langdon, B. B.; Kastantin, M.; Walder, R.; Schwartz, D. K., Interfacial Protein-Protein Associations. *Biomacromolecules* **2014,** *15* (1), 66-74.
75. Kastantin, M.; Schwartz, D. K., Identifying Multiple Populations from Single-Molecule Lifetime Distributions. *Chemphyschem* **2013,** *14* (2), 374-380.

BIBLIOGRAPHY

1. Schwartz, D. K., Mechanisms and kinetics of self-assembled monolayer formation. *Annu. Rev. Phys. Chem.* **2001,** *52*, 107-137.
2. McCloskey, M. A.; Poo, M. M., Rates of membrane-associated reactions: reduction of dimensionality revisited. *J. Cell Biol.* **1986,** *102* (1), 88-96.
3. Nygren, P.; Lundqvist, M.; Broo, K.; Jonsson, B. H., Fundamental design principles that guide induction of helix upon formation of stable peptide-nanoparticle complexes. *Nano Lett.* **2008,** *8* (7), 1844-1852.
4. Thiruvengadathan, R.; Korampally, V.; Ghosh, A.; Chanda, N.; Gangopadhyay, K.; Gangopadhyay, S., Nanomaterial processing using self-assembly-bottom-up chemical and biological approaches. *Rep. Prog. Phys.* **2013,** *76* (6).
5. Whitesides, G. M.; Grzybowski, B., Self-Assembly at All Scales. *Science* **2002,** *295* (5564), 2418-2421.
6. Raghavachari, K.; Saha, A., Accurate Composite and Fragment-Based Quantum Chemical Models for Large Molecules. *Chem. Rev.* **2015**.
7. Han, D.; Pal, S.; Nangreave, J.; Deng, Z.; Liu, Y.; Yan, H., DNA Origami with Complex Curvatures in Three-Dimensional Space. *Science* **2011,** *332* (6027), 342-346.
8. Martins, S. A.; Sousa, S. F.; Ramos, M. J.; Fernandes, P. A., Prediction of Solvation Free Energies with Thermodynamic Integration Using the General Amber Force Field. *J. Chem. Theory Comput.* **2014,** *10* (8), 3570-3577.
9. Hansson, T.; Oostenbrink, C.; van Gunsteren, W., Molecular dynamics simulations. *Curr. Opin. Struct. Biol.* **2002,** *12* (2), 190-196.
10. Pierce, L. C. T.; Salomon-Ferrer, R.; Augusto F. de Oliveira, C.; McCammon, J. A.; Walker, R. C., Routine Access to Millisecond Time Scale Events with Accelerated Molecular Dynamics. *J. Chem. Theory Comput.* **2012,** *8* (9), 2997-3002.
11. Lindsey, R. K.; Rafferty, J. L.; Eggimann, B. L.; Siepmann, J. I.; Schure, M. R., Molecular simulation studies of reversed-phase liquid chromatography. *J. Chromatogr. A* **2013,** *1287*, 60-82.
12. Rimola, A.; Costa, D.; Sodupe, M.; Lambert, J.-F.; Ugliengo, P., Silica Surface Features and Their Role in the Adsorption of Biomolecules: Computational Modeling and Experiments. *Chem. Rev.* **2013,** *113* (6), 4216-4313.
13. Weisz, P. B.; Swegler, E. W., Catalytic Activity Induced by Neutron Irradiation of Inert Silica. *J. Chem. Phys.* **1955,** *23* (9), 1567-1568.
14. Peri, J. B.; Hensley, A. L., The surface structure of silica gel. *J. Phys. Chem.* **1968,** *72* (8), 2926-2933.
15. Maschmeyer, T.; Rey, F.; Sankar, G.; Thomas, J. M., Heterogeneous catalysts obtained by grafting metallocene complexes onto mesoporous silica. *Nature* **1995,** *378* (6553), 159-162.
16. Gill, R. S.; Singh, S.; Singh, P. P., Design and development of desiccant seed dryer with airflow inversion and recirculation. *J. Food Sci. Technol.-Mysore* **2014,** *51* (11), 3418-3424.

17. Handbook of HPLC. In *Chromatogr. Sci. Ser.*, 2nd ed.; Taylor & Francis: Boca Raton, 2010.
18. Tong, H. M., Microelectronics Packaging - Present and Future. *Mater. Chem. Phys.* **1995,** *40* (3), 147-161.
19. Kingon, A. I.; Maria, J.-P.; Streiffer, S. K., Alternative dielectrics to silicon dioxide for memory and logic devices. *Nature* **2000,** *406* (6799), 1032-1038.
20. Zhao, B.; Haasch, R. T.; MacLaren, S., Solvent-Induced Self-Assembly of Mixed Poly(methyl methacrylate)/Polystyrene Brushes on Planar Silica Substrates: Molecular Weight Effect. *J. Am. Chem. Soc.* **2004,** *126* (19), 6124-6134.
21. Cheng, J. Y.; Ross, C. A.; Smith, H. I.; Thomas, E. L., Templated Self-Assembly of Block Copolymers: Top-Down Helps Bottom-Up. *Adv. Mater.* **2006,** *18* (19), 2505-2521.
22. Bij, K. E.; Horvath, C.; Melander, W. R.; Nahum, A., Surface Silanols in Silica-Bonded Hydrocarbonaceous Stationary Phases .2. Irregular Retention Behavior and Effect of Silanol Masking. *J. Chromatogr.* **1981,** *203* (Jan), 65-84.
23. Spialter, L.; Pazdernik, L.; Bernstein, S.; Swansiger, W. A.; Buell, G. R.; Freeburger, M. E., Mechanism of the reaction of ozone with the silicon-hydrogen bond. *J. Am. Chem. Soc.* **1971,** *93* (22), 5682-5686.
24. Zhuravlev, N. D.; Siepmann, J. I.; Schure, M. R., Surface Coverages of Bonded-Phase Ligands on Silica: A Computational Study. *Anal. Chem.* **2001,** *73* (16), 4006-4011.
25. Rafferty, J. L.; Zhang, L.; Siepmann, J. I.; Schure, M. R., Retention mechanism in reversed-phase liquid chromatography: A molecular perspective. *Anal. Chem.* **2007,** *79* (17), 6551-6558.
26. Walba, D. M.; Liberko, C. A.; Korblova, E.; Farrow, M.; Furtak, T. E.; Chow, B. C.; Schwartz, D. K.; Freeman, A. S.; Douglas, K.; Williams, S. D.; Klittnick, A. F.; Clark, N. A., Self-assembled monolayers for liquid crystal alignment: simple preparation on glass using alkyltrialkoxysilanes. *Liq. Cryst.* **2004,** *31* (4), 481-489.
27. Zhuravlev, L. T., The surface chemistry of amorphous silica. Zhuravlev model. *Colloids Surf. Physicochem. Eng. Aspects* **2000,** *173* (1–3), 1-38.
28. Rafferty, J. L.; Siepmann, J. I.; Schure, M. R., Influence of bonded-phase coverage in reversed-phase liquid chromatography via molecular simulation: I. Effects on chain conformation and interfacial properties. *J. Chromatogr. A* **2008,** *1204* (1), 11-19.
29. Sandoval, J. E.; Pesek, J. J., Hydrolytically stable bonded chromatographic phases prepared through hydrosilylation of olefins on a hydride-modified silica intermediate. *Anal. Chem.* **1991,** *63* (22), 2634-2641.
30. Gritti, F.; Guiochon, G., Heterogeneity of the adsorption mechanism of low molecular weight compounds in reversed-phase liquid chromatography. *Anal. Chem.* **2006,** *78* (16), 5823-5834.
31. Felinger, A., Molecular dynamic theories in chromatography. *J. Chromatogr. A* **2008,** *1184* (1-2), 20-41.
32. Giddings, J. C., Kinetic Origin of Tailing in Chromatography. *Anal. Chem.* **1963,** *35* (13), 1999-&.

33. Giddings, J. C.; Eyring, H., A Molecular Dynamic Theory of Chromatography. *J. Phys. Chem.* **1955,** *59* (5), 416-421.
34. Rafferty, J. L.; Siepmann, J. I.; Schure, M. R., Influence of bonded-phase coverage in reversed-phase liquid chromatography via molecular simulation. II. Effects on solute retention. *J. Chromatogr. A* **2008,** *1204* (1), 20-27.
35. Woo, S.; Rothemund, P. W. K., Self-assembly of two-dimensional DNA origami lattices using cation-controlled surface diffusion. *Nat. Commun.* **2014,** *5*.
36. Rafferty, J. L.; Siepmann, J. I.; Schure, M. R., Molecular Simulations of Retention in Chromatographic Systems: Use of Biased Monte Carlo Techniques to Access Multiple Time and Length Scales. *Multiscale Molecular Methods in Applied Chemistry* **2012,** *307*, 181-200.
37. Denis, F. A.; Hanarp, P.; Sutherland, D. S.; Gold, J.; Mustin, C.; Rouxhet, P. G.; Dufrene, Y. F., Protein adsorption on model surfaces with controlled nanotopography and chemistry. *Langmuir* **2002,** *18* (3), 819-828.
38. Domke, K. F.; Pettinger, B., Studying Surface Chemistry beyond the Diffraction Limit: 10 Years of TERS. *Chemphyschem* **2010,** *11* (7), 1365-1373.
39. Muller, D. J.; Dufrene, Y. F., Atomic force microscopy as a multifunctional molecular toolbox in nanobiotechnology. *Nat Nano* **2008,** *3* (5), 261-269.
40. Dufrene, Y. F.; Martinez-Martin, D.; Medalsy, I.; Alsteens, D.; Muller, D. J., Multiparametric imaging of biological systems by force-distance curve-based AFM. *Nat. Meth.* **2013,** *10* (9), 847-854.
41. Tranchida, D.; Piccarolo, S.; Deblieck, R. A. C., Some experimental issues of AFM tip blind estimation: the effect of noise and resolution. *Meas. Sci. Technol.* **2006,** *17* (10), 2630-2636.
42. Huang, P.; Andersson, S. B., Fast scanning in AFM using non-raster sampling and time-optimal trajectories. *IEEE Decis. Cont.r P* **2012**, 5073-5078.
43. Giessibl, F. J., Atomic Resolution of the Silicon (111)-(7x7) Surface by Atomic Force Microscopy. *Science* **1995,** *267* (5194), 68-71.
44. Atkin, J. M.; Berweger, S.; Jones, A. C.; Raschke, M. B., Nano-optical imaging and spectroscopy of order, phases, and domains in complex solids. *Adv. Phys.* **2012,** *61* (6), 745-842.
45. Soriaga, M. P., Ultra-high vacuum techniques in the study of single-crystal electrode surfaces. *Prog. Surf. Sci.* **1992,** *39* (4), 325-443.
46. Castner, D. G.; Ratner, B. D., Biomedical surface science: Foundations to frontiers. *Surf. Sci.* **2002,** *500* (1–3), 28-60.
47. Ferrin, P.; Kandoi, S.; Nilekar, A. U.; Mavrikakis, M., Hydrogen adsorption, absorption and diffusion on and in transition metal surfaces: A DFT study. *Surf. Sci.* **2012,** *606* (7–8), 679-689.
48. Williams, C. T.; Beattie, D. A., Probing buried interfaces with non-linear optical spectroscopy. *Surf. Sci.* **2002,** *500* (1–3), 545-576.
49. Bain, C. D., Sum-frequency vibrational spectroscopy of the solid/liquid interface. *J. Chem. Soc., Faraday Trans.* **1995,** *91* (9), 1281-1296.
50. Rafferty, J. L.; Siepmann, J. I.; Schure, M. R., Mobile phase effects in reversed-phase liquid chromatography: A comparison of acetonitrile/water and methanol/water

solvents as studied by molecular simulation. *J. Chromatogr. A* **2011,** *1218* (16), 2203-2213.
51. Kisley, L.; Chen, J.; Mansur, A. P.; Dominguez-Medina, S.; Kulla, E.; Kang, M. K.; Shuang, B.; Kourentzi, K.; Poongavanam, M. V.; Dhamane, S.; Willson, R. C.; Landes, C. F., High ionic strength narrows the population of sites participating in protein ion-exchange adsorption: a single-molecule study. *J. Chromatogr. A* **2014,** *1343*, 135-42.
52. Tswett, M., Physikalish-Chemische Studien ueber das Chlorophyll. Die Adsorption. *Berichte der Deutschen botanischen Gesellschaft* **1906,** *24*, 316-326.
53. Keil, F. J., Complexities in modeling of heterogeneous catalytic reactions. *Comp.& Math. with Appl.* **2013,** *65* (10), 1674-1697.
54. Satterfield, C. N.; Sherwood, T. K., *The role of diffusion in catalysis*. Addison-Wesley Pub. Co.: Reading, Mass.,, 1963; p vii, 118 p.
55. Miyabe, K.; Guiochon, G., Surface diffusion in reversed-phase liquid chromatography. *J. Chromatogr. A* **2010,** *1217* (11), 1713-1734.
56. Wirth, M. J.; Swinton, D. J.; Ludes, M. D., Adsorption and diffusion of single molecules at chromatographic interfaces. *J. Phys. Chem. B* **2003,** *107* (26), 6258-6268.
57. Chan, V.; Graves, D. J.; McKenzie, S. E., The biophysics of DNA hybridization with immobilized oligonucleotide probes. *Biophys. J.* **1995,** *69* (6), 2243-2255.
58. Squires, T. M.; Messinger, R. J.; Manalis, S. R., Making it stick: convection, reaction and diffusion in surface-based biosensors. *Nat. Biotechnol.* **2008,** *26* (4), 417-426.
59. Ulman, A., Formation and Structure of Self-Assembled Monolayers. *Chem. Rev.* **1996,** *96* (4), 1533-1554.
60. Doudevski, I.; Schwartz, D. K., Concentration dependence of self-assembled monolayer island nucleation and growth. *J. Am. Chem. Soc.* **2001,** *123* (28), 6867-6872.
61. Zhang, R.; Somasundaran, P., Advances in adsorption of surfactants and their mixtures at solid/solution interfaces. *Adv. Colloid Interface Sci.* **2006,** *123*, 213-229.
62. Honciuc, A.; Baptiste, D. J.; Campbell, I. P.; Schwartz, D. K., Solvent Dependence of the Activation Energy of Attachment Determined by Single Molecule Observations of Surfactant Adsorption. *Langmuir* **2009,** *25* (13), 7389-7392.
63. Mrksich, M.; Sigal, G. B.; Whitesides, G. M., Surface Plasmon Resonance Permits in Situ Measurement of Protein Adsorption on Self-Assembled Monolayers of Alkanethiolates on Gold. *Langmuir* **1995,** *11* (11), 4383-4385.
64. Silin, V.; Weetall, H.; Vanderah, D. J., SPR studies of the nonspecific adsorption kinetics of human IgG and BSA on gold surfaces modified by self-assembled monolayers (SAMs). *J. Col. Interf. Sci.* **1997,** *185* (1), 94-103.
65. Kastantin, M.; Langdon, B. B.; Schwartz, D. K., A bottom-up approach to understanding protein layer formation at solid–liquid interfaces. *Adv. Colloid Interface Sci.* **2014,** *207* (0).
66. Bychuk, O. V.; Oshaughnessy, B., Anomalous Surface-Diffusion - a Numerical Study. *J. Chem. Phys.* **1994,** *101* (1), 772-780.
67. Hlushkou, D.; Gritti, F.; Daneyko, A.; Guiochon, G.; Tallarek, U., How Microscopic Characteristics of the Adsorption Kinetics Impact Macroscale Transport in Chromatographic Beds. *J. Phys. Chem. C* **2013,** *117* (44), 22974-22985.

68. Honciuc, A.; Howard, A. L.; Schwartz, D. K., Single Molecule Observations of Fatty Acid Adsorption at the Silica/Water Interface: Activation Energy of Attachment. *J Phys Chem C* **2009,** *113* (6), 2078-2081.
69. Ge, G.; Brus, L. E., Fast Surface Diffusion of Large Disk-Shaped Nanocrystal Aggregates. *Nano Lett.* **2001,** *1* (4), 219-222.
70. Benichou, O.; Loverdo, C.; Moreau, M.; Voituriez, R., Optimizing intermittent reaction paths. *PCCP* **2008,** *10* (47), 7059-7072.
71. Bénichou, O.; Loverdo, C.; Moreau, M.; Voituriez, R., Intermittent search strategies. *Rev. Mod. Phys.* **2011,** *83* (1), 81--129.
72. Bouchaud, J. P.; Georges, A., Anomalous diffusion in disordered media: Statistical mechanisms, models and physical applications. *Phys. Rep.* **1990,** *195* (4-5), 127-293.
73. Bychuk, O. V.; O'Shaughnessy, B., Anomalous diffusion at liquid surfaces. *Phys. Rev. Lett.* **1995,** *74* (10), 1795--1798.
74. Skaug, M. J.; Mabry, J.; Schwartz, D. K., Intermittent Molecular Hopping at the Solid-Liquid Interface. *Phys. Rev. Lett.* **2013,** *110* (25).
75. Skaug, M. J.; Mabry, J. N.; Schwartz, D. K., Single-Molecule Tracking of Polymer Surface Diffusion. *J. Am. Chem. Soc.* **2014,** *136* (4), 1327-1332.
76. Yu, C.; Guan, J.; Chen, K.; Bae, S. C.; Granick, S., Single-Molecule Observation of Long Jumps in Polymer Adsorption. *ACS Nano* **2013,** *7* (11), 9735-9742.
77. Wang, Y.; Rajagopalan, R.; Mattice, W., Kinetics of Detachment of Homopolymers from a Solid Surface. *Phys. Rev. Lett.* **1995,** *74* (13), 2503-2506.
78. Sukhishvili, S. A.; Chen, Y.; Muller, J. D.; Gratton, E.; Schweizer, K. S.; Granick, S., Materials science - Diffusion of a polymer 'pancake'. *Nature* **2000,** *406* (6792), 146-146.
79. Baugh, L.; Vogel, V., Structural changes of fibronectin adsorbed to model surfaces probed by fluorescence resonance energy transfer. *J. Biomed. Mater. Res. A.* **2004,** *69A* (3), 525-534.
80. Maste, M. C. L.; Norde, W.; Visser, A. J. W. G., Adsorption-Induced Conformational Changes in the Serine Proteinase Savinase: A Tryptophan Fluorescence and Circular Dichroism Study. *J. Coll. Interf. Sci.* **1997,** *196* (2), 224-230.
81. Kong, J.; Yu, S., Fourier Transform Infrared Spectroscopic Analysis of Protein Secondary Structures. *Acta Biochimica et Biophysica Sinica* **2007,** *39* (8), 549-559.
82. McLoughlin, S. Y.; Kastantin, M.; Schwartz, D. K.; Kaar, J. L., Single-molecule resolution of protein structure and interfacial dynamics on biomaterial surfaces. *Proc. Natl. Acad. Sci. U. S. A.* **2013,** *110* (48), 19396-19401.
83. Roach, P.; Farrar, D.; Perry, C. C., Interpretation of protein adsorption: Surface-induced conformational changes. *J. Am. Chem. Soc.* **2005,** *127* (22), 8168-8173.
84. Mermut, O.; Phillips, D. C.; York, R. L.; McCrea, K. R.; Ward, R. S.; Somorjai, G. A., In situ adsorption studies of a 14-amino acid leucine-lysine peptide onto hydrophobic polystyrene and hydrophilic silica surfaces using quartz crystal microbalance, atomic force microscopy, and sum frequency generation vibrational spectroscopy. *J. Am. Chem. Soc.* **2006,** *128* (11), 3598-3607.

85. Datta, S.; Christena, L. R.; Rajaram, Y. R. S., Enzyme immobilization: an overview on techniques and support materials. *3 Biotech* **2013,** *3* (1), 1-9.
86. Introduction to Fluorescence. In *Principles of Fluorescence Spectroscopy*, Lakowicz, J., Ed. Springer US: 2006; pp 1-26.
87. Weiss, S., Fluorescence Spectroscopy of Single Biomolecules. *Science* **1999,** *283* (5408), 1676-1683.
88. Lavis, L. D.; Raines, R. T., Bright Ideas for Chemical Biology. *ACS Chem. Biol.* **2008,** *3* (3), 142-155.
89. Meyvis, T. L.; De Smedt, S.; Van Oostveldt, P.; Demeester, J., Fluorescence Recovery After Photobleaching: A Versatile Tool for Mobility and Interaction Measurements in Pharmaceutical Research. *Pharm. Res.* **1999,** *16* (8), 1153-1162.
90. Walder, R. B.; Honciuc, A.; Schwartz, D. K., Phospholipid Diffusion at the Oil–Water Interface. *J. Phys. Chem. B* **2010,** *114* (35), 11484-11488.
91. Malmsten, M., *Biopolymers at Interfaces* 2nd ed.; Marcel Dekker: New York, 2003; p xii, 908 p.
92. Hansen, R. L.; Harris, J. M., Measuring reversible adsorption kinetics of small molecules at solid/liquid interfaces by total internal reflection fluorescence correlation spectroscopy. *Anal. Chem.* **1998,** *70* (20), 4247-4256.
93. Wirth, M. J.; Swinton, D. J., Single-molecule probing of mixed-mode adsorption at a chromatographic interface. *Anal. Chem.* **1998,** *70* (24), 5264-5271.
94. Thompson, N., Fluorescence Correlation Spectroscopy. In *Top. Fluoresc. Spectrosc.*, Lakowicz, J., Ed. Springer US: 1999; Vol. 1, pp 337-378.
95. Fluorescence Correlation Spectroscopy. In *Principles of Fluorescence Spectroscopy*, Lakowicz, J. R., Ed. Springer US: 2006; pp 797-840.
96. Swinton, D. J.; Wirth, M. J., Lateral diffusion of 1,1 '-dioctadecyl-3,3,3 ' 3 '-tetramethylindocarbocyanine perchlorate at the interfaces of C-18 and chromatographic solvents. *Anal. Chem.* **2000,** *72* (16), 3725-3730.
97. Ludes, M. D.; Wirth, M. J., Single-molecule resolution and fluorescence imaging of mixed-mode sorption of a dye at the interface of C-18 and acetonitrile/water. *Anal. Chem.* **2002,** *74* (2), 386-393.
98. Wirth, M. J.; Legg, M. A., Single-molecule probing of adsorption and diffusion on silica surfaces. *Annu. Rev. Phys. Chem.* **2007,** *58*, 489-510.
99. Bae, S. C.; Granick, S., Molecular motion at soft and hard interfaces: from phospholipid bilayers to polymers and lubricants. *Annu. Rev. Phys. Chem.* **2007,** *58*, 353-374.
100. Desai, T. G.; Keblinski, P.; Kumar, S. K.; Granick, S., Modeling diffusion of adsorbed polymer with explicit solvent. *Phys. Rev. Lett.* **2007,** *98* (21).
101. Douglas, J. F.; Johnson, H. E.; Granick, S., A Simple Kinetic-Model of Polymer Adsorption and Desorption. *Science* **1993,** *262* (5142), 2010-2012.
102. Douglas, J. F.; Schneider, H. M.; Frantz, P.; Lipman, R.; Granick, S., The origin and characterization of conformational heterogeneity in adsorbed polymer layers. *J. of Phys.-Cond. Matter* **1997,** *9* (37), 7699-7718.
103. Frantz, P.; Granick, S., Kinetics of Polymer Adsorption and Desorption. *Phys. Rev. Lett.* **1991,** *66* (7), 899-902.

104. Granick, S.; Bae, S. C., Open questions about polymer interfacial diffusion. *J. Polym. Sci. Part B Polym. Phys.* **2006,** *44* (24), 3434-3435.
105. Granick, S.; Kumar, S. K.; Amis, E. J.; Antonietti, M.; Balazs, A. C.; Chakraborty, A. K.; Grest, G. S.; Hawker, C. J.; Janmey, P.; Kramer, E. J.; Nuzzo, R.; Russell, T. P.; Safinya, C. R., Macromolecules at surfaces: Research challenges and opportunities from tribology to biology. *J. Polym. Sci. Part B Polym. Phys.* **2003,** *41* (22), 2755-2793.
106. Sukhishvili, S. A.; Chen, Y.; Muller, J. D.; Gratton, E.; Schweizer, K. S.; Granick, S., Surface diffusion of poly(ethylene glycol). *Macromolecules* **2002,** *35* (5), 1776-1784.
107. Harris, J. M.; Marshall, D. B., Direct measurement of sorption/desorption kinetics in reversed-phase chromatographic systems. *J. Microcolumn Sep.* **1997,** *9* (3), 185-191.
108. He, H.-T.; Marguet, D., Detecting Nanodomains in Living Cell Membrane by Fluorescence Correlation Spectroscopy. *Annu. Rev. Phys. Chem.* **2011,** *62* (1), 417-436.
109. Axelrod, D., Total Internal Reflection Fluorescence Microscopy in Cell Biology. *Traffic* **2001,** *2* (11), 764-774.
110. Horn, D.; Klingler, J.; Schorf, W.; Graf, K., Experimental progress in the characterization of colloidal systems. *Structure, Dynamics and Properties of Disperse Colloidal Systems* **1998,** *111*, 27-33.
111. Honciuc, A.; Harant, A. W.; Schwartz, D. K., Single-molecule observations of surfactant diffusion at the solution-solid interface. *Langmuir* **2008,** *24* (13), 6562-6566.
112. Stryer, L., Fluorescence Energy Transfer as a Spectroscopic Ruler. *Annu. Rev. Biochem* **1978,** *47* (1), 819-846.
113. Energy Transfer. In *Principles of Fluorescence Spectroscopy*, Lakowicz, J., Ed. Springer US: 2006; pp 443-475.
114. Langdon, B. B.; Kastantin, M.; Walder, R.; Schwartz, D. K., Interfacial Protein-Protein Associations. *Biomacromolecules* **2014,** *15* (1), 66-74.
115. Monserud, J. H.; Schwartz, D. K., Mechanisms of surface-mediated DNA hybridization. *ACS Nano* **2014,** *8* (5), 4488-99.
116. Kastantin, M.; Schwartz, D. K., DNA Hairpin Stabilization on a Hydrophobic Surface. *Small* **2013,** *9* (6), 933-941.
117. Walder, R.; Kastantin, M.; Schwartz, D. K., High throughput single molecule tracking for analysis of rare populations and events. *Analyst* **2012,** *137* (13), 2987-2996.
118. *Handbook of HPLC*. 2nd ed.; Taylor & Francis: Boca Raton, 2010.
119. Vandeemter, J. J.; Zuiderweg, F. J.; Klinkenberg, A., Longitudinal Diffusion and Resistance to Mass Transfer as Causes of Nonideality in Chromatography. *Chem. Eng. Sci.* **1956,** *5* (6), 271-289.
120. Gritti, F.; Guiochon, G., Mass transfer kinetics, band broadening and column efficiency. *J. Chromatogr. A* **2012,** *1221*, 2-40.
121. Pasti, L.; Cavazzini, A.; Felinger, A.; Martin, M.; Dondi, F., Single-molecule observation and chromatography unified by levy process representation. *Anal. Chem.* **2005,** *77* (8), 2524-2535.
122. Zhong, Z. M.; Lowry, M.; Wang, G. F.; Geng, L., Probing strong adsorption of solute onto cis-silica gel by fluorescence correlation imaging and single-molecule spectroscopy under RPLC conditions. *Anal. Chem.* **2005,** *77* (8), 2303-2310.

123. Zhong, Z. M.; Wang, G. F.; Geng, M. L., Probing strong adsorption of individual solute molecules at solid/liquid interfaces with model-based statistical two-dimensional correlation analysis. *J. Mol. Struct.* **2006,** *799* (1-3), 204-210.
124. Cooper, J. T.; Peterson, E. M.; Harris, J. M., Fluorescence imaging of single-molecule retention trajectories in reversed-phase chromatographic particles. *Anal. Chem.* **2013,** *85* (19), 9363-70.
125. Kisley, L.; Chen, J.; Mansur, A. P.; Shuang, B.; Kourentzi, K.; Poongavanam, M. V.; Chen, W. H.; Dhamane, S.; Willson, R. C.; Landes, C. F., Unified superresolution experiments and stochastic theory provide mechanistic insight into protein ion-exchange adsorptive separations. *Proc. Natl. Acad. Sci. U. S. A.* **2014,** *111* (6), 2075-80.
126. Wirth, M. J.; Smith, E. A.; Anthony, S. R., Measurement and simulation of tailing zones of a cationic dye in analytical-scale reversed phase chromatography. *J. Chromatogr. A* **2004,** *1034* (1-2), 69-75.
127. Rafferty, J. L.; Siepmann, J. I.; Schure, M. R., Understanding the Retention Mechanism in Reversed-Phase Liquid Chromatography: Insights from Molecular Simulation. *Advances in Chromatography, Vol 48* **2010,** *48*, 1-55.
128. Kohler, J.; Chase, D. B.; Farlee, R. D.; Vega, A. J.; Kirkland, J. J., Comprehensive Characterization of Some Silica-Based Stationary Phases for High-Performance Liquid-Chromatography. *J. Chromatogr.* **1986,** *352*, 275-305.
129. Skaug, M. J.; Mabry, J.; Schwartz, D. K., Intermittent Molecular Hopping at the Solid-Liquid Interface. *Phys. Rev. Lett.* **2013,** *110* (25), 256101
130. Veatch, S. L.; Machta, B. B.; Shelby, S. A.; Chiang, E. N.; Holowka, D. A.; Baird, B. A., Correlation Functions Quantify Super-Resolution Images and Estimate Apparent Clustering Due to Over-Counting. *PLoS One* **2012,** *7* (2).
131. Chen, J. X.; Bremauntz, A.; Kisley, L.; Shuang, B.; Landes, C. F., Super-Resolution mbPAINT for Optical Localization of Single-Stranded DNA. *Acs Applied Materials & Interfaces* **2013,** *5* (19), 9338-9343.
132. Kastantin, M.; Schwartz, D. K., Identifying Multiple Populations from Single-Molecule Lifetime Distributions. *Chemphyschem* **2013,** *14* (2), 374-380.
133. Poole, C. F.; Poole, S. K., Foundations of retention in partition chromatography. *J. Chromatogr. A* **2009,** *1216* (10), 1530-1550.
134. Gritti, F.; Guiochon, G., Effect of the mobile phase composition on the isotherm parameters and the high concentration band profiles in reversed-phase liquid chromatography. *J. Chromatogr. A* **2003,** *995* (1-2), 37-54.
135. Felinger, A., Determination of rate constants for heterogeneous mass transfer kinetics in liquid chromatography. *J. Chromatogr. A* **2006,** *1126* (1-2), 120-128.
136. Felinger, A.; Cavazzini, A.; Remelli, M.; Dondi, F., Stochastic-dispersive theory of chromatography. *Anal. Chem.* **1999,** *71* (20), 4472-4479.
137. Bacskay, I.; Felinger, A., Macroscopic and microscopic analysis of mass transfer in reversed phase liquid chromatography. *J. Chromatogr. A* **2009,** *1216* (8), 1253-1262.
138. Bocian, S.; Vajda, P.; Felinger, A.; Buszewski, B., Effect of End-Capping and Surface Coverage on the Mechanism of Solvent Adsorption. *Chromatographia* **2010,** *71*, S5-S11.

139. Gritti, F.; Kazakevich, Y. V.; Guiochon, G., Effect of the surface coverage of endcapped C-18-silica on the excess adsorption isotherms of commonly used organic solvents from water in reversed phase liquid chromatography. *J. Chromatogr. A* **2007,** *1169* (1-2), 111-124.
140. Masel, R. I., *Principles of Adsorption and Reaction on Solid Surfaces*. Wiley: New York, 1996; p xiv, 804 p.
141. Horvath, C.; Melander, W.; Molnar, I., Solvophobic Interactions in Liquid-Chromatography with Nonpolar Stationary Phases. *J. Chromatogr.* **1976,** *125* (1), 129-156.
142. Dorsey, J. G.; Dill, K. A., The Molecular Mechanism of Retention in Reversed-Phase Liquid-Chromatography. *Chem. Rev.* **1989,** *89* (2), 331-346.
143. Honciuc, A.; Harant, A. W.; Schwartz, D. K., Single-Molecule Observations of Surfactant Diffusion at the Solution- Solid Interface. *Langmuir* **2008,** *24* (13), 6562-6566.
144. Zhang, L.; Rafferty, J. L.; Siepmann, J. I.; Chen, B.; Schure, M. R., Chain conformation and solvent partitioning in reversed-phase liquid chromatography: Monte Carlo simulations for various water/methanol concentrations. *J. Chromatogr. A* **2006,** *1126* (1-2), 219-231.
145. Fornstedt, T.; Zhong, G. M.; Guiochon, G., Peak tailing and slow mass transfer kinetics in nonlinear chromatography. *J. Chromatogr. A* **1996,** *742* (1-2), 55-68.
146. Miyabe, K.; Guiochon, G., Comparison of the Characteristics of Adsorption Equilibrium and Surface Diffusion in Liquid–Solid and Gas–Solid Adsorption on C18-Silica Gels. *J. Phys. Chem. B* **2004,** *108* (9), 2987-2997.
147. Schunack, M.; Linderoth, T. R.; Rosei, F.; Lægsgaard, E.; Stensgaard, I.; Besenbacher, F., Long Jumps in the Surface Diffusion of Large Molecules. *Phys. Rev. Lett.* **2002,** *88* (15), 156102.
148. Lomholt, M. A.; Koren, T.; Metzler, R.; Klafter, J., Levy strategies in intermittent search processes are advantageous. *Proc. Natl. Acad. Sci. U. S. A.* **2008,** *105* (32), 11055-11059.
149. Calandre, T.; Bénichou, O.; Grebenkov, D. S.; Voituriez, R., Splitting probabilities and interfacial territory covered by two-dimensional and three-dimensional surface-mediated diffusion. *Physical Review E* **2014,** *89* (1), 012149.
150. Loverdo, C.; Benichou, O.; Moreau, M.; Voituriez, R., Enhanced reaction kinetics in biological cells. *Nature Physics* **2008,** *4* (2), 134-137.
151. Krapivsky, P. L., Kinetics of monomer-monomer surface catalytic reactions. *Phys. Rev. A* **1992,** *45* (2), 1067-1072.
152. Sriram, I.; Walder, R.; Schwartz, D. K., Stokes-Einstein and desorption-mediated diffusion of protein molecules at the oil-water interface. *Soft Matter* **2012,** *8* (22), 6000-6003.
153. Wang, B.; Kuo, J.; Bae, S. C.; Granick, S., When Brownian diffusion is not Gaussian. *Nature Materials* **2012,** *11* (6), 481-485.
154. Mabry, J. N.; Skaug, M. J.; Schwartz, D. K., Single-Molecule Insights into Retention at a Reversed-Phase Chromatographic Interface. *Anal. Chem.* **2014,** *86* (19), 9451-9458.

155. Langdon, B. B.; Mirhossaini, R. B.; Mabry, J. N.; Sriram, I.; Lajmi, A.; Zhang, Y.; Rojas, O. J.; Schwartz, D. K., Single-Molecule Resolution of Protein Dynamics on Polymeric Membrane Surfaces: The Roles of Spatial and Population Heterogeneity. *ACS Applied Materials & Interfaces* **2015,** *7* (6), 3607-3617.
156. Bychuk, O. V.; O'Shaughnessy, B., Anomalous diffusion of surface-active species at liquid-fluid and liquid-solid interfaces. *J. Phys. II France* **1994,** *4*, 1135-1156.
157. Wang, D.; He, C.; Stoykovich, M. P.; Schwartz, D. K., Nanoscale Topography Influences Polymer Surface Diffusion. *ACS nano* **2015,** *9* (2), 1656-1664.
158. Tauzin, L. J.; Shuang, B.; Kisley, L.; Mansur, A. P.; Chen, J. X.; de Leon, A.; Advincula, R. C.; Landes, C. F., Charge-Dependent Transport Switching of Single Molecular Ions in a Weak Polyelectrolyte Multilayer. *Langmuir* **2014,** *30* (28), 8391-8399.
159. Chechkin, A. V.; Zaid, I. M.; Lomholt, M. A.; Sokolov, I. M.; Metzler, R., Bulk-mediated diffusion on a planar surface: Full solution. *Physical Review E* **2012,** *86* (4).
160. Jung, L. S.; Campbell, C. T., Sticking Probabilities in Adsorption from Liquid Solutions: Alkylthiols on Gold. *Phys. Rev. Lett.* **2000,** *84* (22), 5164-5167.
161. Cooper, J. T.; Harris, J. M., Imaging Fluorescence-Correlation Spectroscopy for Measuring Fast Surface Diffusion at Liquid/Solid Interfaces. *Anal. Chem.* **2014,** *86* (15), 7618-7626.
162. Maune, H. T.; Han, S.-p.; Barish, R. D.; Bockrath, M.; Goddard, W. A.; Rothemund, P. W. K.; Winfree, E., Self-assembly of carbon nanotubes into two-dimensional geometries using DNA origami templates. *Nat Nano* **2010,** *5* (1), 61-66.
163. Kuzyk, A.; Schreiber, R.; Fan, Z.; Pardatscher, G.; Roller, E.-M.; Hogele, A.; Simmel, F. C.; Govorov, A. O.; Liedl, T., DNA-based self-assembly of chiral plasmonic nanostructures with tailored optical response. *Nature* **2012,** *483* (7389), 311-314.
164. Hyman, P.; Valluzzi, R.; Goldberg, E., Design of protein struts for self-assembling nanoconstructs. *Proc. Nat. Acad. Sci. U.S.A.* **2002,** *99* (13), 8488-8493.
165. Park, S. Y.; Lytton-Jean, K. R. A.; Lee, B.; Weigand, S.; Schatz, G. C.; Mirkin, C. A., DNA programmable nanoparticle crystallization. *Nature* **2008,** *451*, 553-556.
166. Jones, M. R.; Macfarlane, R. J.; Lee, B.; Zhang, J. A.; Young, K. L.; Senesi, A. J.; Mirkin, C. A., DNA-nanoparticle superlattices formed from anisotropic building blocks. *Nature Materials* **2010,** *9* (11), 913-917.
167. Merzlyak, A.; Lee, S.-W., Phage as templates for hybrid materials and mediators for nanomaterial synthesis. *Curr. Opin. Chem. Biol.* **2006,** *10* (3), 246-252.
168. Oshea, E. K.; Rutkowski, R.; Kim, P. S., Evidence That the Leucine Zipper Is a Coiled Coil. *Science* **1989,** *243* (4890), 538-542.
169. Gopinath, A.; Rothemund, P. W. K., Optimized Assembly and Covalent Coupling of Single-Molecule DNA Origami Nanoarrays. *ACS Nano* **2014,** *8* (12), 12030-12040.
170. Nuraje, N.; Banerjee, I. A.; MacCuspie, R. I.; Yu, L. T.; Matsui, H., Biological bottom-up assembly of antibody nanotubes on patterned antigen arrays. *J. Am. Chem. Soc.* **2004,** *126* (26), 8088-8089.
171. Heller, M. J., DNA Microarray Technology: Devices, Systems, and Applications. *Annu. Rev. Biomed. Eng.* **2002,** *4* (1), 129-153.

172. Cretich, M.; Damin, F.; Pirri, G.; Chiari, M., Protein and peptide arrays: Recent trends and new directions. *Biomol. Eng* **2006,** *23* (2–3), 77-88.
173. Jamadagni, S. N.; Godawat, R.; Dordick, J. S.; Garde, S., How Interfaces Affect Hydrophobically Driven Polymer Folding. *Journal of Physical Chemistry B* **2009,** *113* (13), 4093-4101.
174. Claesson, P. M.; Blomberg, E.; Froberg, J. C.; Nylander, T.; Arnebrant, T., Protein Interactions at Solid-Surfaces. *Advances in Colloid and Interface Science* **1995,** *57*, 161-227.
175. Raffaini, G.; Ganazzoli, F., Protein adsorption on biomaterial and nanomaterial surfaces: a molecular modeling approach to study non-covalent interactions. *J. Appl. Biomater. Biomech.* **2010,** *8* (3), 135-145.
176. Jones, R. A. L.; Richards, R. W., *Polymers at Surfaces and Interfaces*. Cambridge University Press 1999.
177. Balamurugan, K.; Gopalakrishnan, R.; Raman, S. S.; Subramanian, V., Exploring the Changes in the Structure of α-Helical Peptides Adsorbed onto a Single Walled Carbon Nanotube Using Classical Molecular Dynamics Simulation. *J. Phys. Chem. B* **2010,** *114* (44), 14048-14058.
178. Gong, P.; Levicky, R., DNA surface hybridization regimes. *Proc. Natl. Acad. Sci. U.S.A* **2008,** *105* (14), 5301-5306.
179. Doshi, D. A.; Watkins, E. B.; Israelachvili, J. N.; Majewski, J., Reduced water density at hydrophobic surfaces: Effect of dissolved gases. *Proc. Natl. Acad. Sci. U.S.A* **2005,** *102* (27), 9458-9462.
180. Scatena, L. F.; Brown, M. G.; Richmond, G. L., Water at hydrophobic surfaces: Weak hydrogen bonding and strong orientation effects. *Science* **2001,** *292* (5518), 908-912.
181. Patel, A. J.; Varilly, P.; Chandler, D.; Garde, S., Quantifying Density Fluctuations in Volumes of All Shapes and Sizes Using Indirect Umbrella Sampling. *J. Stat. Phys.***2011,** *145* (2), 265-275.
182. Mrksich, M.; Whitesides, G. M., Using self-assembled monolayers to understand the interactions of man-made surfaces with proteins and cells. *Annu. Rev. Biophys. Biomol. Struct.* **1996,** *25*, 55-78.
183. Ramos, R.; Gordon, M. J., Reflection-mode, confocal, tip-enhanced Raman spectroscopy system for scanning chemical microscopy of surfaces. *Rev. Sci. Instrum.* **2012,** *83* (9), -.
184. Mazzola, L. T.; Frank, C. W.; Fodor, S. P.; Mosher, C.; Lartius, R.; Henderson, E., Discrimination of DNA hybridization using chemical force microscopy. *Biophys. J.* **1999,** *76* (6), 2922-2933.
185. Woo, S.; Rothemund, P. W. K., Self-assembly of two-dimensional DNA origamilattices using cation-controlled surface diffusion. *Nat. Comm.* **2014,** *5*, 4889.
186. Walder, R.; Nelson, N.; Schwartz, D. K., Super-resolution surface mapping using the trajectories of molecular probes. *Nat. Comm.* **2011,** *2*.
187. Lakowicz, J. R., Energy Transfer. In *Principles of Fluorescence Spectroscopy*, 3rd ed.; Lakowicz, J., Ed. Springer: New York, 2006; pp 443-475.

188. Huang, Y.; Duan, X.; Wei, Q.; Lieber, C. M., Directed Assembly of One-Dimensional Nanostructures into Functional Networks. *Science* **2001,** *291* (5504), 630-633.
189. Penzo, E.; Wang, R.; Palma, M.; Wind, S. J., Selective placement of DNA origami on substrates patterned by nanoimprint lithography. *J. Vac. Sci. Technol. B* **2011,** *29* (6), 06F205.
190. Marqusee, S.; Robbins, V. H.; Baldwin, R. L., Unusually Stable Helix Formation in Short Alanine-Based Peptides. *Proc. Natl. Acad. Sci. U. S. A.* **1989,** *86* (14), 5286-5290.
191. Scholtz, J. M.; Baldwin, R. L., The Mechanism of Alpha-Helix Formation by Peptides. *Annu. Rev. Biophys. Biomol. Struct.* **1992,** *21*, 95-118.
192. Jas, G. S.; Hegefeld, W. A.; Middaugh, C. R.; Johnson, C. K.; Kuczera, K., Detailed Microscopic Unfolding Pathways of an alpha-Helix and a beta-Hairpin: Direct Observation and Molecular Dynamics. *J. Phys. Chem. B* **2014,** *118* (26), 7233-7246.
193. Zagrovic, B.; Jayachandran, G.; Millett, I. S.; Doniach, S.; Pande, V. S., How large is an alpha-helix? Studies of the radii of gyration of helical peptides by small-angle X-ray scattering and molecular dynamics. *J. Mol. Biol.* **2005,** *353* (2), 232-241.
194. Gnanakaran, S.; Hochstrasser, R. M.; Garcia, A. E., Nature of structural inhomogeneities on folding a helix and their influence on spectral measurements. *Proc. Natl. Acad. Sci. U. S. A.* **2004,** *101* (25), 9229-9234.
195. Thompson, P. A.; Munoz, V.; Jas, G. S.; Henry, E. R.; Eaton, W. A.; Hofrichter, J., The helix-coil kinetics of a heteropeptide. *J. Phys. Chem. B* **2000,** *104* (2), 378-389.
196. Wang, T.; Zhu, Y.; Getahun, Z.; Du, D.; Huang, C. Y.; Degrado, W. F.; Gai, F., Length Dependent Helix-Coil Transition Kinetics of Nine Alanine-Based Peptides. *J. Phys. Chem. B* **2004,** *108* (39).
197. Sorin, E. J.; Pande, V. S., Exploring the helix-coil transition via all-atom equilibrium ensemble simulations. *Biophys. J.* **2005,** *88* (4), 2472-2493.
198. Nymeyer, H.; Garcia, A. E., Simulation of the folding equilibrium of alpha-helical peptides: A comparison of the generalized born approximation with explicit solvent. *Proc. Natl. Acad. Sci. U. S. A.* **2003,** *100* (24), 13934-13939.
199. Chakrabartty, A.; Kortemme, T.; Baldwin, R. L., Helix Propensities of the Amino-Acids Measured in Alanine-Based Peptides without Helix-Stabilizing Side-Chain Interactions. *Protein Sci.* **1994,** *3* (5), 843-852.
200. Doig, A. J.; Chakrabartty, A.; Klingler, T. M.; Baldwin, R. L., Determination of Free Energies of N-Capping in .alpha.-Helixes by Modification of the Lifson-Roig Helix-Coil Theory To Include N- and C-Capping. *Biochem.***1994,** *33* (11), 3396-3403.
201. Lundqvist, M.; Nygren, P.; Jonsson, B. H.; Broo, K., Induction of structure and function in a designed peptide upon adsorption on a silica nanoparticle. *Angew. Chem.-Int. Edit.* **2006,** *45* (48), 8169-8173.
202. Zhao, X.; Liu, R.; Chi, Z.; Teng, Y.; Qin, P., New Insights into the Behavior of Bovine Serum Albumin Adsorbed onto Carbon Nanotubes: Comprehensive Spectroscopic Studies. *J. Phys. Chem. B* **2010,** *114* (16), 5625-5631.

203. Matsuura, K.; Saito, T.; Okazaki, T.; Ohshima, S.; Yumura, M.; Iijima, S., Selectivity of water-soluble proteins in single-walled carbon nanotube dispersions. *Chem. Phys. Lett.* **2006,** *429* (4–6), 497-502.
204. Wang, S.; Humphreys, E. S.; Chung, S.-Y.; Delduco, D. F.; Lustig, S. R.; Wang, H.; Parker, K. N.; Rizzo, N. W.; Subramoney, S.; Chiang, Y.-M.; Jagota, A., Peptides with selective affinity for carbon nanotubes. *Nat Mater* **2003,** *2* (3), 196-200.
205. Dieckmann, G. R.; Dalton, A. B.; Johnson, P. A.; Razal, J.; Chen, J.; Giordano, G. M.; Muñoz, E.; Musselman, I. H.; Baughman, R. H.; Draper, R. K., Controlled Assembly of Carbon Nanotubes by Designed Amphiphilic Peptide Helices. *J. Am. Chem. Soc.* **2003,** *125* (7), 1770-1777.
206. Lu, D. R.; Park, K., Effect of Surface Hydrophobicity on the Conformational-Changes of Adsorbed Fibrinogen. *J. Colloid Interface Sci.* **1991,** *144* (1), 271-281.
207. Burkett, S. L.; Read, M. J., Adsorption-Induced Conformational Changes of α-Helical Peptides. *Langmuir* **2001,** *17* (16), 5059-5065.
208. Lai, P. Y., STATICS AND DYNAMICS OF A POLYMER-CHAIN ADSORBED ON A SURFACE - MONTE-CARLO SIMULATION USING THE BOND-FLUCTUATION MODEL. *Physical Review E* **1994,** *49* (6), 5420-5430.
209. Eisenriegler, E.; Kremer, K.; Binder, K., Adsorption of polymer chains at surfaces: Scaling and Monte Carlo analyses. *J. Chem. Phys.* **1982,** *77* (12), 6296-6320.
210. Wong, J. S. S.; Hong, L.; Bae, S. C.; Granick, S., Polymer Surface Diffusion in the Dilute Limit. *Macromolecules* **2011,** *44* (8), 3073-3076.
211. Skaug, M. J.; Schwartz, D. K., Using the dynamics of fluorescent cations to probe and map charged surfaces. *Soft Matter* **2012,** *8* (48), 12017-12024.
212. Sulpizi, M.; Gaigeot, M.-P.; Sprik, M., The Silica–Water Interface: How the Silanols Determine the Surface Acidity and Modulate the Water Properties. *J. Chem. Theory Comput.* **2012,** *8* (3), 1037-1047.
213. Kastantin, M.; Langdon, B. B.; Chang, E. L.; Schwartz, D. K., Single-Molecule Resolution of Interfacial Fibrinogen Behavior: Effects of Oligomer Populations and Surface Chemistry. *J. Am. Chem. Soc.* **2011,** *133* (13), 4975-4983.
214. Skaug, M. J.; Schwartz, D. K., Using the dynamics of fluorescent cations to probe and map charged surfaces. *Soft Matter* **2012,** *8*, 12017-12024.
215. Kastantin, M.; Schwartz, D. K., Connecting Rare DNA Conformations and Surface Dynamics Using Single-Molecule Resonance Energy Transfer. *ACS Nano* **2011,** *5* (12), 9861-9869.
216. HiLyte Fluor. http://www.anaspec.com/content/pdfs/c_literature168.pdf (accessed March 1, 2015).
217. Mukhopadhyay, S.; Krishnan, R.; Lemke, E. A.; Lindquist, S.; Deniz, A. A., A natively unfolded yeast prion monomer adopts an ensemble of collapsed and rapidly fluctuating structures. *Proc. Nat. Acad. Sci. U.S.A.* **2007,** *104* (8), 2649-2654.
218. Honciuc, A.; Schwartz, D. K., Probing Hydrophobic Interactions Using Trajectories of Amphiphilic Molecules at a Hydrophobic/Water Interface. *J. Am. Chem. Soc.* **2009,** *131* (16), 5973-5979.
219. Steinbach, P. J., Filtering artifacts from lifetime distributions when maximizing entropy using a bootstrapped model. *Anal. Biochem.* **2012,** *427* (1), 102-105.

220. Steinbach, P. J., Inferring lifetime distributions from kinetics by maximizing entropy using a bootstrapped model. *J. Chem. Inf. Comput. Sci.* **2002,** *42* (6), 1476-1478.
221. Steinbach, P. J.; Ionescu, R.; Matthews, C. R., Analysis of kinetics using a hybrid maximum-entropy/nonlinear-least-squares method: Application to protein folding. *Biophys. J.* **2002,** *82* (4), 2244-2255.
222. Gensch, T.; Bohmer, M.; Aramendia, P. F., Single molecule blinking and photobleaching separated by wide-field fluorescence microscopy. *J. Phys. Chem. A* **2005,** *109* (30), 6652-6658.
223. Foley, J. P.; Dorsey, J. G., Equations for Calculation of Chromatographic Figures of Merit for Ideal and Skewed Peaks. *Anal. Chem.* **1983,** *55* (4), 730-737.
224. Horvath, K.; Olajos, M.; Felinger, A.; Hajos, P., Retention controlling and peak shape simulation in anion chromatography using multiple equilibrium model and stochastic theory. *J. Chromatogr. A* **2008,** *1189* (1-2), 42-51.
225. Bindhu, C. V.; Harilal, S. S.; Nampoori, V. P. N.; Vallabhan, C. P. G., Solvent effect on absolute fluorescence quantum yield of rhodamine 6G determined using transient thermal lens technique. *Mod. Phys. Lett. B* **1999,** *13* (16), 563-576.
226. Stirling Churchman, L.; Flyvbjerg, H.; Spudich, J. A., A Non-Gaussian Distribution Quantifies Distances Measured with Fluorescence Localization Techniques. *Biophys. J.* **2006,** *90* (2), 668-671.
227. Greenfield, N. J., Using circular dichroism spectra to estimate protein secondary structure. *Nat. Protoc.* **2006,** *1* (6), 2876-2890.
228. Greenfield, N. J.; Fasman, G. D., Computed circular dichroism spectra for the evaluation of protein conformation. *Biochem.***1969,** *8* (10), 4108-4116.
229. Pauling, L.; Corey, R. B.; Branson, H. R., The structure of proteins: Two hydrogen-bonded helical configurations of the polypeptide chain. *Proc. Nat. Acad. Sci. U.S.A.* **1951,** *37* (4), 205-211.
230. Tran, H. T.; Pappu, R. V., Toward an Accurate Theoretical Framework for Describing Ensembles for Proteins under Strongly Denaturing Conditions. *Biophys. J.* **2006,** *91* (5), 1868-1886.
231. Zagrovic, B.; Pande, V. S., Structural correspondence between the [alpha]-helix and the random-flight chain resolves how unfolded proteins can have native-like properties. *Nat. Struct. Mol. Biol.* **2003,** *10* (11), 955-961.
232. Bishop, M.; Clarke, J. H. R., Investigation of the end-to-end distance distribution function for random and self-avoiding walks in two and three dimensions. *J. Chem. Phys.* **1991,** *94* (5), 3936-3942.
233. des Cloizeaux, J., Lagrangian theory for a self-avoiding random chain. *Phys. Rev. A* **1974,** *10* (5), 1665-1669.
234. Kohn, J. E.; Millett, I. S.; Jacob, J.; Zagrovic, B.; Dillon, T. M.; Cingel, N.; Dothager, R. S.; Seifert, S.; Thiyagarajan, P.; Sosnick, T. R.; Hasan, M. Z.; Pande, V. S.; Ruczinski, I.; Doniach, S.; Plaxco, K. W., Random-coil behavior and the dimensions of chemically unfolded proteins. *Proc. Natl. Acad. Sci. U. S. A.* **2004,** *101* (34), 12491-12496.
235. Vig, J. R., UV/ozone cleaning of surfaces. *J. Vac. Sci. Technol. A* **1985,** *3* (3), 1027-1034.

236. Honciuc, A.; Baptiste, D. J.; Schwartz, D. K., Hydrophobic Interaction Microscopy: Mapping the Solid/Liquid Interface Using Amphiphilic Probe Molecules. *Langmuir* **2009,** *25* (8), 4339-4342.

APPENDIX A: SUPPORTING INFORMATION FOR CH. 2

A.1 SINGLE-MOLECULE IMAGING EXPERIMENTAL DETAILS

A.1.1 Surface Preparation

Two-inch diameter highly polished fused silica wafers (Mark Optics) were cleaned in piranha solution (hazardous corrosive, strongly oxidizing solution) and a UV/ozone cleaner[1] and then coated with a trimethylsilyl (TMS) monolayer (i.e. end-capped) by exposure to hexamethyldisilazane vapor in a sealed beaker for 18 hours.[2] A custom-built contact angle goniometer was used to check the quality of TMS monolayers.[3] Contact angle measurements were made by imaging an ~1μL sessile drop on three different positions on the wafer and recording the contact angle, which was 91° ± 1°.

A.1.2 Single-Molecule TIRFM

BODIPY 530/550 C_{12} (BFA) was purchased from Life Technologies, reconstituted in methanol, and stored at –20 °C. Dilute solutions of BFA for imaging experiments were prepared in HPLC-grade methanol and water. Our TIRF microscope, which has been described in detail elsewhere,[4] consists of an inverted Nikon TE-2000 microscope with 60X objective with 1.5X auxiliary magnification, flow cell, prism-based illumination,

532 nm laser, 547 nm long-pass filter and electron multiplied CCD-camera. The microscope is focused at the interface of the TMS surface and bulk solution. Only BFA molecules adsorbed to the interface were localized during image processing because diffusion in solution was too fast to allow localization at the 75 ms frame times (13.03 frames per second) used in these experiments. During single-molecule experiments, the flow cell was at room temperature, and the bulk BFA concentration in the flow cell was set such that adsorbed BFA molecules were separated by about 10 μm. The BFA concentration C_o was 10^{-12} M, 10^{-11} M, and 10^{-10} M for 50%, 56%, and 62% methanol respectively. All image processing was performed in Mathematica 9, as previously described.[5] In brief, diffraction-limited objects in each frame were identified by convoluting the image with a disk matrix, subtracting the local background, and binarizing the image. The images were binarized using a discrete threshold. To set the threshold, the low-intensity half of the lowest intensity peak in the distribution of pixel intensities (attributed to noise in the background of the processed image) was fit to a Gaussian distribution, and the threshold for binarization was defined as 5 standard deviations above the mean of the peak. After binarization, object positions were calculated as the centroid of intensity of contiguous pixels. Objects were tracked by identifying the closest objects in sequential frames for which the distance between closest objects (tracking radius) was less than 0.145 μm. Trajectories were selected that had objects larger than one pixel in size and were at least two frames long to minimize the impact of noise on identification of molecules.

A.2 Range of Retention Measurements

We found that the measurements in 50% methanol neared the upper bound of single-molecule retention measurement in prism-based TIRFM using stagnant solutions of approximately constant solute concentration C_o. The adsorption depth $K = k_{ads}/k_{des}$ varied logarithmically with the solution composition, and in 50% methanol, the value of *K* was 0.29 μm ± 0.15 μm. A value of *K* three orders of magnitude greater would almost equal the ~ 100 μm thickness of the solution and the assumption of constant bulk solution concentration would no longer be valid. We note that the thickness of the solutions was limited by the working distance of the microscope objective and the practicality of the required mixing time. In a stagnant solution of thickness *L*, with a solute with molecular diffusivity *D*, the characteristic mixing time τ_{mix} is defined by the following relation:

$$\tau_{mix} = {L^2}/{6D} \qquad \text{(A1)}$$

The assumption of constant bulk concentration is generally true for $L \gg K$. For BFA with a *D* value of ~400 μm^2 s^{-1}, the mixing time when *L* = 100 μm is only 4 seconds. However, it would become severely limiting for solutions orders of magnitude thicker. (For the interested reader, Squires and co-workers provide an excellent tutorial on transport of solutes to surfaces.[6])

As we increased the concentration of methanol in solution, higher values of C_o were required to observe a significant number of adsorbed molecules on the surface. As C_o increases, the background fluorescence in the image increases, while the signal intensity

remains relatively constant, and so we limited our measurements to 62% methanol in solution, where the background fluorescence was acceptably low and molecules could be identified by our image processing routines using similar threshold values (3.5 - 4.5% of max intensity) for the binarization of the images. With 75% methanol solutions, the threshold values were 7.6 - 9.6% of max intensity which were significantly different from those for data collected in 50% - 62% methanol conditions.

A.3 Fitting Adsorption Event Count Data

Each adsorption site had x molecules adsorb over the course of the experiment. The probability histogram for x was fit to a multicomponent Poisson distribution$f_{ads}(x)$ normalized for $x > 0$

$$f_{ads}(x) = \sum_{i=1}^{n} p_i \frac{{\lambda_i}^x \, e^{-\lambda_i}}{x!\,(1 - e^{-\lambda_i})} \qquad (3)$$

where for the i^{th} population of sites, λ_i is the mean number of adsorption events and p_i is the fraction of total sites, with $\sum p_i = 1$. The average site has $\bar{\lambda} = \sum p_i \lambda_i$ adsorption events. If N molecules adsorb on an area a, the total number of sites S is given by $S = N/\bar{\lambda}$, and the density of sites is S/a. The fit parameters for the fits in Fig 2.3 are reported for the different solution conditions in the table below. We used the minimum number of populations (3 in all cases) required to fit the distributions such that the

residual errors were uncorrelated. Fig A1 shows fits to the 62% methanol data, demonstrating that 3 populations were required to fit the data.

Table A1: Adsorption event count histogram fit parameters. The parameters are for the fits shown in Fig 2.3. The values in parentheses represents the uncertainty (standard error) in the last significant digit of each value. $a = 4{,}300\ \mu m^2$

Percent Methanol	N	$\bar{\lambda}$	S/a (μm^{-2})	p_i	λ_i
50	22,900	0.43(6)	15(2)	0.88(2)	0.17(2)
				0.10(2)	1.9(3)
				0.013(4)	7(1)
56	39,984	0.31(3)	18(2)	0.94(1)	0.18(1)
				0.05(1)	1.8(3)
				0.007(2)	7(1)
62	29,674	0.26(2)	10(1)	0.93(1)	0.13(1)
				0.06(1)	1.4(1)
				0.006(1)	8.3(6)

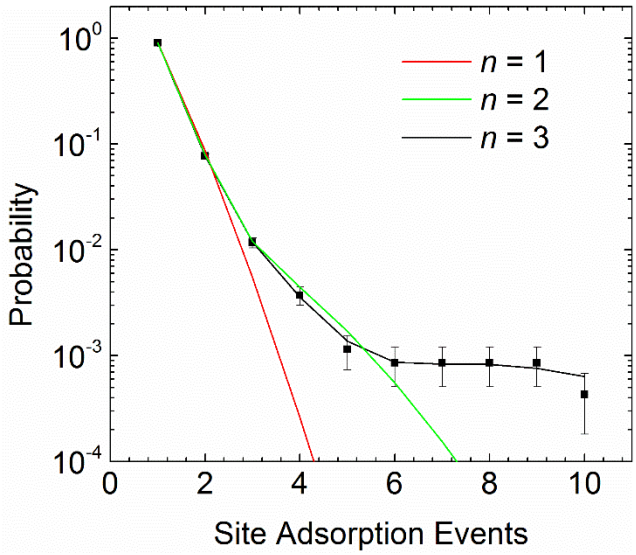

Figure A1: Adsorption event count histogram fit with increasing numbers of components. The 62% methanol data from Fig 2.3 is shown by black squares. The solid lines show best fits of Eq 3 with the specified number of components n.

A.4 Fitting Single-Molecule Residence Time Distributions

A.4.1 Number of Populations

The complementary cumulative distributions $F_S(t)$ of observed surface residence times t were fit to

$$F_S(t) = \sum_{i=1}^{n} p_i \, e^{-t/\tau_i} \qquad (4)$$

where $F_S(t)$ represents the fraction of objects with a residence time $\geq t$. We used the minimum number of populations n required to fit the distributions. The residence time distributions had very similar shapes in the different solvent conditions, and so we show the residence time data and resulting fits for different values of n for a representative condition (62% methanol) in Fig A2. With two populations, there was significant

systematic deviation between the experimental data and the fit of Eq 4. For three or more populations, the distributions were fit with R^2 values greater than 0.99.

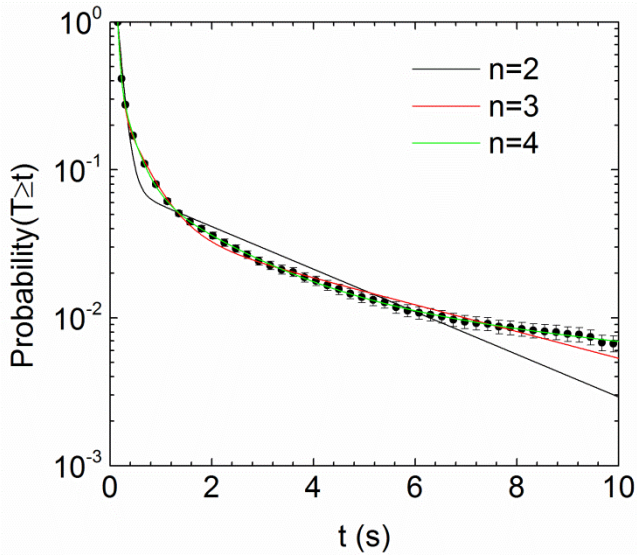

Figure A2: Residence time distribution fits for increasing numbers of populations. Data from 62% methanol experiments (●) with standard error. Fits of Eq. 4 with different numbers of populations n as annotated. R^2: 0.9539 (n = 2), 0.9967 (n = 3), 0.9998 (n = 4).

The approach to fitting the residence time distributions outlined above is based on describing the kinetics as a sum of discrete exponential processes. Alternatively, the residence time distributions can be fit with a quasi-continuous distribution of first-order kinetic lifetimes, using a regularization method such as the maximum entropy method (MEM), which we used here as implemented in MemExp 4.0.[7-9] In MEM fitting, structure is introduced to the residence time distribution conservatively starting from a uniform prior distribution and without the bias introduced by having to provide initial values for parameters in a nonlinear fitting scheme like that used for the mixture of discrete exponential fits.[9] The fit to the complementary cumulative residence time distribution is given by

$$F_S(t) = \int_0^\infty p\,(\log(\tau))e^{-\frac{t}{\tau}}\; dlog(\tau) \qquad (A2)$$

where p is the probability of a given value of $\log(\tau)$. A more detailed overview of the fitting procedure and underlying theory have previously been reported.[10] If the lifetime kinetics are well-described by a discrete mixture of first order processes, then the distribution of lifetimes p will contain sharp, well-resolved peaks centered at the characteristic lifetimes. Figure A3 shows the distribution p that was fit to the 62% methanol residence time distribution. We plot the characteristic residence times from the fit of the discrete model (Eq 4) as lines centered at τ_i with height proportional to the fit fraction p_i. The peaks from the MEM fit were similar in relative height and location to the discrete characteristic residence times from the mixture model. Figure A4 shows the fit of Eq A2 to the 62% methanol data, which matched the experimental residence time distribution within error. Thus by two very different fitting procedures we determined

that three first order exponential processes gave a satisfactory description of the experimental residence time distribution.

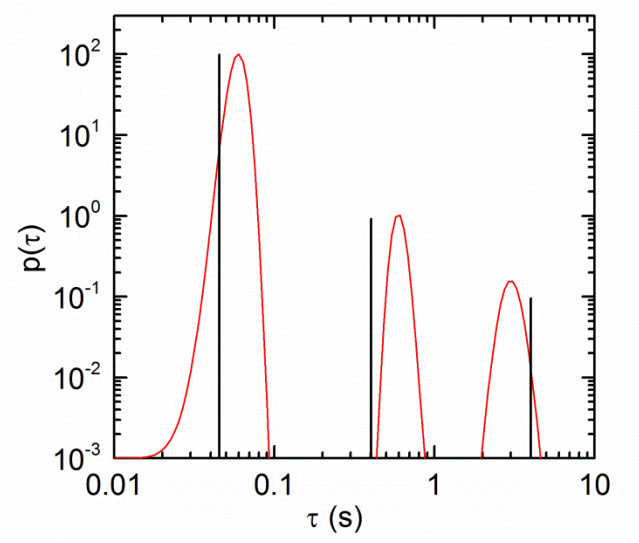

Figure A3: Fitted distributions of residence times. Probability *p(τ)* of characteristic first-order residence time τ from MEM fit of Eq. A2 (red) to 62% methanol data. Discrete fit of Eq 4, bars (black) centered at τ_i with height 100 f_i.

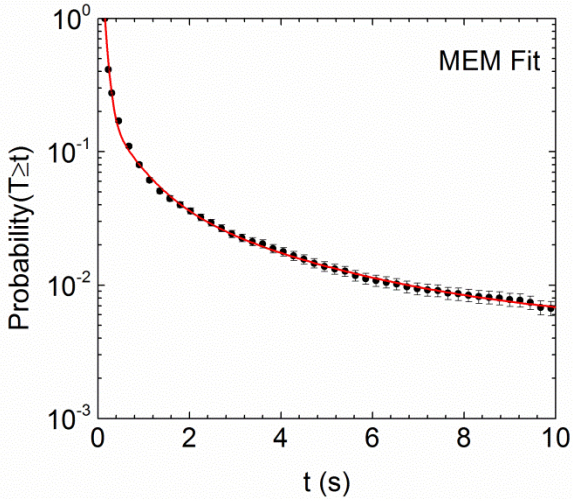

Figure A4: Residence time distribution fit by maximum entropy method. Data from 62% methanol experiments (black circles) with standard error. Fit by maximum entropy method according to Eq A2 (red line).

A.4.2 Dependence of Population Fractions on Solution Conditions

Each component distribution of the mixture model (Eq 4) had a characteristic residence time τ_i and represented a fraction p_i of the adsorption events. The most common physical interpretation of this model is that the surface adsorption sites have n possible binding energies, giving rise to n characteristic times for first-order desorption. We refer to this as having n populations in the desorption kinetics. The distribution of binding energies can arise from having physically different surface sites or from the adsorbed molecule having different binding configurations. Our adsorption kinetics data (Table A1) showed small shifts in the population fractions across the different solution conditions, leading us to conclude that the different kinetic populations could be mostly attributed to having different types of surface sites. However, independent fits of the residence time data for different solution conditions showed slightly greater differences in the population fractions (Table 1). If the exact composition of the active adsorption sites was totally independent of solution conditions, then the residence time distributions for the different solution conditions could be fit using the same population fractions. We show fits according to this scheme in Fig A5. We found that while the fits recapitulated some of the trends in the data, they did not fit the tails of the distribution within error. Thus, we concluded that the exact composition of the active adsorption sites may have had a weak solution dependence.

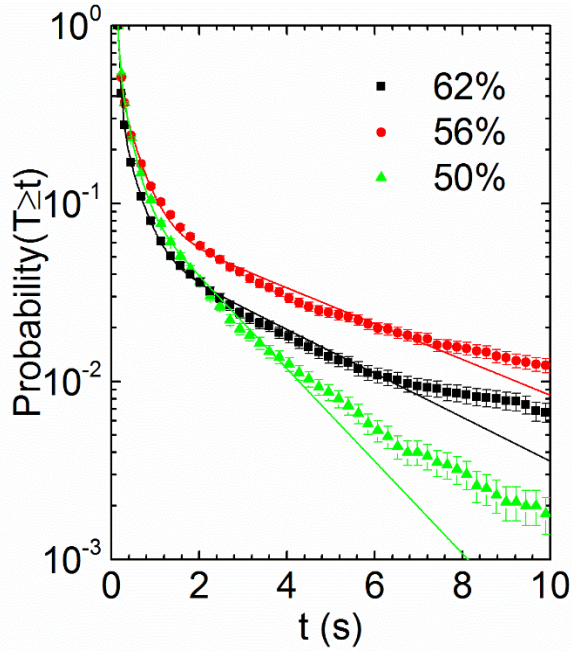

Figure A5: Residence time distribution fits with fixed population fractions. Experimental data are shown with standard error for percent methanol in solution as annotated. Fits using Eq 4 with three populations are shown with solid lines.

Table A2: Parameters for residence time distribution fits. The parameter values are for the fits shown in Fig A5. The numbers in parentheses represents the uncertainty in the last significant digit of each value (standard error).

Percent Methanol	$\overline{\tau_S}$	p_i	τ_i
50	0.053(4)	0.961(5)	0.037(2)
		0.035(8)	0.25(2)
		0.0049(5)	1.7(1)
56	0.08(1)	0.961(5)	0.045(4)
		0.035(8)	0.42(6)
		0.0049(5)	4.6(4)
62	0.078(5)	0.961(5)	0.051(2)
		0.035(8)	0.33(1)
		0.0049(5)	3.5(3)

A.5 Correlation between Site Residence Times and Adsorption Rates

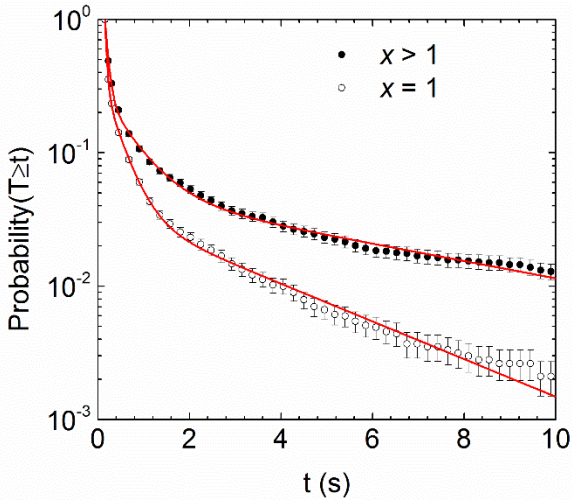

Figure A6: Adsorption site residence time distributions. Data from sites (in 62% methanol) with adsorption event count $x = 1$ and from sites with $x > 1$ showing that longer site residence times were correlated with higher adsorption rates. Fits to 3-component exponential mixture distributions (Eq 4) shown with red solid lines. 2.3 adsorption events μm^{-2} were observed.

Table A3: Adsorption site residence time distribution fit parameters at different site adsorption event counts. Eq 4 fits. The numbers in parentheses represents the uncertainty (standard error) in the last significant digit of each value. 2.3 adsorption events μm^{-2} were observed at each solution condition. 43% - 55% of adsorption events occurred on the sites with x > 1, and so the amount of residence time data for both types of sites was roughly equal.

Percent Methanol	$x = 1$			$x > 1$		
	$\overline{\tau_S}$	τ_i	p_i	$\overline{\tau_S}$	τ_i	p_i
50	0.066(2)	0.052(2)	0.965(3)	0.23(1)	0.094(7)	0.83(2)
		0.35(2)	0.033(2)		0.6(1)	0.141(1)
		2.1(6)	0.0025(8)		3.1(7)	0.026(8)
56	0.078(9)	0.054(4)	0.967(2)	0.4(1)	0.01(1)	0.84(2)
		0.43(8)	0.029(2)		0.8(2)	0.13(2)
		3.8(8)	0.0036(6)		9(2)	0.025(3)
62	0.051(9)	0.042(2)	0.984(2)	0.16(1)	0.074(4)	0.945(8)
		0.36(4)	0.015(2)		0.6(1)	0.047(5)
		3.4(7)	0.0013(1)		7(1)	0.009(3)

A.6 Calculation of Single-Molecule Step Size Distributions

We analyzed the 1D step size distributions using the self-part of the van Hove correlation function

$$G_s(\Delta x, \Delta t) = \frac{1}{N}\langle \sum_{i=1}^{N} \delta[\Delta x + x_i(t) - x_i(t+\Delta t)]\rangle \quad \text{(A3)}$$

where G_s is the probability that a molecule has moved a distance Δx along the x or y coordinate during time Δt. N is the total number of trajectories in the dataset, and the brackets here denote time averaging. The step size distributions are sensitive to the mechanism of surface diffusion. For this analysis, the tracking radius was increased to 1.74 μm so that hops from site-to-site could be observed if present. Figure A7 shows a narrow central peak representing periods of apparent immobility and broad tails consistent with a hopping mechanism as found in recent simulations of a similar system.[11-12]

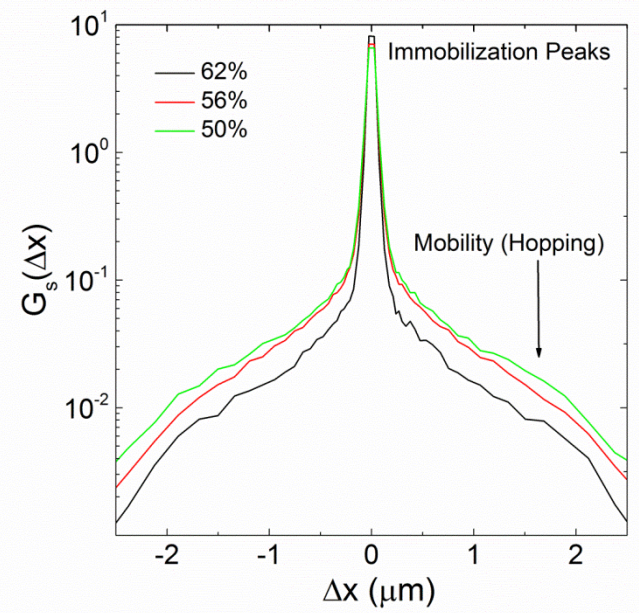

Figure A7: Single-molecule step-size distributions. Lag-time (Δt) of 150 ms. Methanol content of aqueous solvent as annotated.

A.7 Power Studies Demonstrating No Photophysical Effects

Light can induce fluorescent dyes to enter a dark state temporarily (photoblinking) or permanently (photobleaching); the rates of these processes have a strong dependence (typically quadratic) on the light intensity.[13] If either of these processes was significant on the timescale of our imaging, then our measured desorption kinetics would not be accurate. To check if this was the case, we measured surface residence time distributions for ensembles of molecules in 50% methanol excited with 100% laser power (12 $\mu W/\mu m^2$) and with 50% laser power. The tracking radius in this analysis was increased to 1.74 μm, which allowed us to track individual molecules for longer time durations if they hopped from site-to-site. We saw no change in the residence time distributions at different laser powers, leading us to conclude that our measured desorption kinetics reflected the interaction of the adsorbate with the surface and were not biased by photophysical effects.

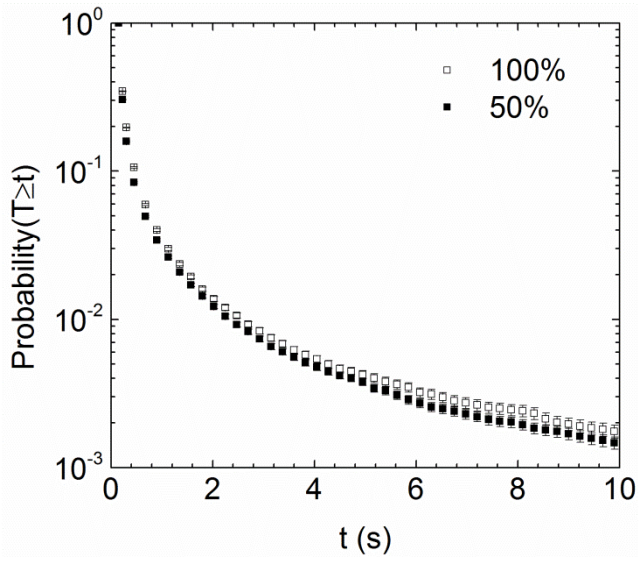

Figure A8: Residence time distributions at different laser power levels. Data from 50% methanol experiments with standard error at 100% and 50% laser power as annotated.

A.8 Chromatograms Showing No Dependence on Analyte Concentration

Chromatographic peak tailing can occur when the analyte interacts with a heterogeneous stationary phase (kinetic effect) or when the concentration of the analyte reaches the nonlinear regime of the adsorption isotherm (overloading effect).[14-15] To verify that our chromatogram shapes reflect kinetic effects and not overloading effects, we increased the BFA concentration by a factor of 3 from the standard concentration (180 μM) to a higher concentration (550 μM) at the methanol composition (62%) with the lowest value of W (narrowest band and hence highest actual concentration in the column). The chromatographic figures of merit for each condition are summarized in the table below and show no dependence on analyte concentration. We also show representative

chromatograms from each condition, which have qualitatively the same shape. Thus we conclude that the tailing in our chromatograms was due to kinetic effects.

Table A4: Chromatographic figures of merit at different BFA concentrations. Data from three replicate experiments at each BFA concentration. Mobile phase 62% methanol. For each measurement, standard error of the last significant digit given in parentheses.

BFA Concentration (μM)	**t_r (min)**	**M_1 (min)**	**W (min)**	**A_s**
180	1.86(7)	1.8 (1)	0.80(4)	1.1(2)
550	1.858(5)	1.86(1)	0.847(7)	1.10(3)

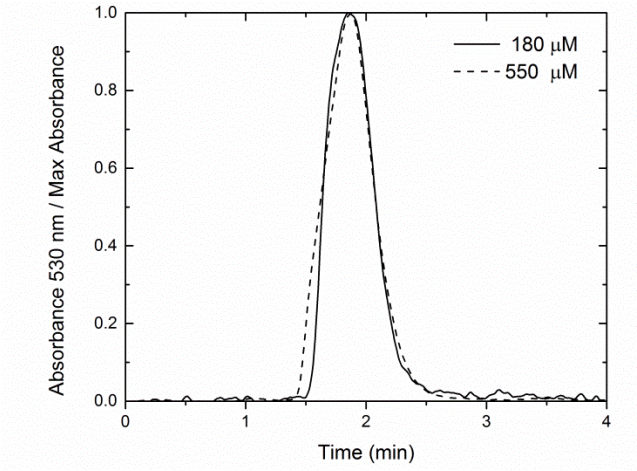

Figure A9: Experimental chromatograms for BFA at different sample concentrations. The BFA concentration of the sample injected into the HPLC system was either the standard (180 μm) or a higher concentration (550 μm). Data for 180 μm shifted 0.14 min to the left.

A.9 Stochastic Model of Chromatography

A.9.1 Theoretical Model

We produced theoretical chromatograms using a procedure developed by Felinger, Dondi, and co-workers[16-18] and briefly present the governing equations here. The theoretical basis for this procedure is the Giddings-Erying model,[19] which views chromatography as a Poisson process, where the number of adsorption events and duration of individual adsorption events (residence times) are randomly distributed. While migrating through the column, a given molecule spends time t_M in the mobile phase and time t_S in the stationary phase with retention time $t_R = t_M + t_S$. The chromatographic peak is the distribution of molecular retention times $f(t_R)$ with first moment $\overline{t_R}$ (average retention time). Assuming the time spent in the mobile phase is constant, the average adjusted retention time is $\overline{t_S} = \overline{t_R} - t_M$.

If the probability distribution of adsorption site residence times $f_S(\tau_S)$ is continuous, with a first moment (average residence time) of $\overline{\tau_S}$, then the average number of adsorption events is given by $\overline{r_M} = \overline{t_S}/\overline{\tau_S}$. (For homogeneous adsorption kinetics, the number of theoretical plates is $\overline{r_M}/2$.) For a given molecule, the probability of adsorbing r_M times follows a Poisson distribution with mean $\overline{r_M} = \mu t_M$, where μ is the frequency of adsorption events. Thus, the distribution of retention times arises from a compound Poisson process involving the random variables r_M and τ_S, which can be described in the frequency domain with a characteristic function ϕ_{τ_S}. (This expression, a Lèvy

representation of the chromatographic process, was formulated by Pasti et. al.,[16] who present an extensive derivation).

$$\phi_{\tau_S}(t_S;\omega|t_M) = \exp\,[t_M \int_0^{\infty}(\exp[i\omega\tau_S] - 1)M(d\tau_S)] \qquad \text{(A4)}$$

where $M(d\tau_S) = \mu\, f(\tau_S)d\tau_S$.

Assuming the time spent in the mobile phase is constant, Eq A4 becomes

$$\phi_{\tau_S}(t_S;\omega|t_M) = \exp\,[\overline{r_M} \int_0^{\infty}(\exp[i\omega\tau_S] - 1)f_S(\tau_S)d\tau_S] \qquad \text{(A5)}$$

In this work, we modeled $f_S(\tau_S)$ as a mixture of exponential distributions defined by

$$f_S(\tau_S) = \sum_{i=1}^{n} \frac{p_i}{\tau_i} \exp\,[-\tau_S/\tau_i] \qquad \text{(A6)}$$

where $\sum_{i=1}^{n} p_i = 1$ and $\overline{\tau_S} = \sum_{i=1}^{n} p_i\,\tau_i$. Substituting Eq A6 into Eq A5, we obtain

$$\phi_{\tau_S}(t_S;\omega|t_M) = \exp\,\left[\overline{r_M} \sum_{i=1}^{n} p_i \left(\frac{1}{1-i\omega\tau_i} - 1\right)\right] \qquad \text{(A7)}$$

The chromatographic peak $f(t_S)$ is obtained by transforming ϕ_{τ_S} to the time domain using the fast Fourier transform algorithm. (We used the Mathematica code provided by Pasti et. al.[16]) To obtain $f(t_r)$, we shift $f(t_S)$ along the time axis by t_M. The obtained chromatogram reflects heterogeneity in the adsorption-desorption kinetics, but does not account for other processes that contribute to band broadening (intraparticle diffusion, external film resistance, longitudinal diffusion, eddy diffusion and extra-column dispersion).[20-21] Felinger[17] introduced an approach to account for mobile phase effects (longitudinal diffusion, eddy diffusion and extra-column dispersion) based on the assumption that the peak shape of the unretained maker (uracil in our experiments)

characterizes these processes. (The molecular diffusivity of the analyte and unretained marker must be similar for this approach to be valid.) The unretained marker peak $f(t_0)$ is convoluted with $f(t_r)$ to produce a theoretical model peak capturing the effects of adsorption-desorption kinetics and mobile-phase effects. We followed this procedure, modeling the uracil peak as a Gaussian since the peak features were not smooth and the peak exhibited no asymmetry (Table A6). (The detector sampling time interval was relatively large compared to the width of the peak). The Gaussian peak used in the convolution was defined as

$$g(t) = \exp\left[{}^{-t}/_{2\sigma_0^2}\right] \qquad \text{(A8)}$$

The peak standard deviation σ_0 was estimated using Foley and Dorsey's expression[22]

$$\sigma_0(uracil) = \frac{W}{3.27A_s+1.2} = 0.014\,min \qquad \text{(A9)}$$

A.9.2 Estimation of True Residence Time Distribution

The whole spectrum of adsorption site residence times cannot be observed with present technology.[10,16,23] With single-molecule TIRFM, we observed adsorption on rare, spatially distinct "specific" (SP) adsorption sites with slow kinetics over the timescale 10 ms to 1 s that comprise an unknown fraction p_{SP} of the total adsorption events. We can infer that the rest of the "nonspecific" (NS) adsorption sites with characteristic adsorption time $\overline{\tau_{NS}}$ involved much faster kinetics and a large fraction $(1 - p_{SP})$ of adsorption

events.[16] The primary effect of the SP sites in a chromatographic process would be to increase the asymmetry (A_s) of the chromatographic peaks.[16-18,23-24]

Following the strategy of Pasti et. al.,[16] we formulated an *ad hoc* estimate of the true residence time distribution $f_S(\tau_S)$ by adding an additional term for the NS kinetics to the distribution $f_{SP}(\tau_S)$ of residence times observed with single-molecule TIRFM.

$$f_S(\tau_S) = p_{SP} f_{SP}(\tau_S) + (1 - p_{SP}) f_{NS}(\tau_S) \qquad \text{(A10)}$$

The experimental distribution of residence times $f_{SP}(\tau_S)$ was a mixture of exponential distributions. We assumed the distribution of residence times on the NS sites, $f_{NS}(\tau_S)$, was an exponential distribution with mean $\overline{\tau_{NS}}$ to come up with the following expression.

$$f_S(\tau_S) = p_{SP} \sum_{i=1}^{n} \frac{p_i}{\tau_i} \exp\left[-\tau_S/\tau_i\right] + (1 - p_{SP}) \exp\left[-\tau_S/\overline{\tau_{NS}}\right] \qquad \text{(A11)}$$

Since the NS sites represent weak adsorption sites, $\overline{\tau_{NS}} \ll \tau_i$ for all i.

The mean residence time $\overline{\tau_S}$ is given by the following expression.

$$\overline{\tau_S} = (1 - p_{SP})\overline{\tau_{NS}} + p_{SP}\overline{\tau_{SP}} \qquad \text{(A12)}$$

where $\overline{\tau_{SP}} = \sum_{i=1}^{n} p_i \tau_i$. For consistency across conditions, we set $\overline{\tau_{NS}} = \frac{1}{\alpha} Minimum\{\tau_1, \tau_2, \ldots\}$. We set α = 10, which represents an upper limit for $\overline{\tau_{NS}}$ as longer residence times would have been recorded by in our single-molecule TIRFM measurements. We discuss the significance of this choice in more detail in the next section.

While we could not measure the absolute value of p_{SP}, we inferred how it changed with solution conditions by comparing our single-molecule measurements of adsorption equilibrium K (presumably dominated by interactions with rare, strong SP sites) to our measurements of the chromatography capacity factor k' (presumably dominated by interactions with abundant, weak NS sites). K was calculated by the following expression.

$$K = \frac{k_{ads}}{k_{des}} = \frac{N/(t_{exp} c\ a)}{1/\overline{\tau_S}} \qquad \text{(A13)}$$

where in the single-molecule experiment N is the total number of adsorption events, t_{exp} is the duration of the experiment, c is the concentration of the adsorbate in solution, and a is the area of the field of view. Since the very short NS adsorption events are not observed in single-molecule experiments, we make the simplifying assumption that $\overline{\tau_S} \approx \overline{\tau_{SP}}$. For a chromatographic system equivalent to the single-molecule experiment, $N \approx p_{SP}\overline{r_M}$ and $t_{exp} = t_0$. Thus the expression for K in an equivalent chromatographic system is

$$K = \frac{p_{SP}\overline{r_M}/(t_0 c\ a)}{1/\overline{\tau_{SP}}} \qquad \text{(A15)}$$

where a is the effective surface area of the stationary phase and c the concentration of solution in equilibrium with the mobile phase. We note that the single-molecule experiments can be thought of as observations of one theoretical plate in an equivalent column. In the context of the stochastic theory of chromatography, the capacity factor can be defined as

$$k' = \overline{r_M}\frac{\overline{\tau_S}}{t_0} \qquad \text{(A14)}$$

where t_0 is the elution time of an unretained compound (uracil). In the chromatography experiments, which are presumed to be dominated by NS adsorption events, we assumed that the SP sites did not contribute to the measured value of k' such that $\overline{\tau_S} \approx \overline{\tau_{NS}}$ giving the following expression for the capacity factor.

$$k' = \overline{r_M}\frac{\overline{\tau_{NS}}}{t_0} \qquad \text{(A16)}$$

Therefore, the ratio of the measured chromatographic capacity factor to the measured equilibrium constant in an equivalent chromatographic system is given by

$$\frac{k\prime}{K} = \frac{ac\overline{\tau_{NS}}}{p_{SP}\,\overline{\tau_{SP}}} \qquad \text{(A17)}$$

We rearranged the above expression such that

$$p_{SP} = \varphi/\delta \qquad (9)$$

where $\varphi = \frac{K}{k\prime}\frac{\overline{\tau_{NS}}}{\overline{\tau_{SP}}}$ and $\delta = \frac{1}{c\,a}$. We note that in our chromatography experiments the area of the stationary phase was constant across the different solution conditions as was the concentration of analyte injected into the mobile phase. For a given theoretical plate, the concentration c of analyte in equilibrium with the surface with effective area *a* was unknown but was assumed to be independent of solvent composition and constant throughout the column. So the parameter δ was treated as a fitting parameter in matching the experimental chromatograms to the theoretical modeled chromatograms. By adopting this approach, we estimated how the contribution of the SP sites to the theoretical modeled chromatograms changed with solution conditions in a systematic and self-consistent manner.

A.9.3 Fitting Experimental Peak Asymmetry Results

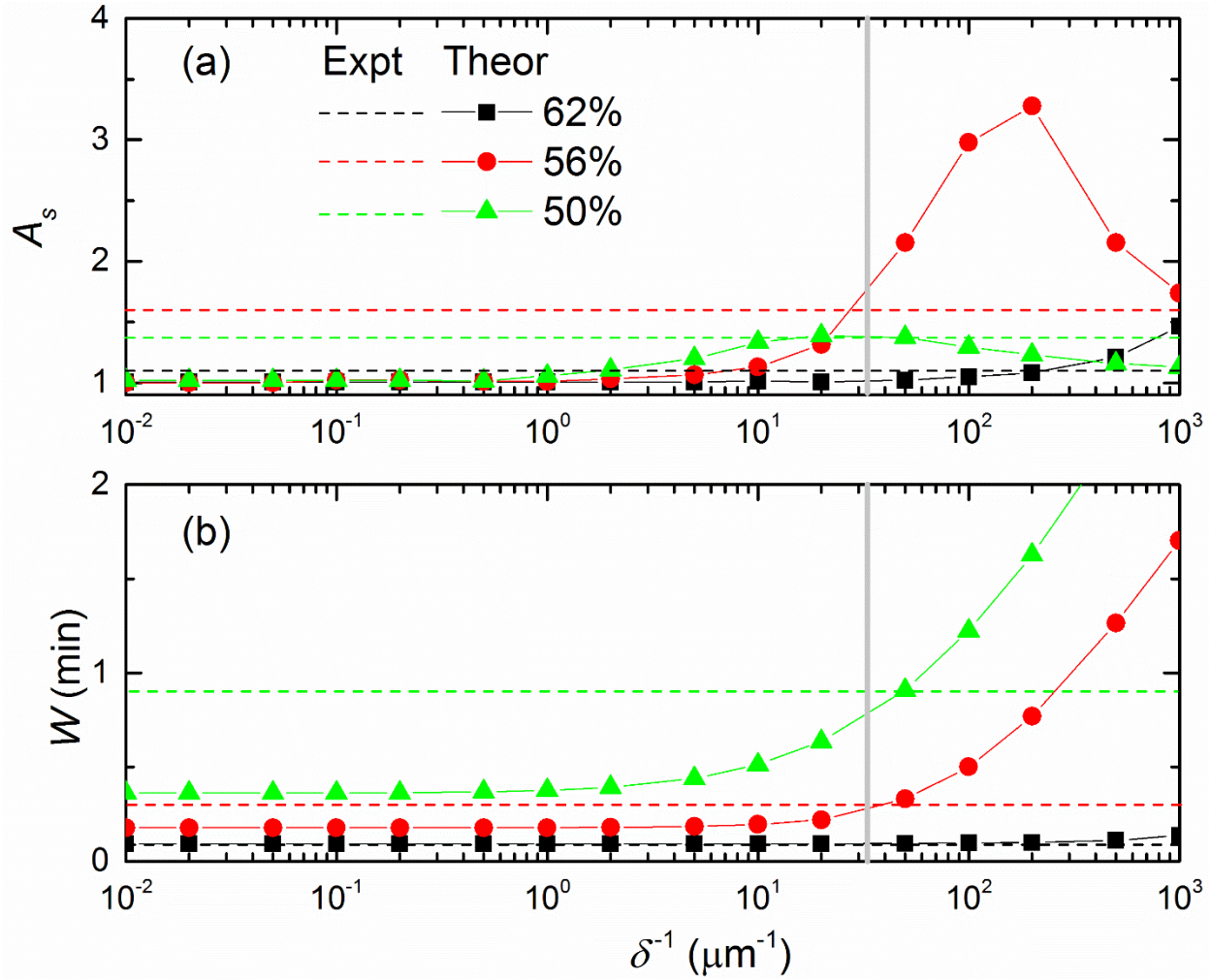

Figure A10: Experimental and theoretical chromatographic figures of merit. The theoretical chromatograms were generated for different values of δ with $\alpha = 10$. Results are shown by the solid data points and compared to experimental chromatography results shown by dashed lines. Panel (a) shows the peak asymmetry data. The best fit to the peak asymmetry data is shown by a gray line at $\delta^{-1} = 33\ \mu m^{-1}$. Panel (b) shows correlation between the theoretical model and experimental values of peak width. Note that experimental values of W were multiplied by a factor of 1/9. The correlation was strong for $\delta^{-1} = 33\ \mu m^{-1}$.

A.9.4 Sensitivity to Characteristic Residence Time Constants

In the context of a two-site model, Felinger and co-workers[25] showed that greater differences in the strong site and weak site characteristic residence times (higher α) result in more asymmetric peaks; as this difference increases, the onset of skew occurs at lower fractions of strong sites. We investigated the sensitivity of our model chromatograms by increasing α from 10 to 100. For both values of α, A_s and W had similar values at the same values of δ^{-1} across the different solution conditions (Fig A11). We note however that $p_{SP} \propto (\alpha\,\delta)^{-1}$ so the fraction of strong sites needed to replicate similar chromatograms decreased as the difference in the strong and weak site residence times increased in agreement with Felinger's results.

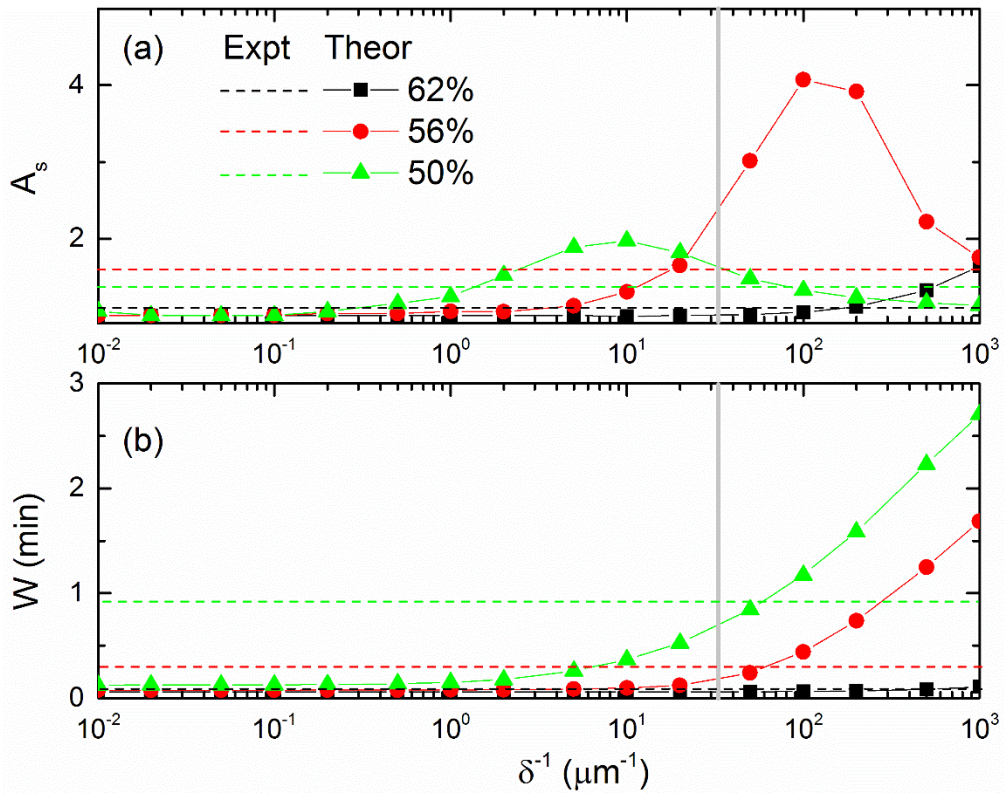

Figure A11: Experimental and theoretical chromatographic figures of merit for $\alpha = 100$. The experimental and theoretical model chromatography results are presented as in Fig A9. The best fit to the peak asymmetry data is shown by a gray line at $\delta^{-1} = 33\ \mu m^{-1}$.

A.10 Experimental and Model Chromatograms

Table A5: Model parameters and results for best fit to peak asymmetry data. Theoretical chromatograms were generated with parameter $\delta^{-1} = 33\ \mu m^{-1}$ for $\alpha = 10$. The fraction of adsorption events onto SP sites p_{SP} was calculated by Eq 9. Peak width W and asymmetry A_s measured as in Fig 6.

	Parameters				Results	
Percent Methanol (v/v)	$\overline{t_S}$ (min)	p_{SP}	$\overline{\tau_S}$ (ms)	$\overline{r_M} = \overline{t_S}/\overline{\tau_S}$	W (min)	A_s
50	29.3	0.0020	7.3	239,000	0.77	1.42
56	6.63	0.0007	7.2	56,000	0.26	1.67
62	1.72	0.0001	5.5	19,000	0.09	1.01

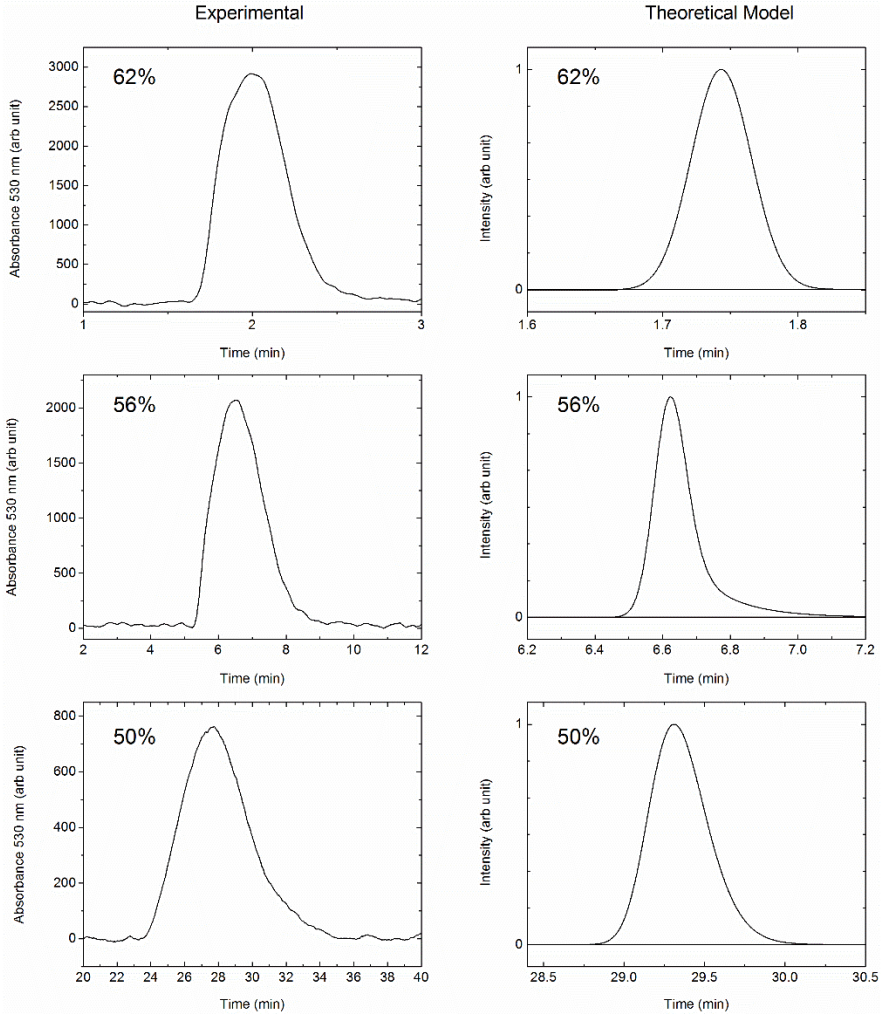

Figure A12: Experimental and theoretical model chromatograms. Model results with $\delta^{-1} = 33\,\mu m^{-1}$ for $\alpha = 10$.

A.10.1 Analysis of Uracil Chromatographic Peaks

Table A6: Chromatographic figures of merit for uracil. For each measurement, uncertainty in the last significant digit given in parentheses. Uncertainty was zero when repeated measurements were the same within instrument resolution. The average across all experimental conditions is also reported and was used in the modeling of chromatographic peaks.

Percent Methanol (v/v)	t_r (min)	M_1 (min)	W (min)	A_s
50	0.108(0)	0.111 (1)	0.063(4)	1.2(2)
56	0.114(3)	0.112(2)	0.067(0)	0.99(2)
62	0.108(0)	0.108(1)	0.067(0)	1.03(0)
Average	0.110(1)	0.110(1)	0.066(1)	1.05(5)

A.11 REFERENCES

1. Kastantin, M.; Langdon, B. B.; Chang, E. L.; Schwartz, D. K., Single-Molecule Resolution of Interfacial Fibrinogen Behavior: Effects of Oligomer Populations and Surface Chemistry. *J. Am. Chem. Soc.* **2011,** *133* (13), 4975-4983.
2. Skaug, M. J.; Schwartz, D. K., Using the dynamics of fluorescent cations to probe and map charged surfaces. *Soft Matter* **2012,** *8*, 12017-12024.
3. Honciuc, A.; Schwartz, D. K., Probing Hydrophobic Interactions Using Trajectories of Amphiphilic Molecules at a Hydrophobic/Water Interface. *J. Am. Chem. Soc.* **2009,** *131* (16), 5973-5979.
4. Honciuc, A.; Harant, A. W.; Schwartz, D. K., Single-Molecule Observations of Surfactant Diffusion at the Solution- Solid Interface. *Langmuir* **2008,** *24* (13), 6562-6566.
5. Walder, R.; Kastantin, M.; Schwartz, D. K., High throughput single molecule tracking for analysis of rare populations and events. *Analyst* **2012,** *137* (13), 2987-2996.
6. Squires, T. M.; Messinger, R. J.; Manalis, S. R., Making it stick: convection, reaction and diffusion in surface-based biosensors. *Nat. Biotechnol.* **2008,** *26* (4), 417-426.
7. Steinbach, P. J., Filtering artifacts from lifetime distributions when maximizing entropy using a bootstrapped model. *Anal. Biochem.* **2012,** *427* (1), 102-105.
8. Steinbach, P. J., Inferring lifetime distributions from kinetics by maximizing entropy using a bootstrapped model. *J. Chem. Inf. Comput. Sci.* **2002,** *42* (6), 1476-1478.
9. Steinbach, P. J.; Ionescu, R.; Matthews, C. R., Analysis of kinetics using a hybrid maximum-entropy/nonlinear-least-squares method: Application to protein folding. *Biophys. J.* **2002,** *82* (4), 2244-2255.
10. Kastantin, M.; Schwartz, D. K., Identifying Multiple Populations from Single-Molecule Lifetime Distributions. *ChemPhysChem* **2013,** *14* (2), 374-380.
11. Skaug, M. J.; Mabry, J.; Schwartz, D. K., Intermittent Molecular Hopping at the Solid-Liquid Interface. *Phys. Rev. Lett.* **2013,** *110* (25), 256101

12. Skaug, M. J.; Mabry, J. N.; Schwartz, D. K., Single-Molecule Tracking of Polymer Surface Diffusion. *J. Am. Chem. Soc.* **2014,** *136* (4), 1327-1332.
13. Gensch, T.; Bohmer, M.; Aramendia, P. F., Single molecule blinking and photobleaching separated by wide-field fluorescence microscopy. *J. Phys. Chem. A* **2005,** *109* (30), 6652-6658.
14. Fornstedt, T.; Zhong, G. M.; Guiochon, G., Peak tailing and slow mass transfer kinetics in nonlinear chromatography. *J. Chromatogr. A* **1996,** *742* (1-2), 55-68.
15. Wirth, M. J.; Smith, E. A.; Anthony, S. R., Measurement and simulation of tailing zones of a cationic dye in analytical-scale reversed phase chromatography. *J. Chromatogr. A* **2004,** *1034* (1-2), 69-75.
16. Pasti, L.; Cavazzini, A.; Felinger, A.; Martin, M.; Dondi, F., Single-molecule observation and chromatography unified by levy process representation. *Anal. Chem.* **2005,** *77* (8), 2524-2535.
17. Felinger, A., Determination of rate constants for heterogeneous mass transfer kinetics in liquid chromatography. *J. Chromatogr. A* **2006,** *1126* (1-2), 120-128.
18. Felinger, A., Molecular dynamic theories in chromatography. *J. Chromatogr. A* **2008,** *1184* (1-2), 20-41.
19. Giddings, J. C.; Eyring, H., A Molecular Dynamic Theory of Chromatography. *J. Phys. Chem.* **1955,** *59* (5), 416-421.
20. Bacskay, I.; Felinger, A., Macroscopic and microscopic analysis of mass transfer in reversed phase liquid chromatography. *J. Chromatogr. A* **2009,** *1216* (8), 1253-1262.
21. Hlushkou, D.; Gritti, F.; Daneyko, A.; Guiochon, G.; Tallarek, U., How Microscopic Characteristics of the Adsorption Kinetics Impact Macroscale Transport in Chromatographic Beds. *J Phys Chem C* **2013,** *117* (44), 22974-22985.
22. Foley, J. P.; Dorsey, J. G., Equations for Calculation of Chromatographic Figures of Merit for Ideal and Skewed Peaks. *Anal. Chem.* **1983,** *55* (4), 730-737.
23. Wirth, M. J.; Swinton, D. J., Single-molecule probing of mixed-mode adsorption at a chromatographic interface. *Anal. Chem.* **1998,** *70* (24), 5264-5271.
24. Horvath, K.; Olajos, M.; Felinger, A.; Hajos, P., Retention controlling and peak shape simulation in anion chromatography using multiple equilibrium model and stochastic theory. *J. Chromatogr. A* **2008,** *1189* (1-2), 42-51.
25. Felinger, A.; Cavazzini, A.; Remelli, M.; Dondi, F., Stochastic-dispersive theory of chromatography. *Anal. Chem.* **1999,** *71* (20), 4472-4479.

APPENDIX B: SUPPORTING INFORMATION FOR CH. 3

B.1 End-to-End Distances of Molecular Trajectories

To evaluate the effect of solvent composition on hopping, we desired to study a subset of trajectories with appreciable surface diffusion. We show the probability distributions of end-to-end distances for all trajectories in Figure B1. While the trajectories were highly heterogeneous as shown in Figure 3.2, the end-to-end distances indicated two qualitatively different subsets: (1) molecules that exhibited some mobility with end-to-end distance sensitive to solvent condition and (2) molecules that were confined for their entire surface residence time with end-to-end distance insensitive to solvent condition. We selected molecules from the first population with end-to-end distances greater than 200 nm to characterize surface diffusion by hopping. Molecules from the second population with end-to-end distances less than 50 nm were selected to analyze the apparent motion of confined molecules as described in the following section.

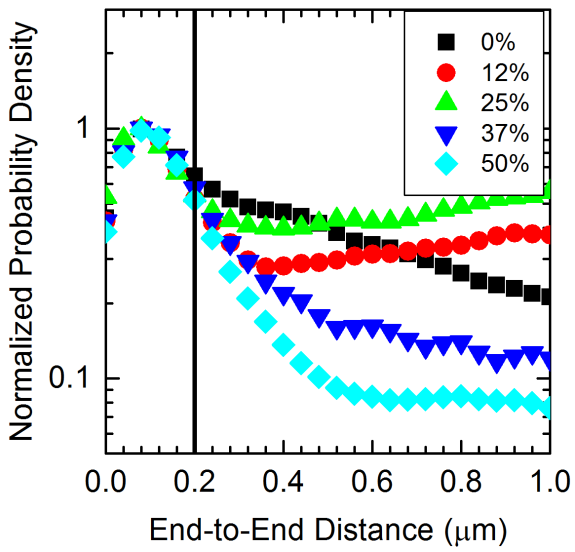

Figure B1: End-to-End Distance Distributions. Probability densities normalized by maximum value. Percent methanol in solution indicated in legend. The vertical line at 200 nm end-to-end distance indicates lower threshold used for selecting subset of mobile molecules.

B.2 Apparent Diffusion of Confined Molecules

When molecules are confined to nanometer-size regions, their apparent motion, i.e. surface diffusion, depends strongly on the localization precision, which is typically ~50 nm in single-molecule TIRFM.[1-3] The localization precision depends on the signal-to-noise ratio of the identified fluorescent objects, which can vary as a function of the solvent environment. The choice of solvent can affect the quantum efficiency of the fluorophore[4] and the effective bulk concentration of fluorophore (contributing to background fluorescence), needed to observe significant numbers of adsorbed single molecules.[2] To estimate the localization precision, we carefully examined the 1-frame step-size distributions of molecules with end-to-end distance < 50 nm for each solution

condition. The step-size distributions for these molecules showed no dependence on lag time (Figure B2), indicating that the population was dominated by confined molecules.

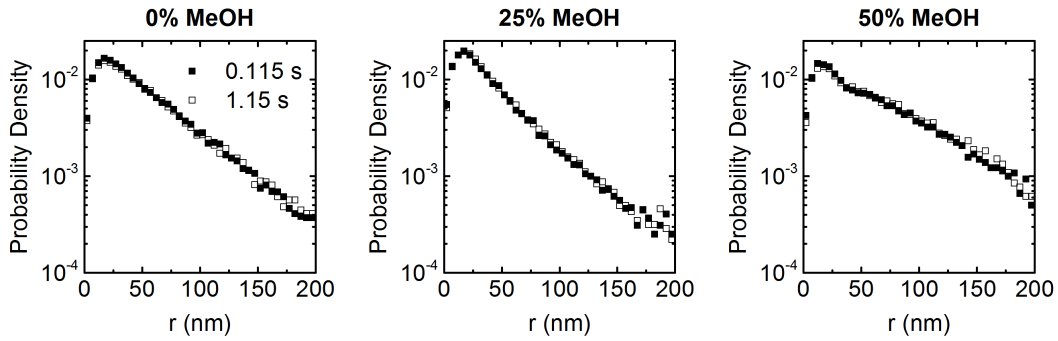

Figure B2: Step-size distributions for trajectories with end-to-end distance < 50 nm at different lag times. The experimental distributions (symbols) of steps observed over Δt = 0.115 s and 1.15 s for the indicated solution conditions. Standard error bars were smaller than the data symbols.

The step-size distribution of truly immobile molecules should depend only upon the accuracy with which the fluorescence point spread function (PSF) can be fit. The PSF is usually described by a Gaussian probability distribution.[5-6] However, if the molecules are not completely immobile but are simply confined at dimensions comparable to the resolution limit or if there is lateral drift in the microscope assembly, the apparent step sizes are described by a heavy-tailed non-Gaussian probability distribution. The apparent step size distribution is a convolution of a Maxwell distribution and a Bessel function, in the special case of the molecule translating a uniform distance over the observation lag time.[7] The experimental step-size distributions of the confined molecules (end-to-end distance < 50 nm) were heavy tailed (Figure B2), indicating there was lateral motion at length scales near the resolution of the technique.

To describe the steps sizes of confined molecules and determine the function $p_{confined}(R, \Delta t)$, we fit the complementary cumulative squared-displacement distributions using Equation 3.2. Figure B3 shows the fit of a representative distribution using increasing numbers of component distributions. In all cases, three component distributions were required to fit the step-size distributions within experimental error (Figure B4). The characteristic step size for confined molecules (i.e. the localization precision) ranged from about 80 nm – 100 nm in the different solution conditions (Table B1).

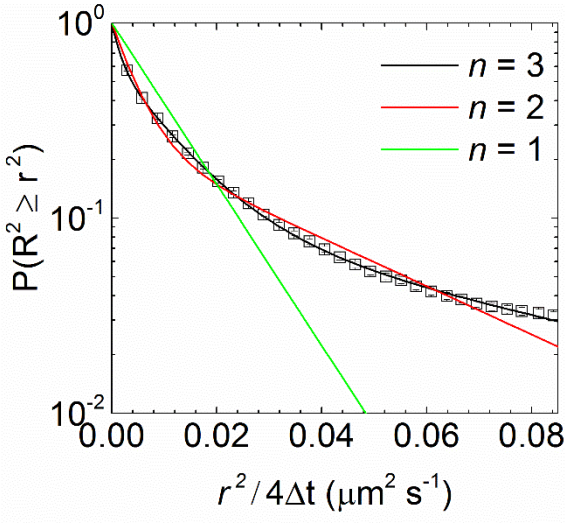

Figure B3: Complementary cumulative squared step-size distributions for trajectories with end-to-end distance < 50 nm in 0% methanol. The experimental distributions (symbols) of squared-step sizes over lag time Δt = 0.115 s with standard error. Fits (solid lines) to Equation 3.2 with the annotated number of component distributions (n).

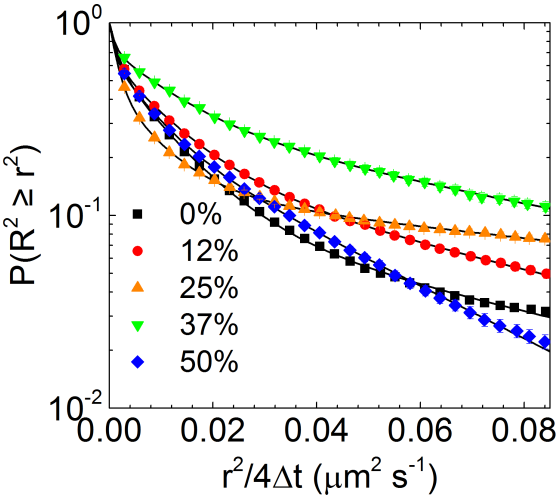

Figure B4: Complementary cumulative squared step-size distributions for trajectories with end-to-end distance < 50 nm. Experimental distributions (symbols) of squared-step sizes over lag time Δt = 0.115 s with standard error for the indicated solution conditions (annotated by percent methanol). Fits of $p_{confined}(R, \Delta t)$ to Equation 3.2 for n = 3 (solid lines).

Table B1: Parameters for the fits of Equation 3.2 shown in Figure B4. The values in parentheses represents the uncertainty (standard error of the mean) in the last significant digit of each value.

Percent Methanol	$\ell_{confined}$ (μm)	**Fraction** f_i	$\ell_{confined,i}$ (μm)
0	0.077(1)	0.46(3)	0.030(6)
		0.43(4)	0.07(1)
		0.12(5)	0.17(6)
12	0.092(1)	0.42(3)	0.028(7)
		0.43(2)	0.06(1)
		0.15(4)	0.20(6)
25	0.098(4)	0.53(3)	0.027(7)
		0.35(3)	0.07(1)
		0.11(4)	0.26(6)
37	0.11(1)	0.40(7)	0.022(6)
		0.35(4)	0.07(2)
		0.25(8)	0.19(5)
50	0.09(1)	0.33(4)	0.03(2)
		0.45(6)	0.08(4)
		0.22(7)	0.16(7)

B.3 Statistical Description of Molecular Mobility

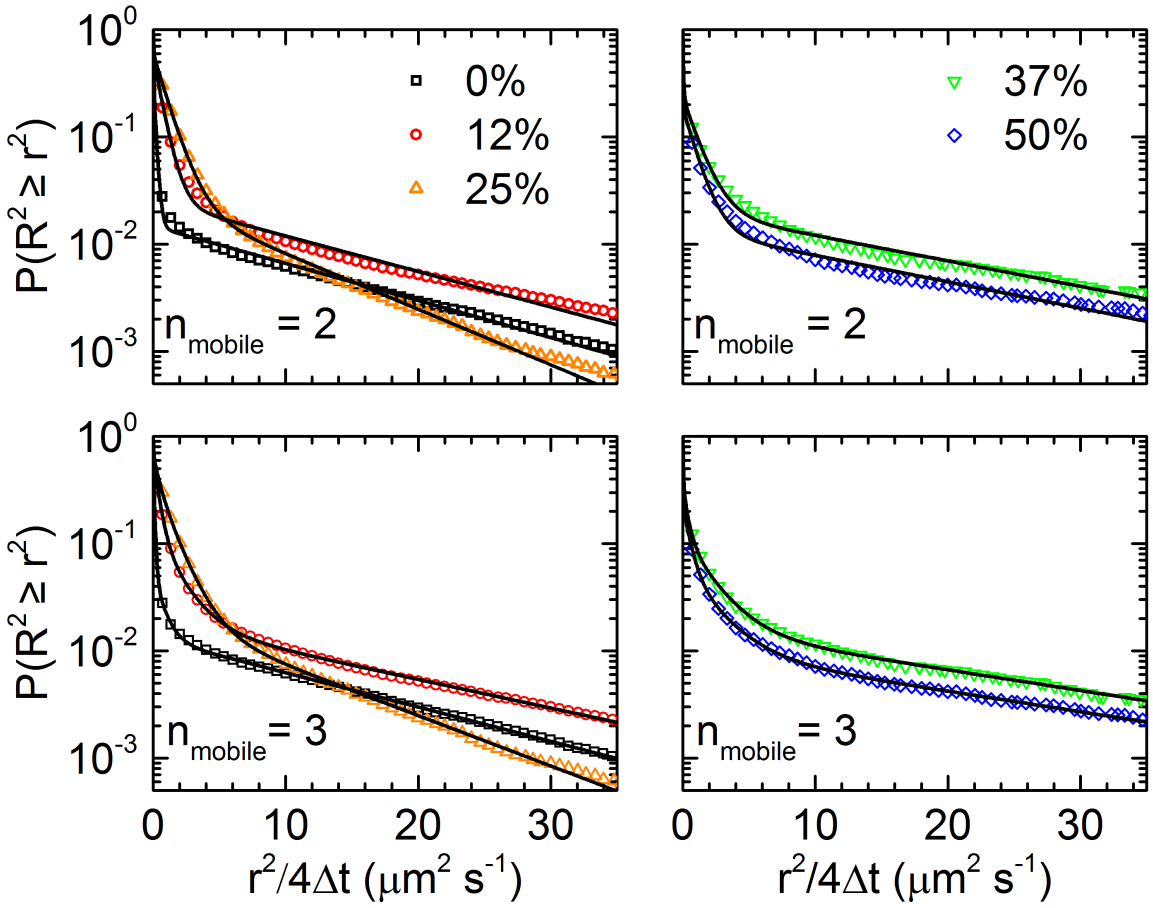

Figure B5: Complementary cumulative squared step-size distributions for trajectories with end-to-end distance > 200 nm. Experimental distributions (symbols) of squared-step sizes over lag time Δt = 0.115 s with standard error for the indicated solution conditions (annotated by percent methanol). Fits of $p_{ensemble}(R, \Delta t)$ to Equation 3.3. The number of components distributions n_{mobile} in $p_{mobile}(R, \Delta t)$ is indicated. In all cases, $p_{ensemble}(R, \Delta t)$ could be fit within error with n_{mobile} = 3.

Table B2: Fit parameters for the Equation 3.3 fits shown in Figure B5. The values in parentheses represents the uncertainty (standard error of the mean) in the last significant digit of each value.

Percent Methanol	**$D_{ensemble}$** ($\mu m^2 B^1$)	**f_{mobile}**	**$f_{mobile,i}$**	**D_{mobile}** ($\mu m^2 B^1$)	**$D_{mobile,i}$** ($\mu m^2 B^1$)
0	0.274(9)	0.49(2)	0.44(2) 0.038(1) 0.0124(3)	0.54(1)	0.114(4) 1.0(1) 14.5(5)
12	0.70(3)	0.65(1)	0.52(1) 0.12(1) 0.0193(4)	1.07(2)	0.43(2) 1.73(7) 14(1)
25	0.88(4)	0.67(4)	0.30(3) 0.35(2) 0.018(2)	1.31(4)	0.54(5) 1.44(8) 12(1)
37	0.60(4)	0.35(3)	0.24(3) 0.095(4) 0.015(1)	1.7(2)	0.30(5) 1.8(1) 23(1)
50	0.49(3)	0.27(2)	0.18(1) 0.07(1) 0.014(2)	1.81(2)	0.36(7) 1.9(2) 21.0(9)

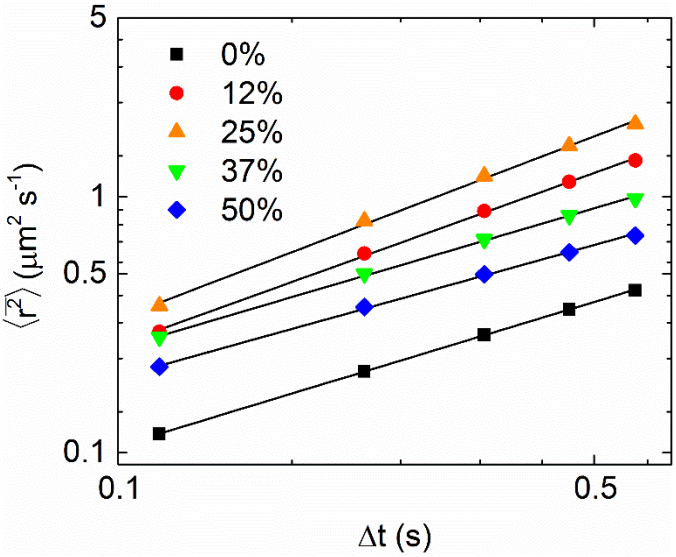

Figure B6: Mean squared displacement as a function of lag time. Experimental data for the indicated solution conditions (annotated by percent methanol). Fits to model $\langle \overline{r^2} \rangle = 4\Gamma\Delta t^{\alpha}$ with power-law exponent α = 0.80(4), 0.930(8), 0.97(2), 0.758(4), and 0.72(3) for 0%, 12%, 25%, 37%, and 50% methanol, respectively.

B.4 Evidence of Surface Heterogeneity

Following our previously reported methodology,[2] we constructed maps of where molecules adsorbed to the surface. Figure B7 shows representative areas from experiments with 0%, 25% and 50% methanol in solution. On a perfectly uniform surface, the probability of more than one molecule adsorbing in the same area was vanishingly low, and so the majority of adsorption events occurred at distinct areas of the surface, which appeared blue in the maps. Rare, anomalously strong adsorption sites were identified in the maps at 0% and 50% methanol and appeared as red areas. So while

molecules observed in these experiments covered only a small fraction of the surface, anomalously strong adsorption sites were sampled in a statistically significant manner.

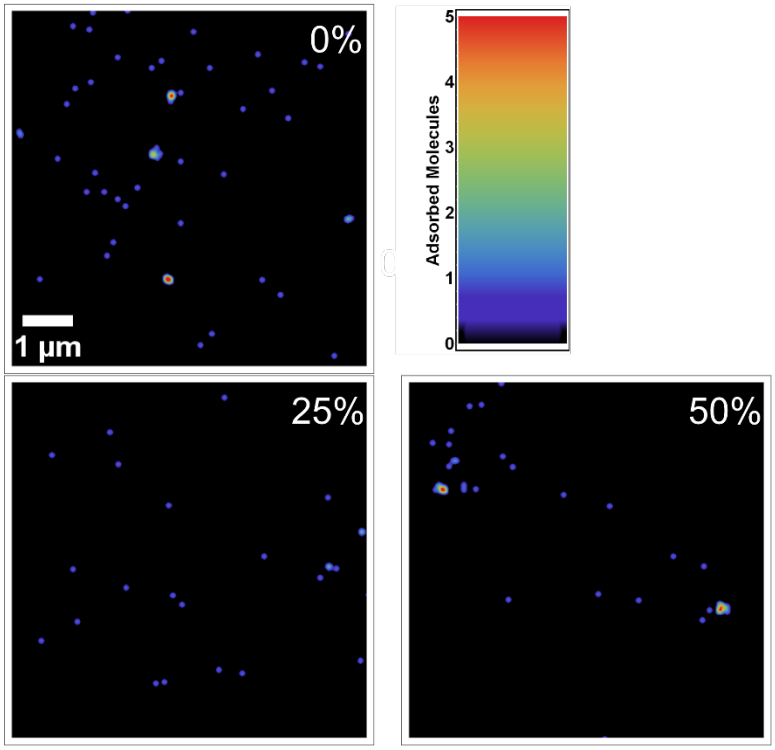

Figure B7: Super-resolution maps of adsorption sites. Experimental data for the indicated solution conditions (annotated by percent methanol). All maps constructed with 0.5 molecules µm2.

The kinetics on these heterogeneous adsorption sites were characterized using a Poisson mixture model.[2,8] The probability distribution for site adsorption events can be modeled with the following equation.

$$f_{ads}(x) = \sum_{i=1}^{n} p_i \frac{{\lambda_i}^x \, e^{-\lambda_i}}{x!\,(1 - e^{-\lambda_i})} \qquad (S-1)$$

where for the i^{th} population of sites, comprising a fraction p_i of adsorption sites, the mean number of adsorption events per site is λ_i. The model is constrained so that $\sum p_i = 1$. The average site has $\bar{\lambda} = \sum p_i \lambda_i$ adsorption events. If *N* molecules adsorb on an area *a* onto *S* discrete sites, the density of sites is given by $S/a = N/\bar{\lambda}$.

The model for adsorption kinetics was fit to the data as shown in Figure B8. The adsorption kinetic distributions were heavy-tailed and required two component distributions to be fit within error. Qualitatively, weak adsorption sites with $\lambda \sim 0.1$ and strong sites with $\lambda \sim 1$ were identified by the fitting procedure. We have previously demonstrated that sites with stronger adsorption kinetics also exhibit slower desorption kinetics i.e. retain molecules to a confined area for longer periods of time for this exact physical system and other surface-molecule-solution combinations.[2,8] Here, we were simply interested in determining if the frequency of confined periods, evident in the step-size distributions, was correlated with the heterogeneous surface properties that lead to anomalous adsorption kinetics. We can quantify the heterogeneity of the surface by comparing the observed density of sites to that expected for a perfectly uniform surface. The so-called heterogeneity parameter is given by

$$h = \frac{maximum\ \ density\ of\ adsorption\ \ sites}{observed\ density\ of\ adsorption\ sites} = \frac{1/a_{molecule}}{S/a} \quad (\mathrm{S}-2)$$

The cross-sectional area of BODIPY fatty acid $a_{molecule}$ has been estimated to be about 4 nm^2.[9] The heterogeneity and fitting parameters are reported in Table B3. As discussed in

the main text, the apparent heterogeneity of the surface had the same non-monotonic dependence on solution conditions as the frequency of confinement ($1 - f_{mobile}$).

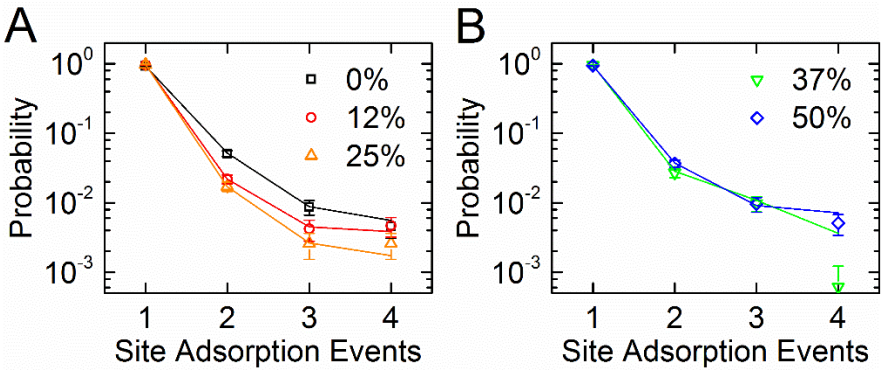

Figure B8: Probability histograms of site adsorption events. Data from indicated methanol-water solution conditions represented by symbols with standard error displayed. Fits to multicomponent Poisson distributions (Equation B1) are shown with solid lines.

Table B3: Adsorption event count histogram fit parameters. The parameters are for the fits shown in Fig B8. The values in parentheses represents the uncertainty (standard error) in the last significant digit of each value. a = 4,770 μm^2 and N = 2,480 for each surface.

Percent Methanol	**h** $\times 10^{-4}$	S/a (μm^{-2})	p_i	λ_i
0	9.5(9)	2.8(3)	0.968(4) 0.031(4)	0.096(5) 3.0(4)
12	5.5(5)	4.8(4)	0.980(2) 0.020(2)	0.038(2) 3.6(4)
25	3.0(9)	9(3)	0.990(4) 0.011(4)	0.029(6) 3(1)
37	3.8(5)	7(1)	1	0.075(1)
50	10(1)	2.8(4)	0.963(5) 0.037(5)	0.065(6) 0.50(3)

B.5 Theoretical Flight Length Distribution

The distribution of flight lengths for a molecule that desorbs from a surface and freely diffuses through solution prior to re-adsorption is given by the following equation.[10]

$$\lambda(r, r^*) = \frac{1}{r^*} - \frac{\pi r}{2{r^*}^2}\left[H_0\left(\frac{r}{r^*}\right) - Y_0\left(\frac{r}{r^*}\right)\right] \quad (B3)$$

It consists of the Struve function H_0, a Bessel function of the second kind Y_0, and the characteristic flight length $r^* = a/\epsilon$. In the context of a lattice model, a is the lattice spacing and ϵ is the probability of an adsorbing onto the surface from an adjacent site in solution. For large r, $\lambda(r, r^*) \sim \left(\frac{r^*}{r}\right)^2$, i.e. the tails of the distribution resemble a power-law. The scaling relationship between adsorption rate and the apparent diffusion coefficient for flying motion is given by

$$D_{flying} \sim \int_0^{r_{max}} r^2 \lambda(r, r^*) dr \quad (B4)$$

which applies when steps up to r_{max} in length can be observed.

B.6 References

1. Skaug, M. J.; Mabry, J. N.; Schwartz, D. K., Single-Molecule Tracking of Polymer Surface Diffusion. *J. Am. Chem. Soc.* **2014,** *136* (4), 1327-1332.

2. Mabry, J. N.; Skaug, M. J.; Schwartz, D. K., Single-Molecule Insights into Retention at a Reversed-Phase Chromatographic Interface. *Anal. Chem.* **2014,** *86* (19), 9451-9458.
3. Skaug, M. J.; Mabry, J.; Schwartz, D. K., Intermittent Molecular Hopping at the Solid-Liquid Interface. *Phys. Rev. Lett.* **2013,** *110* (25).
4. Bindhu, C. V.; Harilal, S. S.; Nampoori, V. P. N.; Vallabhan, C. P. G., Solvent effect on absolute fluorescence quantum yield of rhodamine 6G determined using transient thermal lens technique. *Mod. Phys. Lett. B* **1999,** *13* (16), 563-576.
5. Yu, C.; Guan, J.; Chen, K.; Bae, S. C.; Granick, S., Single-Molecule Observation of Long Jumps in Polymer Adsorption. *ACS Nano* **2013,** *7* (11), 9735-9742.
6. Kisley, L.; Chen, J.; Mansur, A. P.; Shuang, B.; Kourentzi, K.; Poongavanam, M. V.; Chen, W. H.; Dhamane, S.; Willson, R. C.; Landes, C. F., Unified superresolution experiments and stochastic theory provide mechanistic insight into protein ion-exchange adsorptive separations. *Proc. Natl. Acad. Sci. U. S. A.* **2014,** *111* (6), 2075-80.
7. Stirling Churchman, L.; Flyvbjerg, H.; Spudich, J. A., A Non-Gaussian Distribution Quantifies Distances Measured with Fluorescence Localization Techniques. *Biophys. J.* **2006,** *90* (2), 668-671.
8. Langdon, B. B.; Mirhossaini, R. B.; Mabry, J. N.; Sriram, I.; Lajmi, A.; Zhang, Y.; Rojas, O. J.; Schwartz, D. K., Single-Molecule Resolution of Protein Dynamics on Polymeric Membrane Surfaces: The Roles of Spatial and Population Heterogeneity. *ACS Applied Materials & Interfaces* **2015,** *7* (6), 3607-3617.
9. Horn, D.; Klingler, J.; Schorf, W.; Graf, K., Experimental progress in the characterization of colloidal systems. *Structure, Dynamics and Properties of Disperse Colloidal Systems* **1998,** *111*, 27-33.
10. Chechkin, A. V.; Zaid, I. M.; Lomholt, M. A.; Sokolov, I. M.; Metzler, R., Bulk-mediated diffusion on a planar surface: Full solution. *Physical Review E* **2012,** *86* (4).

APPENDIX C: SUPPORTING INFORMATION FOR CH. 4

C.1 CIRCULAR DICHROISM MEASUREMENTS

Circular dichroism (CD) spectra of peptide solution (0.6 μM peptide, 180 μM sodium fluoride) were acquired in a 1 mm quartz cell using an Applied Photophysics ChirascanPlus Circular Dichroism and Fluorescence Spectrometer (Applied Photophysics, Surrey, UK). The data was smoothed using an 8-point Savitzky-Golay filter in Mathematica and is shown in Figure C1 at three different temperatures. The data has dominant features consistent with α-helical spectra including peaks at ~195 nm and minima at ~205 nm. In contrast, random coil spectra have minima around 195 nm.[1] The data was fit to a constrained linear combination of reference α-helix and random coil poly-l-lysine curves[2] by the following equation.[1]

$$\frac{\theta(\lambda,T)}{A} = h(T)S(\lambda, helix) + (1 - h(T))S(\lambda, coil) \qquad \text{(C1)}$$

$\theta(\lambda, T)$ is the measured molar ellipticity of the peptide at temperature T and wavelength λ. The fractional helicity at a given temperature is specified by $h(T)$. $S(\lambda, state)$ is the molar ellipticity value from the reference poly-lysine CD data for the indicated conformational state. We note that the peptide concentration (used in converting the absolute ellipticity to molar ellipticity) was determined by measuring the absorbance at 488 nm (corresponding to the peak absorbance of the HiLyte Fluor 488) and using the

manufacturer's specified molar extinction coefficient for HiLyte Fluor 488 (70,000 M^{-1} cm^{-1}) to convert absorbance to concentration. This provided an approximate measure of the peptide concentration, but the magnitude of the spectra are acutely sensitive to the peptide concentration (and possibly to the presence of the fluorescent dyes as well) and so to enable a more accurate fit of the data we renormalized the measured molar ellipticity θ by the fitted normalization constant A.

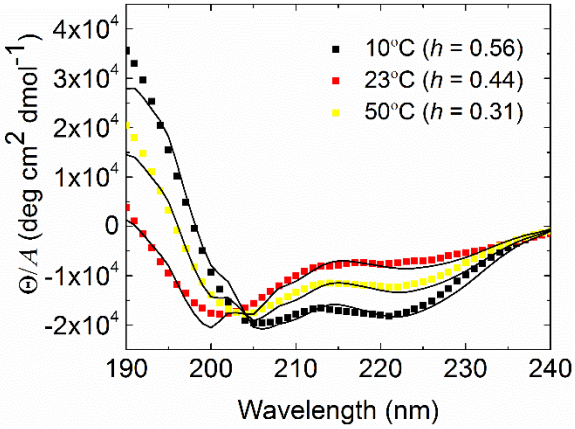

Figure C1: Circular dichroism spectra of peptide in solution. Solid lines show fit of linear combination of reference helix and coil spectra. The legend shows solution temperature and fractional helicity, h from the fit of Eq C1 with $A = 4.8$.

C.2 PEPTIDE END-TO-END DISTANCE CALCULATIONS

We evaluated the end-to-end distance, *r*, for both the helix and coil state to validate our criteria for assigning adsorbed peptides to the coil ($d < 1.14$) or helix ($d > 1.14$) state. The relative end-to-end distance d is proportional to r/R_o. In the full helical state, the end-to-end distance would be about 4.2 nm, the product of the number of residues (28) between dyes and the translation distance along the axis per residue (1.5 Å).[3] In the coil state, peptide conformations resemble self-avoiding random walks when only excluded volume effects are significant.[4] (Under perfect solvent conditions, the conformations may also resemble more compact normal random walks.[5]). Following a previously outlined method,[6-7] we used the following scaling form for the end-to-end distance distribution for a self-avoiding random walk, which has been show to agree well with protein structures simulated with atomistic detail.[4,8]

$$P_\delta(\tilde{r}) \approx \tilde{r}^\theta \exp(-\tilde{r}^t) \qquad \text{(C2)}$$

In Equation C2, the constants θ and t depend on the dimensionality of the walk and are $\theta = 4/9$ and $t = 4.0$ in two dimensions (δ=2) and are $\theta = 5/18$ and $t = 2.5$ in three dimensions (δ=3). P_δ is the probability of observing end-to-end distance $\tilde{r} = r/R_g$, where the radius of gyration $R_g = bN^{3/(\delta+2)}$ for $N = 28$ monomers (the number of residues between the dyes) of length $b = 0.38$ nm.[5] We note that values of *b* (around 0.2 nm) smaller than the residue size have been found to apply at extremely high concentrations of chemical denaturants for large proteins.[9] Following previous literature

estimates of peptide size,[10] we have opted for a more conservative estimate of *b*, based on the actual residue length, for comparing the helix and coil conformations. The radius of gyration is thus estimated as 4.6 nm for δ=2 and 2.8 nm for δ=3. The fraction of configurations with an end-to-end distance greater than $\tilde{r}$ can be calculated by the following equation.

$$x(\tilde{r}) = \int_{\tilde{r}}^{\infty} P_{\delta}(\tilde{r}')dr \Big/ \int_{0}^{\infty} P_{\delta}(\tilde{r}')dr \qquad \text{(C3)}$$

Peptides adsorbed to an interface will adopt a roughly two-dimensional conformation if surface interactions are strong or a roughly three-dimensional conformation if surface interactions are weak. We evaluated the fraction of peptides in the coil state falsely assigned to the helix state, $x(\tilde{r})$ for both limiting cases. The value of $x(\tilde{r})$ for r =4.2 nm was 0.17 in 2D and 0.02 in 3D. This agrees with the data in Figure 1 that shows a finite amount of overlap in the peaks at high and low *d* values.

C.3 SURFACE PATTERNING

C.3.1 Procedure

The TMS surface was patterned using 2000 lines-per-inch (lpi) nickel mesh (Structure Probe Inc., West Chester, PA) as a contact photomask. The masked substrate was then exposed to ultraviolet light from a mercury (254 nm) Pen-Ray lamp (UVP, Upland, CA) with an intensity of 0.3 mW cm^{-2} for 30 minutes.

C.3.2 Photomask Imaging

The mesh photomask was imaged on a #1 glass coverslip (Fisher Scientific), with a drop of ultrapure water on top, using an inverted microscope (Nikon Ti-E, 100X objective) with a mercury lamp (Nikon C-HFIE) for illumination through the objective and beamsplitter (Chroma) in the filter cube to facilitate bright-field imaging. Nikon Elements software was used to capture the image from the cooled CCD camera (Photometrics Cascade 512B).

C.3.4 Dye-Labeled Amine Monolayer Preparation

A piranha and UV/ozone cleaned fused silica wafer was immersed in a 200 mL toluene solution containing 0.50 mL N-(6-aminohexyl)aminopropyltrimethoxysilane at room temperature for one hour. The wafer was then rinsed with toluene, dried with a nitrogen stream, rinsed with water, and dried again. The water contact angle after functionalization was 35° ± 1°. The wafer was then patterned as described above using the contact photomask and ultraviolet illumination. A concentrated dye solution was prepared by dissolving 1 mg Alexa Fluor 532 carboxylic acid, succinimidyl ester in 0.10 mL methanol. This solution was added to 10 mL solution of phosphate buffered saline, pH 7.8. The patterned, amine-functionalized wafer was then placed in the dye solution and kept in the dark overnight at room temperature to facilitate covalent coupling of the

succinimidyl ester with the surface-bound amine groups. The dye-labeled wafer was then rinsed with copious amounts of water and placed in 200 mL of DI water in a beaker in a bath sonicator. This cleaning procedure was then repeated with isopropanol and the wafer was dried with nitrogen and installed in the flow cell. Ultrapure water was flowed into the flow cell, and the patterned surface was imaged using TIRFM as previously described, except that a 532 nm laser (Cobalt Samba) was used for illumination and the image was filtered only with a 585/40 nm bandpass filter (Semrock).

C.3.5 Pattern Characterization

The degradation of the silane coating upon exposure to UV light was presumably due to the generation of ozone and highly reactive radical species.[11] If these reactive species diffused under the contact photomask, then the apparent size of the holes would increase, and the shape would be expected to change from squares to circles, since the boundary for ozone degradation would depend on the radial distance from the ozone source.[12] The mesh had 4.5 μm square holes (Figure C3A). Consistent with the above mechanism for photopatterning, the features in the patterned monolayer were larger and more circular (Figure C3B). These circular surface feature sizes appear very similar to those imaged using the MAPT technique (Figure 1) and so we can infer that the MAPT technique is sensitive to the underlying surface chemistry.

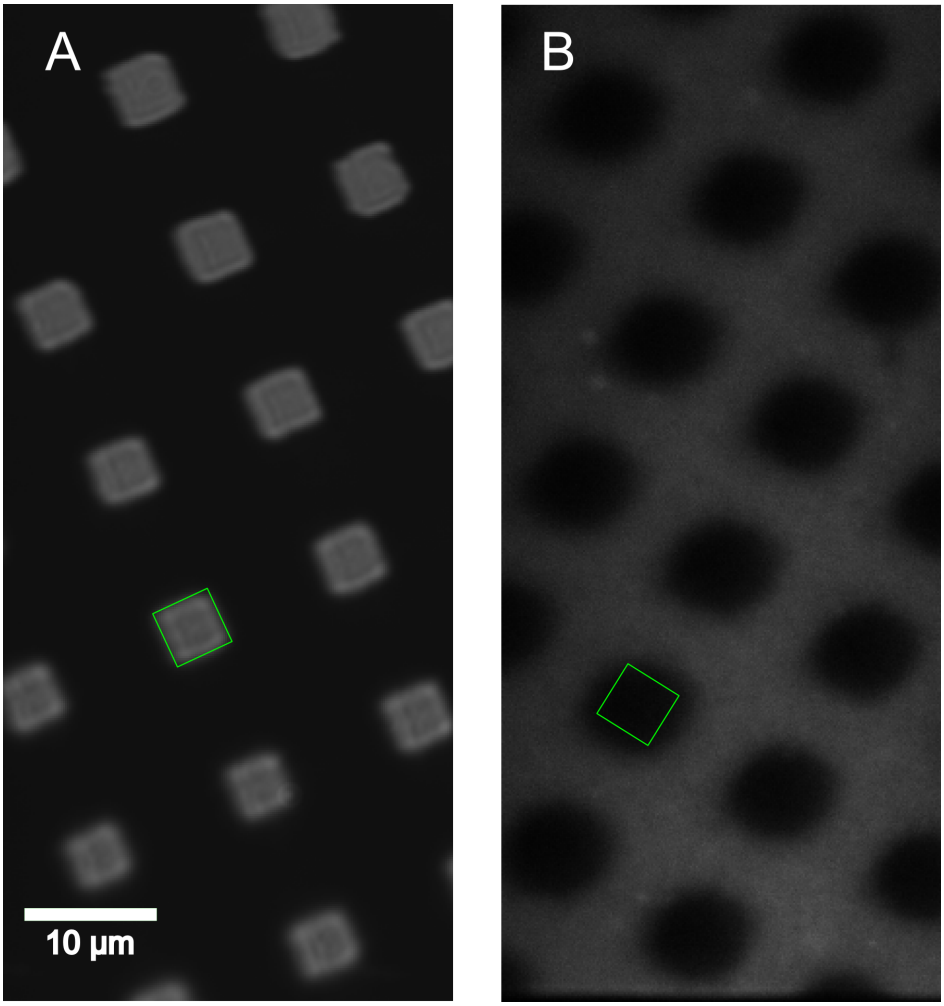

Figure C2: Patterning test images. (A) Bright-field image of nickel mesh (contact photomask). (B) TIRFM image of patterned (photodegraded) amine monolayer with covalently attached Alexa Fluor 532. A 4.5 µm square was placed at the center of a hole in each image. The features in the patterned monolayer were apparently larger than the holes in the mask, presumably due to ozone diffusion.

C.4 MAPT IMAGES OF CONTROL SURFACES

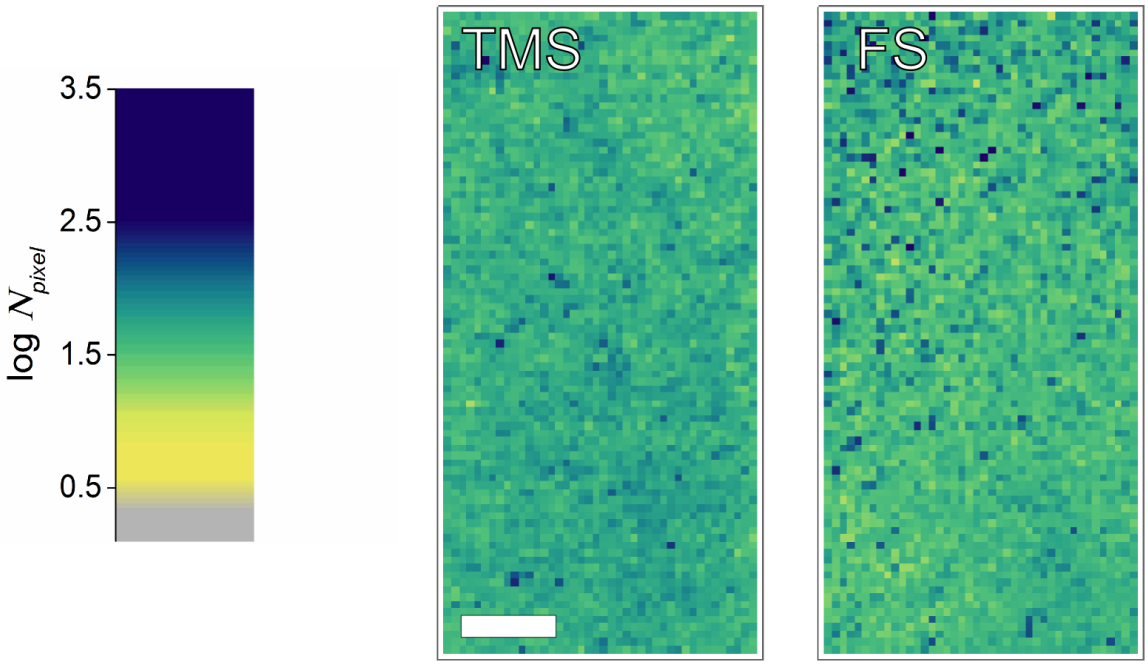

Figure C3: Control adsorption map. Map showing the number of molecules that adsorbed in each pixel (N_{pixel}) on control surfaces with an average N_{pixel} of 52. Pixel width = 770 nm. Scalebar 10 µm.

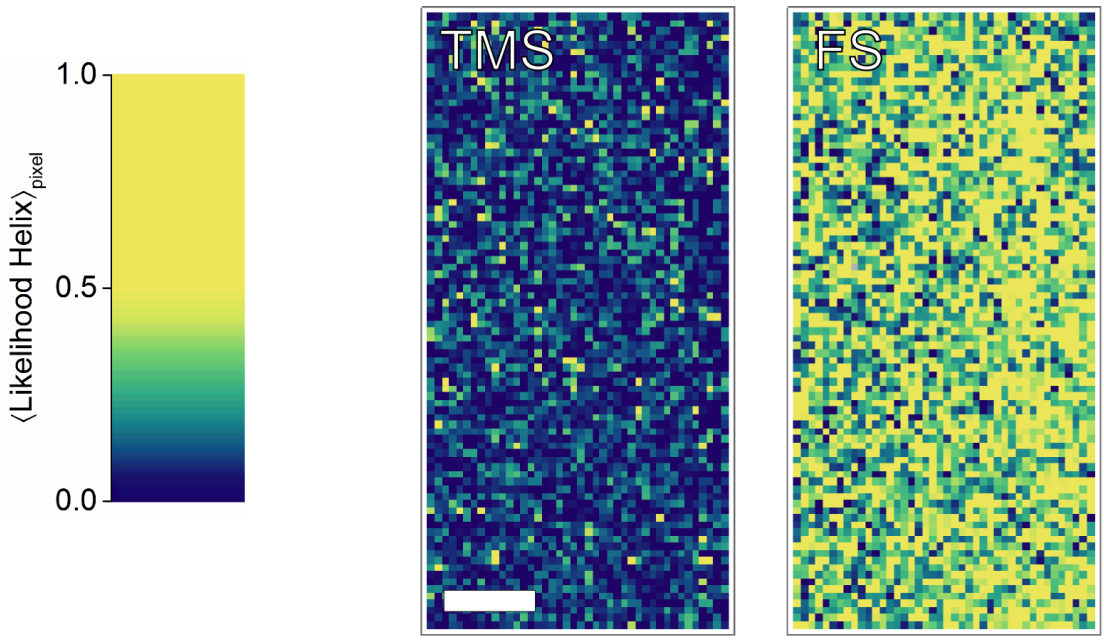

Figure C4: Control conformation map. Map of the likelihood of observing peptides in the helix state in each pixel. Scalebar 10 μm.

C.5 Measurement of Folding and Unfolding Rates

To measure unbiased surface folding and unfolding rates, the timescales for measurable folding and unfolding must be less than the timescale for desorption from the surface. In these experiments, the timescales for measurable folding/unfolding and desorption overlap. This creates an observation bias since molecules can desorb before undergoing a change in conformation. We utilize an established framework to correct for this observation bias,[13] which relies on constructing a corrected probability distribution of initial conformational state residence times. The initial state residence time $t_i = i\, t_{ac}$, where i is the number of frames the adsorbed molecule remains in the initial

conformational state and t_{ac} is the acquisition time (100 ms in these experiments). The probability of observing a given initial state residence time is given by

$$p(t_i) = \frac{n(t_i)}{\rho\, n(t_r > t_i)} \qquad \text{(C4)}$$

In this equation, $n(t_i)$ is the number of trajectories with a given initial state residence time, $n(t_r > t_i)$ is the number of trajectories with the same initial conformational state and a surface residence time t_r greater than the initial state residence time. The normalization constant is given by $\rho = \sum_i \frac{n(t_i)}{n(t_r > t_i)}$. The complementary cumulative distribution $F(t_j)$ is calculated using the below equation.

$$F(t_j) = \sum_{t_i > t_j} p(t_i) \qquad \text{(C5)}$$

C.6 Distributions of Surface Residence and Initial Conformational State Times

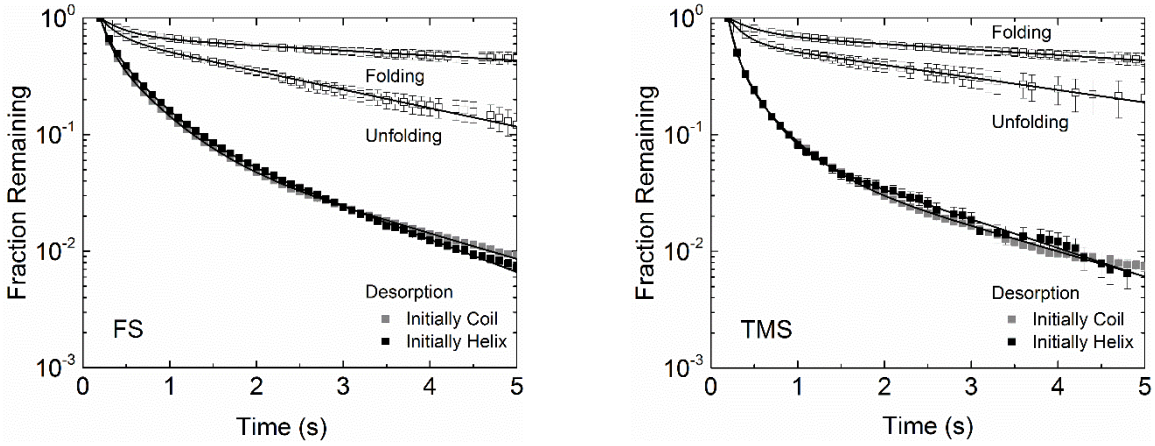

Figure C5: Complementary cumulative distributions of state times. Data (symbols) were fit (solid lines) to Eq. 2 and were labeled according to the rate constants derived from the data and presented in Figure 5B. The distributions and associated rates constants were surface residence times (desorption), initial helix states (unfolding), and initial coil states (folding). Surface residence time distributions were calculated separately for molecules initially in the helix and coil states. Error bars denote standard error.

Table C1: Parameters for surface residence time distribution fits. The parameter values are the best fit values of Eq. 2 shown in Fig C5. The numbers in parentheses represents the uncertainty in the last significant digit of each value (standard error from separately fitting three subsets of the data). Rate constants reported in Figure 5B are given by $\langle\tau\rangle^{-1}$.

Surface (State)	$\langle\tau\rangle$	p_i	τ_i
TMS (Initially Helix)	0.13(2)	0.89(1)	0.08(1)
		0.094(7)	0.34(4)
		0.013(3)	1.83(3)
TMS (Initially Coil)	0.1319(8)	0.902(2)	0.0845(5)
		0.086(1)	0.379(7)
		0.012(1)	2.0(1)
FS (Initially Helix)	0.25(1)	0.716(4)	0.103(7)
		0.240(7)	0.43(2)
		0.045(3)	1.6(1)
FS (Initially Coil)	0.219(3)	0.7975(6)	0.104(3)
		0.176(1)	0.465(3)
		0.027(2)	2.0(1)

Table C2: Parameters for initial conformational state time distribution fits. Data reported using same conventions as in Table C1.

Surface, Initial State (Conformational Change)	$\langle\tau\rangle$	p_i	τ_i
TMS, Coil (Folding)	5.0(8)	0.58(2)	8(1)
		0.42(2)	0.294(5)
TMS, Helix (Unfolding)	1.5(5)	0.33(2)	4(1)
		0.67(2)	0.19(4)
FS, Coil (Folding)	6(2)	0.53(4)	10(3)
		0.47(4)	0.32(1)
FS, Helix (Unfolding)	1.54(9)	0.46(2)	3.1(3)
		0.54(2)	0.24(5)

C.7 Effect of Incident Laser Power on Surface Residence Times

Fluorescent dyes under intense illumination can enter a dark state temporarily (photoblinking) or permanently (photobleaching). These processes have a strong dependence on the illumination intensity (typically quadratic)[14] and usually occur on timescales that are longer than the timescales for a molecule to spontaneously desorb from a surface.[12-13,15] Accordingly, if the surface residence time distributions do not have a strong dependence on incident light intensity, then photophysical process are not significantly affecting the data. We measured surface residence time distributions for the labeled peptides on FS, using 100% laser power (~10 μW/μm^2) and 50% power. We did not see a large difference in the residence time distributions at different laser powers, leading us to conclude that photophysical effects were not significantly affecting our single-molecule observations.

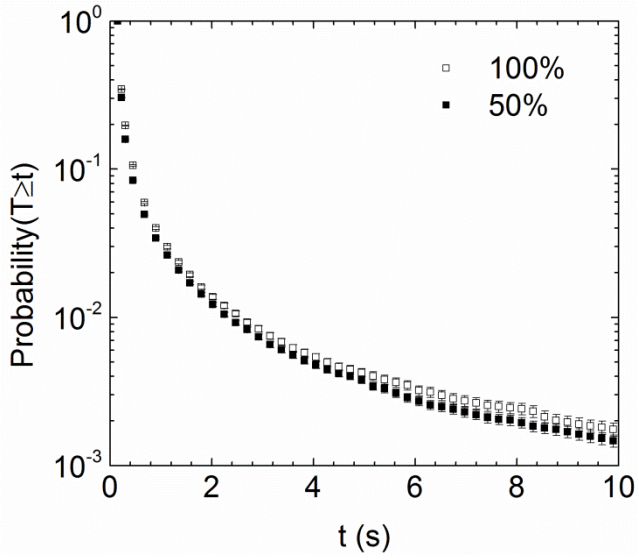

Figure C6: Residence time distributions at different laser power levels. Data acquired for peptides on FS with standard error at 100% and 50% laser power as annotated.

C.8 REFERENCES

1. Greenfield, N. J., Using circular dichroism spectra to estimate protein secondary structure. *Nat. Protoc.* **2006,** *1* (6), 2876-2890.
2. Greenfield, N. J.; Fasman, G. D., Computed circular dichroism spectra for the evaluation of protein conformation. *Biochemistry* **1969,** *8* (10), 4108-4116.
3. Pauling, L.; Corey, R. B.; Branson, H. R., The structure of proteins: Two hydrogen-bonded helical configurations of the polypeptide chain. *Proc. Natl. Acad. Sci. U. S. A.* **1951,** *37* (4), 205-211.
4. Tran, H. T.; Pappu, R. V., Toward an Accurate Theoretical Framework for Describing Ensembles for Proteins under Strongly Denaturing Conditions. *Biophys. J.* **2006,** *91* (5), 1868-1886.
5. Zagrovic, B.; Pande, V. S., Structural correspondence between the [alpha]-helix and the random-flight chain resolves how unfolded proteins can have native-like properties. *Nat. Struct. Mol. Biol.* **2003,** *10* (11), 955-961.
6. Bishop, M.; Clarke, J. H. R., Investigation of the end-to-end distance distribution function for random and self-avoiding walks in two and three dimensions. *The Journal of Chemical Physics* **1991,** *94* (5), 3936-3942.
7. Kastantin, M.; Schwartz, D. K., Connecting Rare DNA Conformations and Surface Dynamics Using Single-Molecule Resonance Energy Transfer. *ACS Nano* **2011,** *5* (12), 9861-9869.
8. des Cloizeaux, J., Lagrangian theory for a self-avoiding random chain. *Phys. Rev. A* **1974,** *10* (5), 1665-1669.
9. Kohn, J. E.; Millett, I. S.; Jacob, J.; Zagrovic, B.; Dillon, T. M.; Cingel, N.; Dothager, R. S.; Seifert, S.; Thiyagarajan, P.; Sosnick, T. R.; Hasan, M. Z.; Pande, V. S.; Ruczinski, I.; Doniach, S.; Plaxco, K. W., Random-coil behavior and the dimensions of chemically unfolded proteins. *Proc. Natl. Acad. Sci. U. S. A.* **2004,** *101* (34), 12491-12496.
10. Zagrovic, B.; Jayachandran, G.; Millett, I. S.; Doniach, S.; Pande, V. S., How large is an alpha-helix? Studies of the radii of gyration of helical peptides by small-angle X-ray scattering and molecular dynamics. *J. Mol. Biol.* **2005,** *353* (2), 232-241.
11. Vig, J. R., UV/ozone cleaning of surfaces. *Journal of Vacuum Science & Technology A* **1985,** *3* (3), 1027-1034.
12. Honciuc, A.; Baptiste, D. J.; Schwartz, D. K., Hydrophobic Interaction Microscopy: Mapping the Solid/Liquid Interface Using Amphiphilic Probe Molecules. *Langmuir* **2009,** *25* (8), 4339-4342.
13. Kastantin, M.; Schwartz, D. K., DNA Hairpin Stabilization on a Hydrophobic Surface. *Small* **2013,** *9* (6), 933-941.
14. Gensch, T.; Bohmer, M.; Aramendia, P. F., Single molecule blinking and photobleaching separated by wide-field fluorescence microscopy. *J. Phys. Chem. A* **2005,** *109* (30), 6652-6658.

15. Honciuc, A.; Baptiste, D. J.; Campbell, I. P.; Schwartz, D. K., Solvent Dependence of the Activation Energy of Attachment Determined by Single Molecule Observations of Surfactant Adsorption. *Langmuir* **2009,** *25* (13), 7389-7392.